DOKUZ EYLÜL UNIVERSITY
GRADUATE SCHOOL OF NATURAL AND APPLIED SCIENCES

IMPROVED EFFECTIVE FIELD THEORY ANALYSIS OF CRITICAL PHENOMENA IN ISING MODEL WITH QUENCHED DISORDER EFFECTS

by

Yusuf YÜKSEL

March, 2013

İZMİR

IMPROVED EFFECTIVE FIELD THEORY ANALYSIS OF CRITICAL PHENOMENA IN ISING MODEL WITH QUENCHED DISORDER EFFECTS

A Thesis Submitted to the
Graduate School of Natural And Applied Sciences of Dokuz Eylül University
In Partial Fulfillment of the Requirements for the Degree of Doctor of
Philosophy in Physics

by

Yusuf YÜKSEL

March, 2013

İZMİR

Ph.D. THESIS EXAMINATION RESULT FORM

We have read the thesis entitled "**IMPROVED EFFECTIVE FIELD THEORY ANALYSIS OF CRITICAL PHENOMENA IN ISING MODEL WITH QUENCHED DISORDER EFFECTS**" completed by **YUSUF YÜKSEL** under supervision of **PROF. DR. HAMZA POLAT** and we certify that in our opinion it is fully adequate, in scope and in quality, as a thesis for the degree of Doctor of Philosophy.
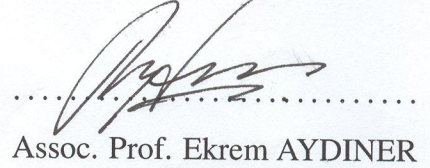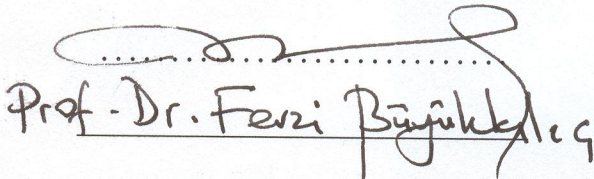

Prof. Dr. Hamza POLAT

Supervisor

Prof. Dr. Kadir YURDAKOÇ
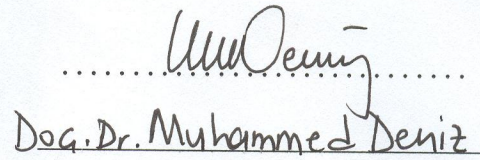
Thesis Committee Member

Assoc. Prof. Ekrem AYDINER

Thesis Committee Member

Prof. Dr. Ferzi Büyükkılıç

Examining Committee Member

Doç. Dr. Muhammed Deniz

Examining Committee Member

Prof. Dr. Ayşe OKUR

Director

Graduate School of Natural and Applied Sciences

ACKNOWLEDGEMENTS

Yusuf YÜKSEL

IMPROVED EFFECTIVE FIELD THEORY ANALYSIS OF CRITICAL PHENOMENA IN ISING MODEL WITH QUENCHED DISORDER EFFECTS

ABSTRACT

This thesis report is essentially based on the results of recent series of papers concerning the critical phenomena and order-disorder phase transition characteristics of Ising model and its various generalizations in the presence of several kinds of quenched disorder effects. In order to investigate the magnetic properties of aforementioned models, we have proposed a formalism based on the effective-field theory (EFT) which improves the results provided by conventional EFT approximations in the literature by systematically including the multi-site, as well as single-site spin correlation functions in the calculations within a heuristic manner.

Numerical computations are performed and the results are analyzed for the cases of spin-1 Blume-Capel model in the presence of longitudinal and transverse magnetic fields (Yüksel & Polat, 2010), site diluted Ising ferromagnets (Akinci, Yuksel, & Polat, 2011c), bond diluted spin-1 Blume-Capel model with transverse and crystal field interactions (Akinci, Yuksel, & Polat, 2011b), spin-1 Blume-Capel model with random crystal field interactions (Yüksel, Akinci, & Polat, 2012a), and Ising model in the presence of random magnetic fields (Akinci, Yuksel, & Polat, 2011a).

Keywords: Ferromagnetism, Dilute ferromagnets, Bond dilution, Effective-field theory, Random-field Ising model

DONMUŞ DÜZENSİZLİK ETKİLERİ İÇEREN ISING MODELİNDE KRİTİK OLAYLARIN GELİŞTİRİLMİŞ ETKİN ALAN TEORİSİ İLE ANALİZİ

ÖZ

Bu tez çalışması temel olarak, çeşitli türlerdeki donmuş düzensizlik etkilerinin varlığında, Ising modelinin ve bu modelin çeşitli genelleştirilmiş hallerinin kritik özellikleri ve faz geçiş karakteristiklerine ilişkin sonuçların detaylı analizini içermektedir. Elde edilen sonuçlar, yazarın da yer aldığı çalışma grubu tarafından üretilen makalelerden derlenmiştir. Söz konusu modellerin manyetik özelliklerini incelemek için etkin-alan teorisi (EFT) temelli bir formülasyon önerilmiştir. Önerilen formülasyonun, hesaplamalarda karşılaşılan çoklu ve tekli spin korelasyon fonksiyonlarını sezgisel, ancak sistematik bir biçimde hesaba katarak, sıradan EFT yaklaşımlarının aynı modeller için ürettiği sonuçları geliştirdiği gözlenmiştir.

Çalışmada yer alan nümerik hesaplamalar ve elde edilen sonuçlar sırasıyla boyuna ve enine alanlı spin-1 Blume-Capel modeli (Yüksel & Polat, 2010), örgü noktaları seyreltilmiş ferromanyetik Ising sistemleri (Akinci, Yuksel, & Polat, 2011c), enine alanlı ve kristal alan etkileşimli bağ seyreltik spin-1 Blume-Capel modeli (Akinci, Yuksel, & Polat, 2011b), rastgele kristal alanlı spin-1 Blume-Capel modeli (Yüksel, Akinci, & Polat, 2012a) ve rastgele manyetik alanlı Ising modeli (Akinci, Yuksel, & Polat, 2011a) için uygulanmıştır.

Anahtar sözcükler: Ferromanyetizma, Seyreltik ferromanyetik sistemler, Bağ seyreltme, Etkin-alan teorisi, Rastgele alanlı Ising modeli

CONTENTS

CHAPTER ONE
INTRODUCTION

1.1 Prologue

Magnetism is probably one of the most fascinating phenomena of nature which can be observed in several shapes such as a significant property of a permanent magnet or in forms of captivating magnetic storms (i.e. northern lights or polar aurora) due to the fluctuations of the magnetic fields in earth's magnetosphere. The interest of mankind in magnetism has been a very long journey dating back to ancient Greek and Chinese cultures and in the course of time, owing to the pioneering and cornerstone efforts by Hans Christian Oersted, Andre-Marie Ampere, Michael Faraday, James Clerk Maxwell and of many other scholars, it is now well established that the essential source of microscopic origin of magnetism is moving electric charges which in quantum mechanical manner leads to the concept of magnetic moment and spin angular momentum. In a macroscopic perspective, manifestation of magnetism appears in different characteristics including diamagnetism, paramagnetism, ferromagnetism, antiferromagnetism and ferrimagnetism. Diamagnetism which is associated with a negative magnetic susceptibility is completely a quantum mechanical phenomena and it can be observed in all materials, although it is generally a weak effect. Paramagnetism is characterized by a positive susceptibility and materials exhibiting paramagnetic behavior can only be magnetized in the presence of external magnetic field whereas ferromagnetic materials such as iron, cobalt and nickel can exhibit a spontaneous magnetization even in the absence of external field. This spontaneous magnetization basically originates as a consequence of parallel alignment of magnetic moments. Antiferromagnetism is similar to ferromagnetism, but it is usually related with antiparallel alignment of magnetic moments with zero net magnetization. On the other hand, in ferrimagnetism, although the magnetic moments are aligned antiparallel to each other as in the anti-ferromagnetic order, ferrimagnetic materials may have non-zero net magnetization.

1.2 Manifestation of Ferromagnetism

The different types of magnetic characteristics mentioned above represent the magnetic order of the system. Physics of magnetic phase transitions particularly deals with the transitions between these different magnetic order types. These phase transitions essentially originate as a result of a macroscopic change in the system due to a small variation in a tunable parameter such as temperature. In the present thesis report, we particularly focus our attention on the models exhibiting ferromagnetic-paramagnetic transitions in the presence of quenched disorder. Ferromagnetism is basically the manifestation of long range order among the magnetic moments of material. A ferromagnetic material undergoes a continuous phase transition at a particular temperature known as the Curie temperature and its value extends from a few to thousands of Kelvin degrees depending on the material. Transition temperature values of some certain ferromagnets are depicted in Table 1.1.

Table 1.1 Properties of some common ferromagnets, (Blundell, 2001).

Material	Fe	Co	Ni	Gd	MnSb	EuO	EuS
Curie Point (K)	1043	1394	631	289	587	70	16.5

There are several kinds of magnetic interactions between magnetic moments leading to the concept of long range order in ferromagnetism. Magnetic dipolar interaction between two magnetic dipoles $\vec{\mu}_1$ and $\vec{\mu}_2$ is one of them and it is given by

$$E = \frac{\mu_0}{4\pi r^3}\left[\vec{\mu}_1.\vec{\mu}_2 - \frac{3}{r^2}(\vec{\mu}_1.\vec{r})(\vec{\mu}_2.\vec{r})\right], \tag{1.2.1}$$

where $\mu_0 = 4\pi \times 10^{-7} N/A^2$ is the magnetic permeability of free space and r is the relative distance between dipole moments. However, for $\mu \approx \mu_B$ and $r \approx 1$ Å, magnitude of this energy will be approximately obtained as $\sim 10^{-23}$ J which is equivalent to 1K temperature. By comparing this result with the transition temperature values shown in Table 1.1, we see that magnetic dipolar interaction energy is not generally responsible for the occurrence of long range magnetic order in real systems, except the materials which order at milliKelvin temperatures (Blundell, 2001). However, as will be discussed in the following chapters, the long range magnetic order in real systems

actually originates due to the presence of exchange interactions. Exchange energy is an electrostatic energy and purely a quantum mechanical phenomena.

1.3 A Brief Note on Models of Interacting Many Body Systems

The most simple model representing an interacting many body system is the spin-1/2 Ising model (Ising, 1925) where the particles are interacting with their nearest-neighbors via discrete local spin variables S_i

$$\mathcal{H} = -J \sum_{<ij>} S_i S_j, \tag{1.3.1}$$

where $S_i = \pm 1$, the summation is carried over nearest neighbor spins, and J is the strength of the spin-spin interaction (i.e. exchange interaction). During the last 40 years more than 16000 publications have appeared using this model (Kobe, 2000). The model Hamiltonian defined in Eq. (1.3.1) successfully explains the magnetic behavior of highly anisotropic materials.

As an extension of the model, in order to explain the first order magnetic phase transitions observed in a variety of systems, Blume-Capel model (Blume, 1966, Capel, 1966)

$$\mathcal{H} = -J \sum_{<ij>} S_i S_j - D \sum_i (S_i)^2, \tag{1.3.2}$$

is often used in the literature where D is the single-ion anisotropy. The model can be briefly explained with the help of energy-level diagram of a magnetic ion shown in Fig. 1.1 (Blume, 1966).

According to Fig. 1.1, we consider a magnetic ion with singlet (non-magnetic) and triplet (magnetic) states which are energetically separated by a crystal-field energy D. As shown in Fig. 1.1a, in the presence of a magnetic field, singlet state is not affected whereas triplet state splits into three non-degenerate energy levels. However, at $T = 0K$, the state with lowest energy is the singlet state, hence at the ground state, the system which is an ensemble of magnetic ions prefers to be in the singlet state. In this case the net magnetization is zero.
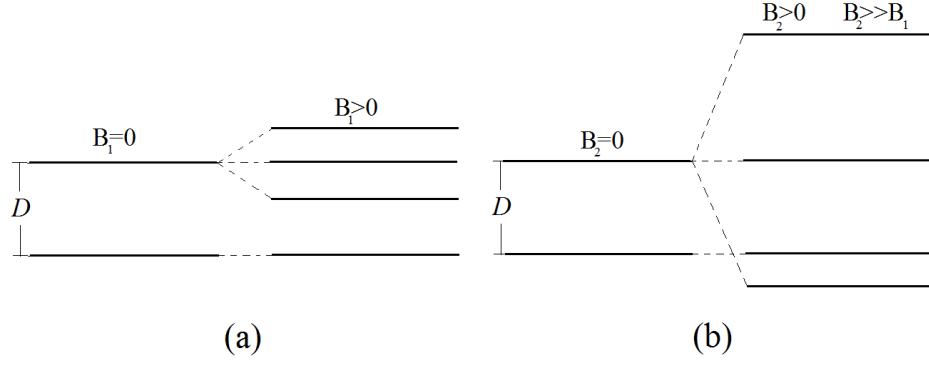
Figure 1.1 Energy-level diagram (a) for magnetic-field splitting smaller than the singlet-triplet separation D, and (b) for magnetic- field splitting larger than D, (Blume, 1966).

On the other hand, if the magnetic field is sufficiently large then the lowest energy level of triplet state may be lower than that of singlet state. In this case the system is magnetically ordered and exhibit a non-zero magnetization. Assuming the magnetic field to be due to the exchange interaction between neighboring ions, the magnetization which is determined from the populations of magnetic triplet and non-magnetic singlet states may exhibit a discontinuous jump with a slight increment in the temperature which yields a first order phase transition (Blume, 1966).

Apart from this, inclusion of a biquadratic exchange interaction in Eq. (1.3.2) yields

$$\mathcal{H} = -J \sum_{<ij>} S_i S_j - K \sum_{<ij>} S_i^2 S_j^2 - D \sum_i (S_i)^2, \qquad (1.3.3)$$

known as Blume-Emergy-Griffiths (BEG) model (Blume, Emery, & Griffiths, 1971) which was introduced to explain the λ transition and phase separation in $\text{He}^3 - \text{He}^4$ mixtures within the framework of an Ising-like model. It is important to note that the local spin in Eq. (1.3.3) must be regarded as a fictitious variable which can take values 0 and ± 1. According to model, a He^3 fermion particle at site i is represented by $S_i = 0$ whereas $S_i = \pm 1$ corresponds to He^4 boson.

The number of He^3 and He^4 atoms are given by

$$N_3 = \sum_i^N (1 - S_i^2), \qquad (1.3.4)$$

$$N_4 = \sum_i^N S_i^2, \qquad (1.3.5)$$

where $N = N_3 + N_4$ is the total number of particles. The Hamiltonian of model consists of two parts. The first one is

$$\mathcal{H} = -J \sum_{<ij>} S_i S_j, \tag{1.3.6}$$

which is responsible for the superfluid ordering in He^3-He^4 mixture. If the He^3 concentration is zero then Eq. (1.3.6) resembles the Hamiltonian of Ising ferromagnet. Hence, in the presence of He^3 atoms, we have $S_i^2 = 0$ for some certain lattice sites which is similar to the problem of Ising ferromagnet with non-magnetic impurities. In this case, we expect that transition temperature T_c decreases with increasing He^3 concentration.

Based on the experimental facts, it is known that below a certain temperature, pairs of He^3 fermions act as a composite boson and phase diagrams in $T(K) - He^3$ fraction plane exhibit a superfluid order by separating into two phases one He^4 rich and one He^3 rich. Theoretically, it order to take into account this fact we should introduce an additional term in the Hamiltonian of the system

$$\mathcal{H}_I = -K_{33} \sum_{<ij>}(1 - S_i^2)(1 - S_j^2) - K_{44} \sum_{<ij>} S_i^2 S_j^2 - K_{34} \sum_{<ij>}[S_i^2(1 - S_j^2) + S_j^2(1 - S_i^2)], \tag{1.3.7}$$

where the summations are taken over nearest-neighbor sites and $K_{\alpha\beta}$ is the effective interaction energy between He^α-He^β atoms. Since $S_i^2 = 0$ for He^3 and $S_i^2 = 1$ for He^4 we can rearrange Eq. (1.3.7) as

$$H_I = -(K_{33} + K_{44} - 2K_{34}) \sum_{ij} S_i^2 S_j^2 - 2q(K_{34} - K_{33}) \sum_i^N S_i^2 - qNK_{33}, \tag{1.3.8}$$

where q is the coordination number of the lattice. Finally, in order to control the number of He^3 and He^4 atoms, it is necessary to include the chemical potentials in total Hamiltonian

$$\mathcal{H} = H_s + H_I - \mu_3 N_3 - \mu_4 N_4, \tag{1.3.9}$$

which can be written in a more compact from

$$\mathcal{H} = -J \sum_{<ij>} S_i S_j - K \sum_{<ij>} S_i^2 S_j^2 - D \sum_i S_i^2 - N(qK_{33} + \mu_3) \tag{1.3.10}$$

where

$$K = K_{33} + K_{44} - 2K_{34}, \qquad (1.3.11)$$

and

$$D = -\mu_3 + \mu_4 - 2q(K_{33} - K_{44}). \qquad (1.3.12)$$

The model Hamiltonian in Eq. (1.3.12) represents spin-1 Ising model with bilinear and biquadratic exchange interactions with crystal field strength D, and the constant term on the right-hand side of Eq. (1.3.12) can be neglected (Blume et al., 1971). Moreover, it is possible to extend these models by including a transverse field term which is called the spin-1 Blume-Capel model in the presence of transverse fields which can be represented by the following Hamiltonian (c.f. see Chapter 4)

$$\mathcal{H} = -J \sum_{<ij>} S_i^z S_j^z - D \sum_i (S_i^2)^2 - \Omega \sum_i S_i^x. \qquad (1.3.13)$$

As will be discussed in Chapter 3, there is not any rigorously exact calculation method for the aforementioned models regarding their critical properties except the one dimensional Ising chain in the presence of external magnetic field and its two dimensional counterpart with zero magnetic field. Hence, in this thesis report, we propose an approximation method which yields almost the best approximate results to the results of some powerful techniques such as Monte Carlo (MC) simulations and series expansion (SE) methods among the other techniques. Our results which will be presented in Chapter 5 are essentially based on our recent publications. A detailed description of our formulation and its relevant variants in the presence of quenched randomness within the framework of our method will be discussed in the following chapters.

For this aim, present thesis report has been organized as follows: In Chapter 2, we discuss some basic and important concepts of magnetism. Chapter 3 concerns with the exact and approximation techniques regarding a variety of spin models. We present a detailed description of our formulation in Chapter 4. Chapter 5 is devoted to our numerical results on the applications of the proposed formalism for the models with quenched disorder effects and related discussions. Finally Chapter 6 contains our final remarks and conclusions.

CHAPTER TWO
SOME BASIC CONCEPTS OF MAGNETISM

This chapter is devoted to the discussion of some basic concepts of magnetism. A widely detailed description of the ideas introduced in this chapter can be found in (Blundell, 2001).

Solid materials may have magnetic moments which exhibit a cooperative behavior. This cooperative behavior completely differs from the case in which all the magnetic moments do not interact with each other. This situation leads to a wide variety of magnetic phenomena in real magnetic materials. In this chapter, we want to depict this picture step by step, and we will describe some properties of magnetic moments based on some elementary tools of classical and quantum physics. First of all, we will focus our attention on the question of how the magnetic moments of a solid behave when large number of them are considered in a solid when they are isolated from each other, as well as from their environment (i.e. from temperature or some other external effects). Next, we will discuss the possibility of magnetic interactions between magnetic moments, as well as their environment, and we will be able to investigate the occurrence of long range magnetic order in the system.

2.1   Magnetic Moments

The fundamental quantity of magnetism is the magnetic moment. According to the principles of electromagnetism, we can imagine a magnetic moment as a current loop. If one considers a current I circulating around an elementary (i.e. vanishingly small) oriented loop with area $|d\vec{S}|$ (see Fig. 2.1a) then the magnetic moment $d\vec{\mu}$ is defined by

$$d\vec{\mu} = Id\vec{S}, \qquad\qquad (2.1.1)$$

and the unit of magnetic moment is Am^2. The length of the vector $d\vec{S}$ is equal to the area of the loop. The direction of the vector is normal to the loop and it is determined by the direction of the current around the elementary loop.
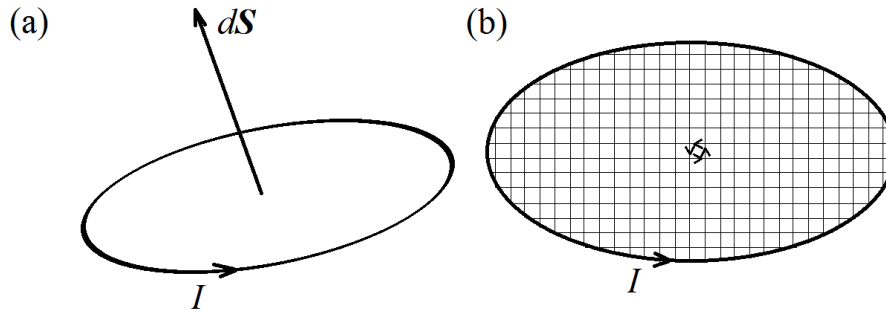
Figure 2.1 (a) An elementary representation of a magnetic moment. $d\mu = IdS$, due to an elementary current loop. (b) A magnetic moment $\mu = I \int dS$ (in perpendicular to the plane of the current loop) associated with a loop of current I can be considered by summing up the magnetic moments with large number of infinitesimal current loops, (Blundell, 2001).

This quantity can also be treated as identical to a magnetic dipole. Hence, we can imagine a magnetic dipole as an object which consists of two magnetic monopoles of opposite magnetic charge separated by a small distance in the same direction as the vector $d\vec{S}$.

The magnetic moment $d\vec{\mu}$ is pointed to the plane of the loop of current and it can align parallel or antiparallel to the angular momentum vector associated with the charge which orbits around the loop. For a loop with finite size, it is possible to calculate the magnetic moment $\vec{\mu}$ by summing up the magnetic moments of various infinitesimal current loops located through the area of the loop (see Fig. 2.1b). All the currents from neighboring infinitesimal loops cancel each other, and only a current running round the perimeter of the loop remains. Hence,

$$\vec{\mu} = \int d\vec{\mu} = I \int d\vec{S}. \tag{2.1.2}$$

2.2 Magnetic Moments and Angular Momentum

A current loop originates as a consequence of the motion of at least one electrical charged particle. These charged particles are also associated with a mass. Hence, there is also an orbital motion due to the mass, in addition to the motion due to the charge. Consequently, a magnetic moment is always connected with an angular momentum. In

atoms, the magnetic moment $\vec{\mu}$ associated with an orbiting electron is directed along the same direction with that of the angular momentum $\vec{L}$ of that electron. Thus, we can write

$$\vec{\mu} = \gamma \vec{L},\tag{2.2.1}$$

where γ is a constant known as the gyromagnetic ratio.

2.2.1 Precession

Now, let us see what happens if a magnetic moment $\vec{\mu}$ is placed in a homogenous magnetic field $\vec{B}$. If we apply a magnetic field on a loop of finite size (e.g. see Fig. 2.1a) then the magnetic moment $\vec{\mu}$ tends to align parallel with the external field due to the existence of torque

$$\vec{G} = \vec{\mu} \times \vec{B}.\tag{2.2.2}$$

On the other hand, the energy E of the magnetic moment is given by

$$E = -\vec{\mu}.\vec{B}.\tag{2.2.3}$$

We see from Eq. (2.2.3) that the energy becomes minimized if the magnetic moment aligns parallel with the magnetic field. However, if the magnetic moment were not associated with any angular momentum then the torque defined in Eq. (2.2.2) would just tend to turn the magnetic moment towards the magnetic field. If we take into account the second law of motion (i.e. Newton's second law), the torque acting on a rotating object can be written as

$$\vec{G} = \Theta \vec{\omega},\tag{2.2.4}$$

where Θ is the moment of inertia and $\vec{\omega}$ is the angular velocity of the moving object. From the definition of the angular momentum

$$\vec{L} = \Theta \vec{\omega},\tag{2.2.5}$$

and using Eqs. (2.1.2) and (2.2.1) we get

$$\frac{d\vec{\mu}}{dt} = \gamma \vec{\mu} \times \vec{B}.\tag{2.2.6}$$

From Eq. (2.2.6) we can conclude that the change in $\vec{\mu}$ is directed perpendicularly to $\vec{\mu}$ and $\vec{B}$. The magnetic field does not only turns $\vec{\mu}$ towards $\vec{B}$ but also it causes the alignment of $\vec{\mu}$ to precess around $\vec{B}$.

2.2.2   The Bohr Magneton

In order to estimate the size of the magnetic moment and the gyromagnetic ratio of an atom, let us consider an electron with charge $-e$ and mass m_e orbiting a circular trajectory around the nucleus of a hydrogen atom, as shown in Fig. 2.2. The current I around the atom is $I = -e/\tau$ where $\tau = 2\pi r/v$ is the orbital period, $v = |\vec{v}|$ is the speed and r is the radius of the circular orbit.
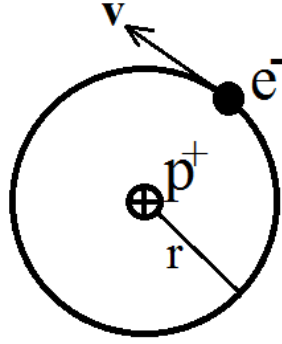
Figure 2.2 An electron in a hydrogen atom orbiting with velocity **v** around the nucleus which consists of a single proton, (Blundell, 2001).

The magnitude of the angular momentum of the electron is $m_e vr$ which must equal $\hbar$ in the ground state. Hence, the magnetic moment of the electron is

$$\mu = \pi r^2 I = -\frac{e\hbar}{2m_e} = -\mu_B, \tag{2.2.7}$$

where μ_B is the Bohr magneton given by

$$\mu_B = \frac{e\hbar}{2m_e}. \tag{2.2.8}$$

Eq. (2.2.8) represents the unit of the size of an atomic magnetic moment and it is numerically equal to the value $9.274 \times 10^{-24} Am^2$. At this point we should note that

the sign of the magnetic moment in Eq. (2.2.7) is negative. This is due to the fact that electron is a negatively charged particle, hence its magnetic moment lies antiparallel to its angular momentum. As a result, the gyromagnetic ratio for the electron is $\gamma = -e/2m_e$.

2.2.3 Magnetization and Field

In a typical magnetic solid, there exists a great number of atoms with magnetic moments. The number of magnetic moments per unit volume is defined as the magnetization $\vec{M}$ of the sample. The magnetization $\vec{M}$ is a smooth vector field which is continuous throughout the sample except at the edges of the magnetic solid. In free space (or vacuum) we can not observe any magnetization. In this case, we can represent the magnetic field by the vector fields $\vec{B}$ and $\vec{H}$, and there is a linear relation between them

$$\vec{B} = \mu_0 \vec{H}, \tag{2.2.9}$$

where $\mu_0 = 4\pi \times 10^{-7}\ Hm^{-1}$ is the permeability of free space. The two magnetic fields $\vec{B}$ and $\vec{H}$ are just scaled versions of each other. The former is measured in Tesla (abbreviated to T) and the latter is measured in Am^{-1}.

However, the relation between $\vec{B}$ and $\vec{H}$ in a medium may become somewhat complicated and these vector fields may differ in both magnitude and direction. The general relation is given as

$$\vec{B} = \mu_0(\vec{H} + \vec{M}). \tag{2.2.10}$$

In a special case where the magnetization $\vec{M}$ linearly depends on the magnetic field $\vec{H}$, the solid is a linear material, and we can write

$$\vec{M} = \chi \vec{H}, \tag{2.2.11}$$

where χ is a dimensionless parameter called the magnetic susceptibility. In this special case there is still a linear relationship between $\vec{B}$ and $\vec{H}$, namely

$$\vec{B} = \mu_0(1 + \chi)\vec{H} = \mu_0 \mu_r \vec{H}, \tag{2.2.12}$$

where $\mu_r = 1 + \chi$ is the relative permeability of the material.

2.3 Classical Mechanics and Magnetic Moments

In this section, we formulate the momentum and kinetic energy expressions of a charged particle in the presence of a magnetic field, and we treat the system within the framework of classical mechanics. In the following two subsections, we deal with a single particle, and then we benefit from this result to evaluate the magnetization of a system of charged particles.

2.3.1 Canonical momentum

According to classical mechanics, if a charged particle with a charge q moves in an electrical field $\vec{E}$ and magnetic field $\vec{B}$ with a velocity $\vec{v}$ then the force acting on the particle is given by Lorentz force

$$\vec{F} = q(\vec{E} + \vec{v} \times \vec{B}). \tag{2.3.1}$$

Using $\vec{F} = md\vec{v}/dt$, $\vec{B} = \vec{\nabla} \times \vec{A}$, and $E = -\vec{\nabla}V - \partial \vec{A}/\partial t$ where V is the electric potential, $\vec{A}$ is the magnetic vector potential and m is the mass of the particle, Eq. (2.3.1) can be written as

$$m\frac{d\vec{v}}{dt} = -q\vec{\nabla}V - q\frac{\partial \vec{A}}{\partial t} + q\vec{v} \times (\vec{\nabla} \times \vec{A}). \tag{2.3.2}$$

If we apply the vector identity $\vec{v} \times (\vec{\nabla} \times \vec{A})$ in Eq. (2.3.2) then we get

$$m\frac{d\vec{v}}{dt} + q\left[\frac{\partial \vec{A}}{\partial t} + (\vec{v}.\nabla)\vec{A}\right] = -q\vec{\nabla}(V - \vec{v}.\vec{A}). \tag{2.3.3}$$

Since

$$\frac{d\vec{A}}{dt} = \frac{\partial \vec{A}}{\partial t} + (\vec{v}.\vec{\nabla})\vec{A}, \tag{2.3.4}$$

which measures the rate of change of $\vec{A}$ at the location of the moving particle, we obtain

$$\frac{d}{dt}(m\vec{v} + q\vec{A}) = -q\vec{\nabla}(V - \vec{v}.\vec{A}). \tag{2.3.5}$$

Eq. (2.3.3) can be regarded as the form of Newton's second law in the presence of an external magnetic field. In this case, the momentum of the particle is defined as canonical momentum

$$\vec{p} = m\vec{v} + q\vec{A}, \tag{2.3.6}$$

with a velocity dependent effective potential $q(V - \vec{v}.\vec{A})$ experienced by the charged particle. Kinetic energy of the system is also $K = \frac{1}{2}mv^2$, and in terms of canonical momentum it is given by $(\vec{p} - q\vec{A})^2/2m$.

2.3.2 The Bohr-van Leeuwen theorem

Now, we are able to calculate the average magnetic moment (i.e. magnetization induced by the magnetic field) for a system of electrons in a solid. By keeping in mind the Lorentz force given by Eq. (2.3.1), it is clear that the work done by the magnetic force acting on the charged particles is zero according to

$$W = \vec{F}.\vec{ds} = q(\vec{v} \times \vec{B})\vec{ds} = 0, \quad (\vec{v} \times \vec{B}) \perp \vec{ds}. \tag{2.3.7}$$

From Eq. (2.3.7), total energy of the system is independent of magnetic field since there is no work due to the magnetic force acting on the charged particle. Therefore, we expect the system to have zero magnetization.

According to Bohr-van Leeuwen theorem, the partition function of a system composed of N particles, each of them having charge q_i is given by

$$Z \propto \int \int ... \int \exp(-\beta E\vec{r}_i, \vec{p}_i)\vec{dr}_1\vec{dr}_2...\vec{dr}_N\vec{dp}_1\vec{dp}_2...\vec{dp}_N, \quad i = 1,...,N. \tag{2.3.8}$$

Eq. (2.3.8) is a $6N$ dimensional integral. In the presence of magnetic field $(\vec{A} \neq 0)$ momentum of each particle is $(\vec{p}_i - q\vec{A})$. For instance, Eq. (2.3.8) reads for a single particle

$$\int_{-\infty}^{\infty} \exp(-\beta(p - qA)^2/2m)dp = 2m \int_{-\infty}^{\infty} \exp(-\beta x^2/2m)dx, \tag{2.3.9}$$

which is independent of magnetic field. Since the partition function (2.3.9) is independent of magnetic field then we have

$$M = -\left(\frac{\partial F}{\partial B}\right)_{T,V} = 0. \tag{2.3.10}$$

However, real magnetic materials do have a net magnetization. Thus we can conclude that classical mechanical treatment of magnetism fails to explain magnetism phenomena in real magnetic systems.

2.4 Quantum Mechanics of Spin

The angular momentum discussed in the preceding sections is associated with the orbital motion of electron around the nucleus. Therefore it is called orbital angular momentum. The $z-$ component of magnetic dipole moment is

$$\mu_z = \gamma L_z = -\frac{e}{2m}m_l\hbar, \qquad (2.4.1)$$

whereas the magnitude of the total magnetic dipole moment is $\sqrt{l(l+1)}\mu_B$.

In addition to orbital angular momentum, an electron has an intrinsic magnetic moment which is associated with an intrinsic angular momentum. This intrinsic angular momentum is called "spin" which is characterized by a spin quantum number s, and it takes the value $1/2$ for electron. The spin angular momentum is associated with a magnetic moment which have a component $-g\mu_B m_s$ on a given axis, and a magnitude equal to $\sqrt{s(s+1)}g\mu_B$. Here, g is a constant known as $g-$ factor which has a value approximately 2. Therefore, the energy for an electron in the presence of magnetic field is given by

$$E = g\mu_B m_s B. \qquad (2.4.2)$$

In general, magnetic moment vector corresponding to spin angular momentum is then given by

$$\vec{\mu} = g_S\gamma\vec{S}, \quad g_S \approx 2. \qquad (2.4.3)$$

2.4.1 Spin-Spin Interaction of Two Spin-1/2 Particles

Now consider two spin-1/2 particles in a magnetic solid such as two electrons of neighboring atoms with one electron in each with spin operators $\vec{S}_a$ and $\vec{S}_b$ interacting with each other via spin-spin interaction

$$\mathcal{H} = \vec{S}_a.\vec{S}_b. \qquad (2.4.4)$$

The total spin angular momentum operator of the system is defined as

$$\vec{S}_{tot} = \vec{S}_a + \vec{S}_b. \qquad (2.4.5)$$

From Eq. (2.4.5), we get

$$(\vec{S}_{tot})^2 = (\vec{S}_a)^2 + (\vec{S}_b)^2 + 2\vec{S}_a.\vec{S}_b. \tag{2.4.6}$$

Our aim is to find the eigenvalues of the Hamiltonian operator given in Eq. (2.4.4). Hence we rearrange Eq. (2.4.6) as

$$\vec{S}_a.\vec{S}_b = \frac{1}{2}\left[(\vec{S}_{tot})^2 - (\vec{S}_a)^2 - (\vec{S}_b)^2\right]. \tag{2.4.7}$$

Eigenvalue of an operator $(\vec{S}_i)^2$ can be determined from

$$(\vec{S}_i)^2\psi_i = \left[(\vec{S}_i^x)^2 + (\vec{S}_i^y)^2 + (\vec{S}_i^z)^2\right], \quad i = a \text{ or } b. \tag{2.4.8}$$

Since the eigenvalues of operators $(\vec{S}_i^x)^2$, $(\vec{S}_i^y)^2$, $(\vec{S}_i^z)^2$ are always $\frac{1}{4} = (\pm 1/2)^2$, we have

$$(\vec{S}_i)^2\psi_i = \frac{3}{4}\psi_i. \tag{2.4.9}$$

On the other hand, for the joint system we have

$$(\vec{S}_{tot})^2\psi = s(s+1)\psi, \tag{2.4.10}$$

where s it the total spin angular momentum quantum number which can be either 0 or 1. Accordingly, using Eqs. (2.4.9) and (2.4.10) we obtain the result

$$\begin{aligned}
\vec{S}_a.\vec{S}_b\psi &= \frac{1}{2}\left[s(s+1) - \frac{3}{2}\right]\psi, \\
&= \begin{cases} -\frac{3}{4}, & s = 0 \quad \text{(singlet)} \\ \frac{1}{4}, & s = 1 \quad \text{(triplet)} \end{cases}
\end{aligned} \tag{2.4.11}$$

Each state has a degeneracy of $2s+1$. Therefore, $s = 0$ state is a singlet whereas the state with $s = 1$ is a triplet.

In a singlet state, the spin vectors of two electrons align antiparallel with each other. Hence, the spin wave function is antisymmetric:

$$\chi_1 = \alpha(s_a)\beta(s_b) - \alpha(s_b)\beta(s_a). \tag{2.4.12}$$

The triplet state is three-fold degenerate. The possible symmetric forms of the total spin wave function are:

$$\begin{aligned}
\chi_2 &= \alpha(s_a)\alpha(s_b), \\
\chi_3 &= \alpha(s_a)\beta(s_b) + \alpha(s_b)\beta(s_a), \\
\chi_4 &= \beta(s_a)\beta(s_b).
\end{aligned} \tag{2.4.13}$$

In Eqs. (2.4.12) and (2.4.13), α and β represent spin-↑ and spin-↓ states of two electrons, respectively.

2.5   Exchange Interaction

At this stage, we are in a position of considering the situation where the magnetic moments are interacting with each other, as well as their environment (i.e. temperature and magnetic field). The magnetic phenomena observed in systems where the individual magnetic moments do not interact with each other completely differs in the presence of interacting magnetic dipole moments leading to a behavior called "*cooperative phenomena*". The long range order observed in real magnetic systems mainly originates from some kind of communication between magnetic dipole moments of material. This electrostatic interaction is called "*exchange interaction*", and it is completely a quantum mechanical phenomenon. Although there are several other interactions such as magnetic dipolar interactions in real materials, the most dominant factor is the exchange interaction. In order to discover the origin of exchange interaction, we should introduce the concept of the symmetry properties of identical particles.

Let us consider two electrons with spatial coordinates $\vec{r}_1$ and $\vec{r}_2$. If one of the electrons is in a state $\psi_a(\vec{r}_1)$ whereas the other is in $\psi_b(\vec{r}_2)$ then the total spatial wave function can be written as

$$\psi(\vec{r}_1, \vec{r}_2) = \psi_a(\vec{r}_1).\psi_b(\vec{r}_2). \tag{2.5.1}$$

When we swap the electrons, the system should remain unchanged. In other words, the probability distribution must be conserved

$$|\psi(\vec{r}_1, \vec{r}_2)|^2 = |\psi(\vec{r}_2, \vec{r}_1)|^2. \tag{2.5.2}$$

As a consequence of Eq. (2.5.2), the spatial wave function has the following property

$$\psi(\vec{r}_1, \vec{r}_2) = +\psi(\vec{r}_2, \vec{r}_1) \quad \text{(symmetric)},$$
$$\psi(\vec{r}_1, \vec{r}_2) = -\psi(\vec{r}_2, \vec{r}_1) \quad \text{(antisymmetric)}. \tag{2.5.3}$$

Since the electron is a fermion, the overall wave function including the spatial and spin parts of the two electron system must be antisymmetric. Recall from preceding section that the singlet spin state has an antisymmetric spin wave function whereas the triplet state has three symmetric spin wave functions. Accordingly, the overall wave functions of singlet and triplet states are given by the following equations

$$\Psi_S = \frac{1}{\sqrt{2}} \left[\psi_a(\vec{r}_1)\psi_b(\vec{r}_2) + \psi_a(\vec{r}_2)\psi_b(\vec{r}_1) \right] \chi_S, \qquad (2.5.4)$$

$$\Psi_T = \frac{1}{\sqrt{2}} \left[\psi_a(\vec{r}_1)\psi_b(\vec{r}_2) - \psi_a(\vec{r}_2)\psi_b(\vec{r}_1) \right] \chi_T, \qquad (2.5.5)$$

where the spin wave functions χ_S and χ_T are given by Eqs. (2.4.12) and (2.4.13), respectively. Energy eigenvalues corresponding to Eqs. (2.5.4) and (2.5.5) can be calculated from

$$
\begin{aligned}
E_S &= \int \Psi_S^* \mathcal{H} \Psi_S \, d\vec{r}_1 \vec{r}_2, \\
E_T &= \int \Psi_T^* \mathcal{H} \Psi_T \, d\vec{r}_1 \vec{r}_2.
\end{aligned}
\qquad (2.5.6)
$$

By assuming that the spin wave functions are normalized (i.e., $\chi_S^* \chi_S = 1$ and $\chi_T^* \chi_T = 1$) we can calculate the energy difference between singlet and triplet states which is given as follows

$$E_S - E_T = 2 \int \psi_a^*(\vec{r}_1)\psi_b^*(\vec{r}_2) \mathcal{H} \psi_a(\vec{r}_2)\psi_b(\vec{r}_1) d\vec{r}_1 d\vec{r}_2. \qquad (2.5.7)$$

Now, let us generalize Eq. (2.4.4) as

$$\mathcal{H} = A + B\vec{S}_a.\vec{S}_b, \qquad (2.5.8)$$

where the terms A and B are the constants to be determined. According to Eq. (2.4.11), singlet and triplet energies corresponding to Eq. (2.5.8) are

$$
\begin{aligned}
E_S &= A - \frac{3B}{4}, \\
E_T &= A + \frac{B}{4},
\end{aligned}
\qquad (2.5.9)
$$

which yields

$$A = \frac{E_S + 3E_T}{4}, \quad B = -(E_S - E_T), \qquad (2.5.10)$$

from which we can define an effective spin Hamiltonian as follows

$$\mathcal{H} = \frac{1}{4}(E_S + 3E_T) - (E_S - E_T)\vec{S}_a.\vec{S}_b. \qquad (2.5.11)$$

Consequently, it follows from Eqs. (2.5.7) and (2.5.11) that the exchange integral J of the system is defined as

$$J = \frac{E_S - E_T}{2} = \int \psi_a^*(\vec{r}_1)\psi_b^*(\vec{r}_2)\mathcal{H}\psi_a(\vec{r}_2)\psi_b(\vec{r}_1)d\vec{r}_1 d\vec{r}_2. \qquad (2.5.12)$$

Therefore we obtain a spin Hamiltonian which can be written as

$$\mathcal{H}^{spin} = -2J\vec{S}_a.\vec{S}_b. \qquad (2.5.13)$$

Eq. (2.5.13) is responsible for the occurrence of magnetism. According to this compact equation, if $J > 0$ then in order to minimize the energy eigenvalue of Eq. (2.5.13), the triplet state with an energy $1/4$ is favored whereas if $J < 0$ then Eq. (2.5.13) becomes minimized if the singlet state with energy $E_s = -3/4$ is preferred. Value of J depends on the material in question and evaluation of it can be possible using certain numerical methods such as density functional theory (DFT), as well as experimental techniques. Moreover, based on Eq. (2.5.13), we can define different types of magnetic order. Namely, $J > 0$ case represents a ferromagnetic order where the spins are aligned parallel with each other, and for $J < 0$ we have an antiferromagnetic order where the spins tend to align antiparallel. Throughout the present report, we will particularly focus our attention on the models characterizing the manifestation of ferromagnetism.

We also note that the result given in Eq. (2.5.13) has been derived for a system of two identical particles. However, it can be generalized to all neighboring atoms in a magnetic solid, and this is known as the Heisenberg model (Heisenberg, 1928):

$$\mathcal{H} = -\sum_{<ij>} J_{ij}\vec{S}_i.\vec{S}_j, \qquad (2.5.14)$$

where the factor 2 is omitted for avoiding the double counting of each pair of spins in the sum. From the experimental point of view, the term $\vec{S}_i$ in Eq. (2.5.14) can be the spin of a single electron localized on a particular atom in a crystal or the combined spin of several d electrons in a transition-metal ion, or the combined spin and orbital moment of a rare-earth ion. However, in a theoretical manner, the magnetic properties of the system do not exhibit variations as long as the Hamiltonian has the same form, hence the origin of the spins is not an important factor. As we shall see in the following parts of this work, the model characterized by Eq. (2.5.14) and its various variants will play a vital role in the foundation of this thesis report.

2.6 Heisenberg and Ising Models

It is possible to determine the magnetic properties of a solid material with the help of microscopic spin Hamiltonian defined in Eq. (2.5.14). If we consider only the nearest neighbor interactions between localized spins with a constant interaction parameter J then we obtain from Eq. (2.5.14)

$$\mathcal{H} = -J \sum_{<ij>} \vec{S}_i.\vec{S}_j, \tag{2.6.1}$$

where J is the exchange interaction constant, and $<ij>$ denotes that the sum is taken over only the nearest neighbors. The spins $\vec{S}_i$ in Eq. (2.6.1) are considered as three dimensional unit vectors in three dimensional space. Hence, it is important to notice that we should distinguish between dimensionality D of spin vector $\vec{S}_i$ and dimensionality d of lattice. For $D = 1, 2,$ and 3, we have Ising, XY, and Heisenberg Hamiltonian, respectively. The situation can also be understood by considering anisotropic counterpart of Eq. (2.6.1),

$$\mathcal{H} = -J_x \sum_{<ij>} S_i^x S_j^x - J_y \sum_{<ij>} S_i^y S_j^y - J_z \sum_{<ij>} S_i^z S_j^z, \tag{2.6.2}$$

with

$$|\vec{S}_i| = \left[(S_i^x)^2 + (S_i^y)^2 + (S_i^z)^2 \right]^{1/2} = 1. \tag{2.6.3}$$

For $J_z = 0$ in Eq. (2.6.2), we get XY model whereas for $J_x = J_y = 0$, the model reduces to Ising model (Ising, 1925).

The most fundamental theoretical difference between Heisenberg, XY and Ising models it that spin operators do not commute with each other in the two former models. Therefore, Ising model is considered as a classical spin model whereas the former two have quantum mechanical origin in some sense. On the other hand, the restriction of the Ising model is that only the $z-$ component of spin operator is taken into account which means that magnetic moments can only align parallel or antiparallel with each other and external magnetic field. Therefore the model is useful in describing a magnet which is highly anisotropic in spin space such as Manganese(II) fluoride (MnF_2). On the other hand, Heisenberg model is capable of describing the magnetic properties

of some magnetic insulators, such as Europium (II) sulfide (EuS). The XY and Heisenberg models have a conventional phase transition at finite temperatures for $d > 2$ whereas we can observe a second order phase transition at a certain finite temperature for $d \geq 2$ in Ising model (Yeomans, 2000).

CHAPTER THREE
EXACT AND APPROXIMATE METHODS

In this chapter, we will discuss the ideas of some certain exact and approximate techniques to treat a spin Hamiltonian. Particular emphasis will be devoted to Ising model and its various generalizations. For this purpose, we will introduce the transfer matrix method as an exact calculation technique. Not so surprisingly, the exact calculations are restricted to a few number of examples, including the linear chain Ising model in the presence of magnetic field, and the two dimensional counterpart of the model in the absence of external magnetic field. Particularly, we have no exact solution of three dimensional Ising model. Hence, it is very convenient to handle more sophisticated models such as spin-S ($S \geq 1$) Ising and Heisenberg models or the systems with next-nearest neighbor interactions, ferrimagnetic systems, nanoparticles etc. by attempting to make reasonable approximations. Series expansion method and Monte Carlo (MC) simulations are among the foremost approximations in theoretical literature. Nevertheless, even those powerful numerical approaches have some deficiencies. For instance, in MC simulations one needs fairly large amount of computer facilities due to the long calculation times originating from the exhausting sampling averaging procedures. On the other hand, the results of series expansions agree well with high accuracy MC simulations, and with exact results for soluble models where these are available (Yeomans, 2000). However, as the order of the expansion is increased then the number and complexity of contributing terms also increases rapidly, hence the method becomes an unfit technique as the complexity of the model increases.

Nonetheless, increasing complexity in problems means that we should make more approximations. In most of the cases, it is possible to overcome the obstacles by considering simple methods. One of the most widely used of these is mean field theory (MFT). However, as it will be shown soon, MFT ignores fluctuations. Namely, each spin is assumed to interact only with the mean field of all the other spins in the system. As a consequence, the results of mean field theory can only be valid when fluctuations

are unimportant. However, it can be used as a starting point for more sophisticated calculations (Yeomans, 2000). On the other hand, despite its mathematical simplicity, effective field theory (EFT) is considered to be quite superior to conventional MFT since the former method exactly takes into account the single-site correlations and neglects the multi-site correlations whereas the latter technique ignores the whole correlations in the calculations. Therefore the results obtained by EFT are expected to be both qualitatively and quantitatively more precise than those obtained by MFT. Here, the crucial point is the consideration of multi-site correlations and it plays a vital role on the qualitative and quantitative features of the model under consideration. The main purpose of this thesis report is to introduce an EFT approximation in a heuristic manner which systematically takes into account the thermal fluctuations, i.e. multi-site as well as the single site correlations which appear when expanding the spin identities. Details of the calculation method and its applications on selected model systems will be the subject of the next two chapters.

3.1   The Transfer Matrix Method

The simplest way of understanding how this technique can be applied on a classical spin model is to consider a model characterized by a one dimensional Ising spin chain. The Hamiltonian of the system is given by

$$\mathcal{H} = -J \sum_{i=0}^{N-1} s_i s_{i+1} - H \sum_{i=0}^{N-1} s_i, \tag{3.1.1}$$

where s_i is the $z-$ component of spin angular momentum which can take values $s_i = \pm 1$. We consider periodic boundary conditions which can be identified by $s_N = s_0$.

The first step is to calculate the partition function of the system,

$$Z = \sum_{\{s\}} \exp\left[-\beta \left(-J \sum_{i=0}^{N-1} s_i s_{i+1} - H \sum_{i=0}^{N-1} s_i \right) \right]. \tag{3.1.2}$$

After a straightforward calculation process we get

$$
\begin{aligned}
Z &= \sum_{\{s\}} \exp\left[\beta J(s_0 s_1 + s_1 s_2 + s_2 s_3 + ...)\right] \exp\left[\beta H(s_0 + s_1 + s_2 + ...)\right], \\
&= \sum_{\{s\}} e^{\beta(J s_0 s_1) + \beta H(s_0 + s_1)/2} e^{\beta(J s_1 s_2) + \beta H(s_1 + s_2)/2} ... \\
&\quad ...e^{\beta(J s_{N-1} s_N) + \beta H(s_{N-1} + s_N)/2}, \\
&= \sum_{\{s\}} \langle s_0|T|s_1\rangle\langle s_1|T|s_2\rangle...\langle s_{N-1}|T|s_0\rangle = \sum_{\{s\}} T_{0,1} T_{1,2}...T_{N-1,0}, \qquad (3.1.3)
\end{aligned}
$$

where

$$
T_{i,i+1} = e^{\beta J s_i s_{i+1} + \beta H(s_i + s_{i+1})/2}. \qquad (3.1.4)
$$

are the elements of a matrix T with rows labeled by the values of s_i and columns by the values of s_{i+1}. Hence, the explicit form of the matrix T is given by

$$
\begin{array}{cc}
s_i = +1 \\
s_i = -1
\end{array}
\left(
\begin{array}{cc}
e^{\beta(J+H)} & e^{-\beta J} \\
e^{-\beta J} & e^{\beta(J-H)}
\end{array}
\right)
\qquad (3.1.5)
$$

$$
\underbrace{\qquad\qquad}_{S_{i+1=1}} \quad \underbrace{\qquad\qquad}_{S_{i+1=-1}}
$$

The transfer matrix T can be obtained by matrix product of $T_{i,i+1}$ which is given by Eq. (3.1.5). Hence we get the following equation for the partition function

$$
Z_N = \sum_{s_0 = \pm 1} (T^N)_{0,0}. \qquad (3.1.6)
$$

In order to proceed further, we must diagonalize Eq. (3.1.6) by calculating the trace of the matrix T as follows

$$
Z_N = \sum_i \lambda_i^N, \qquad (3.1.7)
$$

where λ_i is the ith eigenvalue of matrix T. Here, the size of the transfer matrix depends on the number of spin states and on the range of the interactions.

Now let us investigate the free energy of the system. For a transfer matrix T with size n, the possible eigenvalues in decreasing order can be sorted as $\lambda_0, \lambda_1, \lambda_2,...,\lambda_n$. In the thermodynamic limit we can write free energy of the system in the form

$$
f = -k_B T \lim_{N \to \infty} \frac{1}{N} \ln Z_N. \qquad (3.1.8)
$$

Therefore, with the help of Eq. (3.1.7) we have

$$
\begin{aligned}
f &= -k_B T \lim_{N \to \infty} \frac{1}{N} \ln \left[(\lambda_i)^N \right] = -k_B T \lim_{N \to \infty} \frac{1}{N} \ln \left(\lambda_0^N + \sum_{i=1}^{n-1} \lambda_i^N \right), \\
&= -k_B T \lim_{N \to \infty} \frac{1}{N} \ln \left[\lambda_0^N \left(1 + \sum_{i=1}^{n-1} \frac{\lambda_i^N}{\lambda_0^N} \right) \right].
\end{aligned}
\tag{3.1.9}
$$

Since $\lambda_0 \gg \lambda_i$ $(i = 1, n-1)$, it is clear that $(\lambda_i / \lambda_0)^N \to 0$, and accordingly Eq. (3.1.9) reduces to

$$
f = -k_B T \ln \lambda_0.
\tag{3.1.10}
$$

Eigenvalue λ_0 in Eq. (3.1.10) just corresponds to the highest eigenvalue of determinant

$$
\begin{vmatrix}
e^{\beta(J+H)} - \lambda & e^{-\beta J} \\
e^{-\beta J} & e^{\beta(J-H)} - \lambda
\end{vmatrix} = 0.
\tag{3.1.11}
$$

After some manipulations, we obtain the eigenvalues calculated from Eq. (3.1.11) as follows

$$
\lambda_\pm = e^{\beta J} \cosh(\beta H) \pm \sqrt{e^{2\beta J} \sinh^2(\beta H) + e^{-2\beta J}}, \quad \lambda_0 = \lambda_+.
\tag{3.1.12}
$$

By inserting Eq. (3.1.12) in Eq. (3.1.10) we finally obtain the free energy expression of one dimensional Ising model (Ising, 1925) as follows

$$
f = -k_B T \ln \left[e^{\beta J} \cosh(\beta H) + \sqrt{e^{2\beta J} \sinh^2(\beta H) + e^{-2\beta J}} \right].
\tag{3.1.13}
$$

In the limit $T \to 0$ we have $e^{-2\beta J} \to 0$, and Eq. (3.1.13) reduces to

$$
f = -J - H.
\tag{3.1.14}
$$

This is an expected result. At the ground state of the system entropy reduces to zero and the free energy is equal to the average internal energy per spin.

It is also possible to obtain the magnetization of Ising chain from Eq. (3.1.13),

$$
m = -\left(\frac{\partial f}{\partial H} \right)_T = \frac{e^{\beta J} \sinh(\beta H)}{\left[e^{2\beta J} \sinh^2(\beta H) + e^{-2\beta J} \right]^{1/2}}.
\tag{3.1.15}
$$

We see from Eq. (3.1.15) that in the absence of magnetic field ($H = 0$), magnetization vanishes. This means that the system can not exhibit a long range magnetic order

at any temperature. On the other hand, for $J = 0$ or $T \to \infty$ we get $m = \tanh(\beta H)$, and it corresponds to paramagnetic phase. This problem was solved by Ernst Ising himself (Ising, 1925). In two dimensions, the problem becomes mathematically harder to solve and analytical calculations in two dimensions were originally completed by Lars Onsager (Onsager, 1944), and the calculation details can be found in (Huang, 1987). Based on these exact calculations, lower critical dimension of Ising model at which the system can not exhibit a long range ferromagnetic order is found to be $d_c = 1$.

3.2 Series Expansion Method

As we have stated before, exact power series expansion of free energy is one of the most remarkable techniques for treating the spin Hamiltonians. This approach was introduced by (Domb, 1949). It has led to remarkably precise estimates of the critical properties for both two- and three-dimensional Ising models and has also been applied successfully to the Heisenberg and other model systems (Fisher, 1967). In this approach, $T > T_c$ behavior (i.e. paramagnetic properties) of the model are considered by a method called "high temperature series expansion method" whereas $T < T_c$ region of the temperature spectrum (i.e. ferromagnetic spectrum) is treated by "low temperature series expansion" of free energy. These two approaches will be analyzed in the following two subsections (Yeomans, 2000).

3.2.1 High Temperature Series Expansions

Let us apply the method for a two dimensional zero field Ising model on a square lattice defined by the Hamiltonian

$$\mathcal{H} = -J \sum_{<ij>} s_i s_j. \tag{3.2.1}$$

For Ising model we have $s_i s_j = \pm 1$, therefore we may write

$$e^{\beta J s_i s_j} = \cosh(\beta J) + s_i s_j \sinh(\beta J) = \cosh(\beta J)[1 + s_i s_j v], \tag{3.2.2}$$

where $v = \tanh(\beta J)$ is the expansion parameter which will be used for the limit $v \to 0$ as $T \to \infty$ as required. The partition function of the system is defined by

$$
\begin{aligned}
Z &= \sum_{\{s_i\}} e^{\beta J \sum_{<ij>} s_i s_j} = \sum_{\{s_i\}} \prod_{<ij>} e^{\beta J s_i s_j} = \sum_{\{s_i\}} \prod_{<ij>} \cosh(\beta J)(1 + s_i s_j v), \\
&= \cosh(\beta J)^{N_b} \sum_{\{s_i\}} \prod_{<ij>} (1 + s_i s_j v), \\
&= \cosh(\beta J)^{N_b} \sum_{\{s_i\}} \left(1 + v \sum_{<ij>} s_i s_j + v^2 \sum_{<ij>,<kl>} s_i s_j s_k s_l + ... \right).
\end{aligned}
\tag{3.2.3}
$$

Our aim is to count the number of contributions to Z which are of order v^n up to as large values of n as possible. One should notice that the terms in Eq. (3.2.3) correspond to the graphs plotted on a square lattice. Each product of pair of spins $s_i s_j$ can be associated with a bond which connects the lattice sites i and j. Each term of order v can be represented by a single bond. The terms of order v^2 correspond to two bonds which may or may not touch, and so on. Therefore each term of order v^n is in one-to-one correspondence with a graph with n edges on a square lattice (see Fig. 3.1).

Now assume that the number of occupied bonds originating from site i is denoted by p_i. For each lattice site i, we can define a parameter $s_i^{p_i}$ where $s_i = \pm 1$. Hence, summing over two possible values of s_i, we get two values for $s_i^{p_i}$ which can be either 0 if p_i is odd, or 2 if p_i is even. Thus, the only graphs that survive the sum in Eq. (3.2.3) have an even number of lines passing through each site. Consequently, for N spins we get

$$
\begin{aligned}
\sum_{s_i} (s_i^{p_i} s_j^{p_j} s_k^{p_k} ...) &= 2^N \quad \text{(all } p_i \text{ even)}, \\
&= 0 \quad \text{(otherwise)}.
\end{aligned}
\tag{3.2.4}
$$

Hence, only products in which every spin operator appears an even number of times contribute. Graphically, these terms correspond to closed loops; no free ends are allowed, and each contributes the same weight, 2^N, (Yeomans, 2000).

So finding the contribution to the partition function of order n is reduced to the problem of counting the number of closed loops of n bonds that can be put on the

Figure 3.1 Graphs on the square lattice, each of which corresponds to a product of spins in the sum in Eq. (3.2.3): (a) $s_l s_m$, (b) $s_l s_m s_j s_k$, (c) $s_i s_l^2 s_m$, (d) $s_i^2 s_j^2 s_l^2 s_m^2$, (e) $s_i^2 s_j^3 s_k^2 s_l^3 s_m^3 s_n^2 s_o$, (f) $s_i^2 s_j^2 s_l^2 s_m^4 s_n^2 s_p^2 s_q^2$. Only (d) and (f), where the number of bonds at each vertex is even, give a nonzero contribution to the partition function, (Yeomans, 2000).
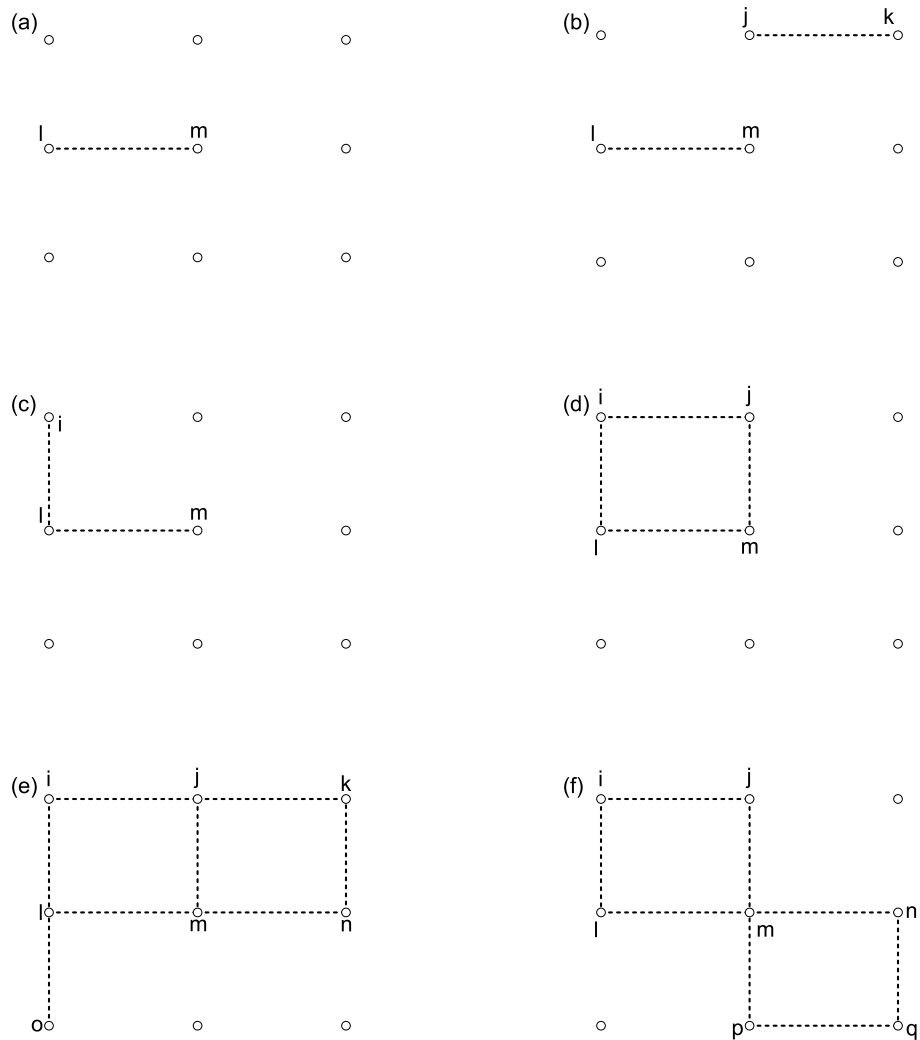
square lattice. Every position and orientation of the loops gives a contribution to the partition function. The closed loop with $n = 4$ edges (or bonds) just corresponds to a square. In our two dimensional problem, the square may be located with a specified (say, lower-left-hand) corner at any lattice site, therefore its contribution is given as N. Another closed loop with $n = 6$ is a 2×1 rectangle (e.g. see Fig. 3.2(a)) which can be located at any of the N lattice sites and oriented in two possible ways, hence its contribution is $2N$. For $n = 8$, the closed loops do not need to be connected. A disconnected loop, however, must consist of two disjoint squares. For instance, the first square can be placed with its lower-left-hand corner at any of the N lattice sites, while the same corner of the "second square" need only avoid nine lattice sites (see Fig. 3.2(b)). Thus, there are $N(N-9)/2$ disconnected even loops with $n = 8$ edges. We should also divide by 2 to eliminate the distinction between the "first" and "second" squares. The connected paths of length 8 are shown in Fig. 3.2(c). We see from this figure that there are four different types with a total of 9 orientations, giving, in all, $9N$ connected loops with 8 edges (Cipra, 1987). Therefore we have

$$N(N-9)/2 + 9N = N(N+9)/2.$$

The terms up to v^{10} are given in (Yeomans, 2000). Accordingly, we have the partition function as follows

$$Z = [\cosh(\beta J)]^{N_b} 2^N \left(1 + Nv^4 + 2Nv^6 + \frac{1}{2}N(N+9)v^8 + 2N(N+6)v^{10} + O(v^{12}) \right).$$
$$(3.2.5)$$

For a square lattice we have $N_b = 2N$, therefore by taking the logarithm of Eq. (3.2.5) we can obtain an expression for the free energy of the system

$$\begin{aligned} \ln Z &= \ln \left[2\cosh^2(\beta J) \right]^N + \ln \left[1 + Nv^4 + 2Nv^6 + \frac{N(N+9)}{2}v^8 + 2N(N+6)v^{10} \right], \\ &= N\ln 2 + 2N\ln\cosh(\beta J) + \ln(1+x), \end{aligned} \qquad (3.2.6)$$

where

$$x = Nv^4 + 2Nv^6 + \frac{N(N+9)}{2}v^8 + 2N(N+6)v^{10}. \qquad (3.2.7)$$

On the other hand, for $T \to \infty$ we have

$$\ln\left[\cosh(\beta J)\right] = \ln\left(1 + \frac{(\beta J)^2}{2!} + \frac{(\beta J)^4}{4!} + \ldots \right) \approx \ln 1 = 0. \qquad (3.2.8)$$
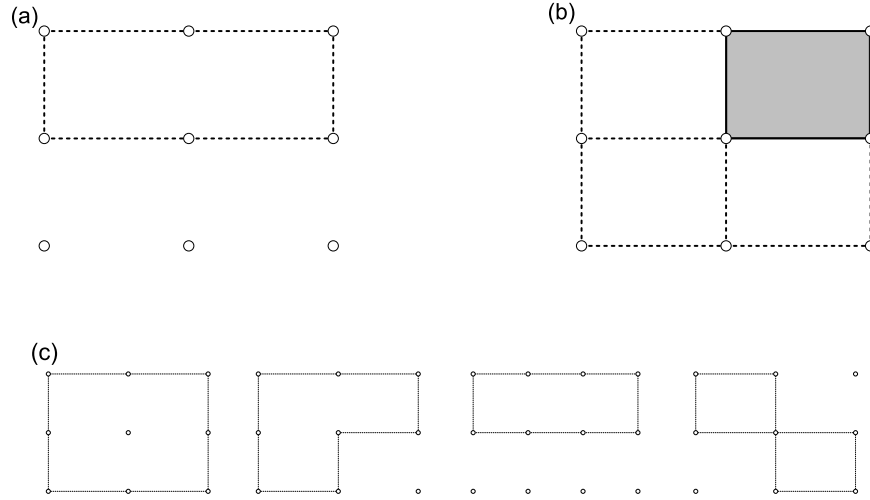
Figure 3.2 (a), (b): Examples of several bond configurations of graphs contributing to the partition function given in Eq. (3.2.5) with $n = 6, 8$. (c) Possible orientations of graphs with $n = 8$ edges, (Cipra, 1987).

Similarly, it is also possible to expand the third term in Eq. (3.2.6) for small v as follows

$$\ln(1+x) = x - \frac{x^2}{2} + \frac{x^3}{3} + O(x^4) \approx x - \frac{x^2}{2}. \tag{3.2.9}$$

By substituting Eq. (3.2.9) in Eq. (3.2.6) and taking the terms up to v^{10}, the terms proportional to N^2 drop out and we obtain

$$F = -k_B T \ln Z = -N k_B T \left[\ln 2 + v^4 + 2v^6 + \frac{9}{2}v^8 + 12v^{10} \right]. \tag{3.2.10}$$

Other thermodynamic quantities such as internal energy per spin, and specific heat at constant magnetic field can be extracted from $\ln Z$ as follows

$$U/N = -\frac{\partial \ln Z}{\partial \beta} = -J\text{sech}^2(\beta J)(4v^3 + 12v^5 + 36v^7 + 120v^9),$$
$$C = \frac{dU}{dT}. \tag{3.2.11}$$

3.2.2 Low Temperature Series Expansions

High temperature series expansion of free energy is not applicable for temperatures below the transition temperature T_c. In order to make a complete treatment of the
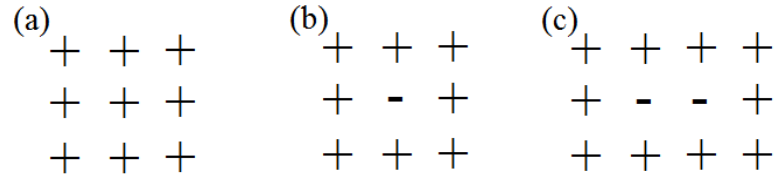
Figure 3.3 Schematic representation of (a) ground state configuration of a two dimensional Ising model where all spins aligned in the same direction, (b) the first excited state configuration, and (c) the second excited state configuration.

problem it is necessary to expand the free energy for $T < T_c$ which is called "low temperature series expansion" method. We assume that for $T < T_c$, major contributions to the partition function are from the states where few spins are flipped in comparison with the ground state of the system.

Again we consider the conventional spin Hamiltonian

$$\beta \mathcal{H} = -\beta J \sum_{<ij>} s_i s_j. \tag{3.2.12}$$

Ground state of the system defined by Eq. (3.2.12) is ferromagnetic with $\beta J > 0$ where all spins are aligned parallel with each other as shown in Fig. 3.3(a). Starting point for determination of a series expansion for partition function is to include the energy excitations around the ground state configuration. The excited state with a lowest energy excitation is to flip a single spin corresponding to configuration depicted in Fig. 3.3(b). Any of N lattice sites can be flipped in the system, and the energy cost is $\triangle E = 8J$ with respect to the ground state energy in two dimensions. The configuration with next lowest energy is the configuration depicted in Fig. 3.3(c) where the number of flipped spins is 2. Now, the energy difference is $\triangle E = 8J + 4J = 12J$. There are two possible orientations for these two flipped spins (namely in horizontal or vertical directions) leading to $2N$ possible orientations in total. In the next configuration, we flip two disjoint spins. There are N possible selections for the first spin. For the second one we have $N - 1$ possibilities. However, four neighboring sites of the first lattice site are not allowed. Consequently, there exist $N - 1 - 4 = N - 5$ remaining possibilities. In order to avoid double counting we should divide the resultant value by two, hence we get $\frac{N(N-5)}{2}$ possible configurations. The amount of energy cost is now

$\triangle E = 8J + 8J = 16J$. Consequently, we can order the terms relative to the ground state energy as follows

$$Z = 2e^{2N\beta J}\left(1 + Ne^{-8\beta J} + 2Ne^{-12\beta J} + \frac{N(N-5)}{2}e^{-16\beta J} + ...\right).\qquad(3.2.13)$$

The factor 2 on the left-hand side of Eq. (3.2.13) is due to the two fold degeneracy of the configurations (for instance the energy of all spin-up configuration is the same as that of all spin-down configuration) which is insignificant in $N \to \infty$ limit, and we finally obtain

$$Z = e^{2N\beta J}\left(1 + Ne^{-8\beta J} + 2Ne^{-12\beta J} + \frac{N(N-5)}{2}e^{-16\beta J} + ...\right).\qquad(3.2.14)$$

The free energy per site is obtained from the series,

$$\begin{aligned}F &= -k_B T \lim_{N\to\infty}\frac{1}{N}\ln Z,\\ &= -k_B T \frac{1}{N}\ln\left[e^{2N\beta J}\left(1 + Ne^{-8\beta J} + 2Ne^{-12\beta J} + \frac{N(N-5)}{2}e^{-16\beta J} + ...\right)\right],\end{aligned}$$
$$(3.2.15)$$

from which we get

$$-\frac{F}{k_B T} = 2\beta J + \frac{1}{N}\ln\left(1 + Nt^4 + 2Nt^6 + \frac{N(N-5)}{2}t^8 + ...\right),\quad t = e^{-2\beta J}.\qquad(3.2.16)$$

By applying Eq. (3.2.9) in Eq. (3.2.16) and taking the powers up to t^8, we can see that the terms proportional to N^2 drop out which is a consequence of the extensivity of the free energy and we get

$$-\frac{F}{k_B T} = 2\beta J + t^4 + 2t^6 - \frac{5}{2}t^8 + O(t^{10}).\qquad(3.2.17)$$

The energy per site and the heat capacity are then obtained from

$$\begin{aligned}U/N &= -\frac{\partial}{\partial\beta}\left(\frac{\ln Z}{N}\right) = -2J + 8Jt^4 + 24Jt^6 - 40Jt^8,\\ C/Nk_B &= \frac{1}{Nk_B}\frac{\partial E}{\partial T} = \left(\frac{J}{k_B T}\right)^2\left[64t^4 + 288t^6 - 640t^8\right].\end{aligned}\qquad(3.2.18)$$

3.3   Monte Carlo Simulations

Until the recent past, the research on physical systems was carried out by completely theoretical or experimental tools, and the validity of a theory could be confirmed

only by an experimental investigation. On the other hand, the reliability, as well as quality standard of an experimental research strictly depend on the preparation of a perfect sample for study or to facilitate a good laboratory equipped with experts which generally costs an expensive expenditure. Moreover, with the advent of computers after the middle of twentieth century, the research on physical systems became possible to carry out by completely numerical methods. As a result of these technological developments, computer simulations or "computational experiments" are regarded as another way of doing academical research at the present time. One of and maybe the most powerful approach among these computational tools is Monte Carlo (MC) simulation technique which was originally introduced in the literature by (Metropolis, Rosenbluth, Rosenbluth, Teller, & Teller, 1953).

MC simulations have a very wide variety of applications in physics. However, we will basically deal with the applications of the method in magnetism. Speaking in a magnetic language, in a typical MC simulation process we actually monitor the time dependence of some properties like magnetization and internal energy of a model system which evolve according to a certain predefined rule (Landau & Binder, 2001). The power and the reliability of the method in applications of magnetic systems originate from the complete consideration of thermal fluctuations and multi-site correlations between neighboring lattice sites. There exist pretty precious references concerning the applications of MC simulations in statistical physics (Landau & Binder, 2001, Newman & Barkema, 2001), and we refer the readers to these worthy studies for further detailed information.

3.3.1 *Importance Sampling Technique*

In statistical mechanics, we generally need to calculate the average value of a certain quantity such as magnetization and internal energy according to

$$\langle \hat{A} \rangle = \frac{\sum_{\{s\}} \hat{A} \exp(-\beta \mathcal{H})}{\sum_{\{s\}} \exp(-\beta \mathcal{H})}, \quad \{s\} : \text{all accessable states.} \qquad (3.3.1)$$

For a regular lattice consisting of N lattice sites, the sums in Eq. (3.3.1) contains 2^N distinct contributions for $s = \pm 1$. Typically, it is almost impossible to calculate these contributions for $N \geq 40$. One possible way to overcome this problem is to create an initial configuration set, and try to extract the desired configuration by following a physically reasonable mechanism. However, some configurations may contribute to the partition function with a major weight whereas the most of the configurations do not make a significant contribution. Moreover, according to the Boltzmann weight $e^{-\beta \hat{H}}$, the number of configurations contributing to the partition function is very small. Therefore, taking the configurations with a weight $e^{-\beta \hat{H}}$, instead of taking the whole configuration set will definitely make things easier and we call it "importance sampling technique".

The first step in this procedure is to create a Markov chain. Namely, if the state of a system at time t can be somehow obtained from the state at $t - 1$, the set of n configurations produced in this manner is called Markov chain. According to the ergodicity hypothesis, a particular configuration of the system must be obtained from another arbitrary configuration in a finite time step.

3.3.2   *Markov Chains and Master Equation*

In a given process for a particular system, if the state at time t can be estimated from previous states by using random elements this process is called a "stochastic process" which can not be defined in a deterministic manner. Let us consider a stochastic process defined by a finite set of possible states $S_1, S_2, S_3, ...$ defined at discrete time steps $t_1, t_2, t_3, ...,$ and denote the state of the system at time t as X_t. According to the conditional probability $X_{t_n} = S_{i_n}$ we have

$$P(X_{t_n} = S_{i_n} | X_{t_{n-1}} = S_{i_{n-1}}, X_{t_{n-2}} = S_{i_{n-2}}, ..., X_{t_1} = S_{i_1}). \qquad (3.3.2)$$

Eq. (3.3.2) tells us that the previous system state $X_{t_{n-1}}$ was the state $S_{i_{n-1}}$, etc. and the state X_{t_n} at time t_n can be obtained from X_{t_1} at time t_1 in successive stochastic iterations. These kind of processes are called stochastic processes. If the conditional probability

in Eq. (3.3.2) is independent of all states and if the probability of the system to be in a state X_{t_n} at time t_n only depends on the previous state at time t_{n-1} then we can write

$$P = P(X_{t_n} = S_{i_n}|X_{t_{n-1}} = S_{i_{n-1}}). \tag{3.3.3}$$

In this case the set of the states $\{X_t\}$ corresponding to Eq. (3.3.3) is a Markov chain, and the conditional probability in Eq. (3.3.3) can be expressed as a transition probability between the states i and j as follows

$$W_{ij} = W(S_i \rightarrow S_j) = P(X_{t_n} = S_j|X_{t_{n-1}} = S_i), \tag{3.3.4}$$

which must obey the following rule as the whole transition probabilities:

$$W_{ij} \geq 0, \quad \sum_j W_{ij} = 1. \tag{3.3.5}$$

Hence, the probability $P(X_{t_n} = S_j)$ of the system to be in a state S_j at time t_n can be defined as

$$P(X_{t_n} = S_j) = P(X_{t_n} = S_j|X_{t_{n-1}} = S_i)P(X_{t_{n-1}} = S_i) = W_{ij}P(X_{t_{n-1}} = S_i). \tag{3.3.6}$$

For $P(X_{t_n} = S_j) = P(S_j, t)$ time dependence of Eq. (3.3.6) is called "Master equation"

$$\frac{dP(S_j,t)}{dt} = -\sum_i W_{ji}P(S_j,t) + \sum_i W_{ij}P(S_i,t). \tag{3.3.7}$$

Moreover, Eq. (3.3.7) can be considered as a "continuity equation", expressing the fact that the total probability is conserved $\left(\sum_j P(S_j,t) \equiv 1 \text{ at all times}\right)$ and all probability of a state i that is "lost" by transitions to state j is gained in the probability of that state, and vice versa. Eq. (3.3.7) just describes the balance of gain and loss processes: since the probabilities of the events $S_j \rightarrow S_{i_1}$, $S_j \rightarrow S_{i_2}$, $S_j \rightarrow S_{i_3}$ are mutually exclusive, the total probability for a move away from the state j simply is the sum $\sum_i W_{ij}P(S_j,t)$ (Landau & Binder, 2001).

3.3.3 Metropolis Algorithm

According to classical Metropolis algorithm (Metropolis et al., 1953), in order to estimate the configuration of the system at time t from a previous configuration at

time $t - 1$, we define a transition probability which depends on the energy difference between initial and final states of the system. The set of produced configurations is a time dependent and non-deterministic sequence, and the evolution of states can be simulated according to the time dependent master equation

$$\frac{\partial P_n(t)}{\partial t} = - \sum_{n \neq m} [P_n(t) W_{n \to m} - P_m(t) W_{m \to n}]. \tag{3.3.8}$$

In Eq. (3.3.8), $P_n(t)$ is the probability of the system to be in a state n at time t, $W_{n \to m}$ is the transition rate between states $n \to m$. In equilibrium we have $\partial P_n(t)/\partial t = 0$, hence we obtain

$$P_n(t) W_{n \to m} = P_m(t) W_{m \to n}, \tag{3.3.9}$$

which is called "detailed balance condition". In a classical system, the occupation probability of state n is given by

$$P_n(t) = e^{-E_n/k_B T}/Z. \tag{3.3.10}$$

Due to the partition function Z in denominator, the exact calculation of Eq.(3.3.10) is generally not possible. In order to overcome this problem, we generate a Markov chain. In other words, a new configuration is generated directly from previous one. If the state n is generated from the state m then according to Eq. (3.3.10), the relative probability is

$$\triangle E = E_n - E_m. \tag{3.3.11}$$

The transition rates satisfying the detailed balance condition in Eq. (3.3.9) are acceptable according to (Metropolis et al., 1953)

$$\begin{aligned} W_{n \to m} &= \tau_0^{-1} \exp(-\triangle E/k_B T), \quad \triangle E > 0 \\ &= \tau_0^{-1}, \qquad\qquad\qquad \triangle E < 0 \end{aligned} \tag{3.3.12}$$

where τ_0 is the spin-flip rate per unit time, and is generally set equal to unity. The implementation of Metropolis algorithm can be summarized as the following recipe:

1. Generate an initial configuration

2. Select the lattice site i

3. Calculate the energy cost $\triangle E$ if the spin at site i overturns

4. If $\triangle E \leq 0$ then accept the new configuration

5. If $\triangle E > 0$ then generate a random number r within the interval $0 < r < 1$

6. If the condition $r < \exp(-\triangle E / k_B T)$ is satisfied then accept the new configuration, else keep the existing configuration

7. Go to the next site and follow the procedure from the step 3

In a typical MC simulation described above the unit of time is measured in terms of MC steps. Namely, one complete sweep of lattice corresponds to a MC step (and also to a step of a Markov chain). Steps $1 - 7$ define one step of a Markov chain, and in each step we calculate the average values of thermodynamic quantities. In the first few iterations (i.e. the first few steps of Markov chain) the system may not reach to the equilibrium. Hence, once the number of states (i.e. the length of Markov chain) is sufficiently large then the configurations produced in these iterations are not added to statistical averaging. There is not any unique method for determining the number of transient steps in MC simulations. However, we can estimate it conventionally as follows: Perform a series of simulations starting from different initial configurations and keeping the system parameters fixed, and monitor the time dependence of magnetization. In most cases, $N = L \times L$ steps are sufficient for thermalization where L is the linear dimension of the regular lattice.

3.3.4   *Application to a Two Dimensional Ferromagnetic Ising Square Lattice*

Now we are capable of calculating some of the thermal and magnetic properties of model systems based on MC simulation technique implemented above. Let us start with a spin-1/2 Ising model defined on a square lattice (see Fig. 3.4). The most simple case can be described by the following Hamiltonian which includes only the nearest-neighbor interactions

$$\mathcal{H} = -J \sum_{<ij>} s_i s_j. \qquad (3.3.13)$$
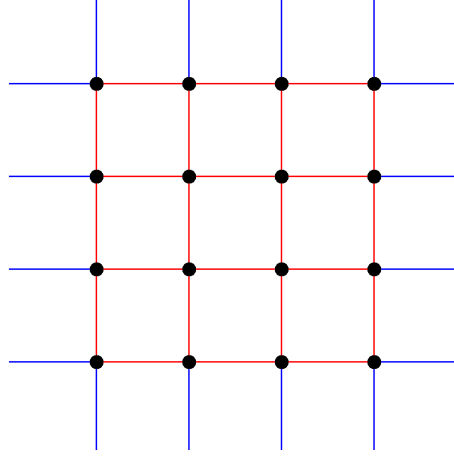
Figure 3.4 Schematic representation of arrangement of spins on a two dimensional square lattice.

In Eq. (3.3.13), $s_i = \pm 1$ represents a discrete spin variable and $J > 0$ is the ferromagnetic exchange interaction parameter value of which has been fixed to unity throughout the simulations. In order to simulate the system, we employ the Metropolis MC simulation algorithm to Eq. (3.3.13) on a $L \times L$ square lattice with periodic boundary conditions (PBCs). Configurations were generated by selecting the sites in sequence through the lattice and making single-spin-flip attempts, which were accepted or rejected according to the Metropolis algorithm, and L^2 sites are visited at each time step (a time step is defined as a MC step per site or simply MCS as explained before). Data were generated over $50 - 100$ independent sample realizations by running most of the simulations for 25000 Monte Carlo steps per site after discarding the first 5000 steps. This number of transient steps is found to be sufficient for thermalization for almost the whole range of the parameter sets. Our program calculates the instantaneous values of various quantities such as magnetization (M), magnetic susceptibility (χ), internal energy (U) and the specific heat (C) which are defined as

- Magnetization:

$$M = \frac{1}{N} \left\langle \sum_i s_i \right\rangle,$$
(3.3.14)

- Internal energy:

$$U = \langle \mathcal{H} \rangle, \qquad (3.3.15)$$

- Magnetic susceptibility:

$$\chi = \frac{1}{k_B T} \left(\langle M^2 \rangle - \langle M \rangle^2 \right), \qquad (3.3.16)$$

- Specific Heat:

$$C = \frac{1}{k_B T^2} \left(\langle U^2 \rangle - \langle U \rangle^2 \right). \qquad (3.3.17)$$
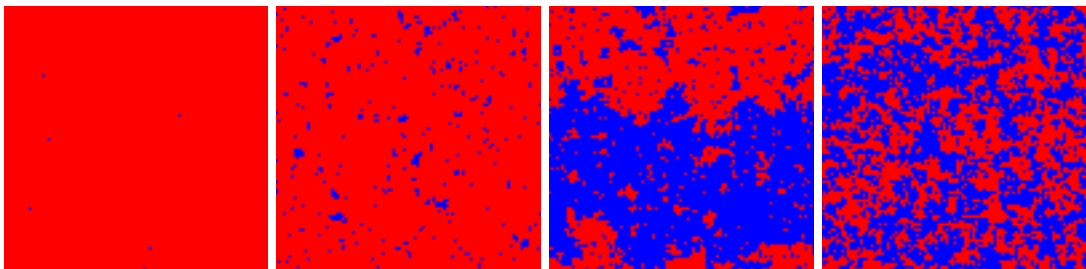
Figure 3.5 Graphical output of several runs of the 2D-Ising model for temperatures $T = 1.0$, $T = 2.0$, $T \approx T_c$, and $T = 3.0$, respectively. Each red (blue) square represents a $s = 1$ (-1) state for ferromagnetism, $J > 0$.
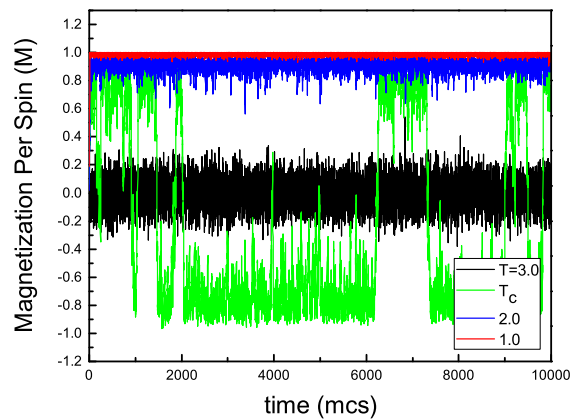
Figure 3.6 Time dependence of magnetization calculated at temperatures $T = 1.0$, $T = 2.0$, $T \approx T_c$, and $T = 3.0$.

In Fig. 3.5 we represent the snapshots of a two dimensional square lattice simulated by Metropolis algorithm in a single run according to Eq. (3.3.13) for temperatures $T = 1.0$ (the leftmost), $T = 2.0$ (middle left), $T \approx T_c$ (middle right) and $T = 3.0$

(the rightmost), respectively. The corresponding time series of magnetization curves are also depicted in Fig. 3.6. It is clear from these figures that at sufficiently low temperatures such as $T = 1.0$ where the thermal fluctuations are negligible ferromagnetic exchange interactions are dominant hence the system is able to establish a long range ferromagnetic order where almost all of the spins point parallel with each other. As the temperature increases (e.g. $T = 2.0$) some of the spins flip their direction due to the thermal agitations originating from increasing temperature. If we increase the temperature further, we get closer to the transition regime. In this regime thermal fluctuations are significantly dominant and the magnetization oscillates between ±1 states. Finally for $T > T_c$, temperature becomes sufficiently dominant against the ferromagnetic exchange coupling J and the system exhibits a paramagnetic state with zero net magnetization. This picture exposes a competition between ferromagnetic coupling J which tends to keep the spins parallel with each other and temperature T which has a tendency to destruct the ferromagnetic order in the system.

Variation of the order parameter M, internal energy U, as well as the response functions C and χ with temperature for this model was investigated by (Landau, 1976a). In the following calculations, we will reproduce the data obtained in this work. In Fig. 3.7 we depict the magnetization and internal energy data for a variety of lattice
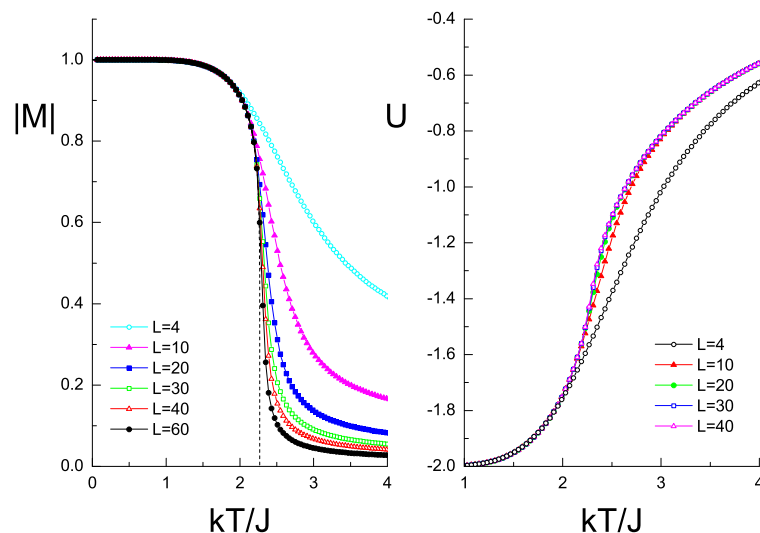
Figure 3.7 Temperature variation of the order parameter (left panel) and internal energy (right panel). The dashed lines on the left represent the exact result (Onsager, 1944).
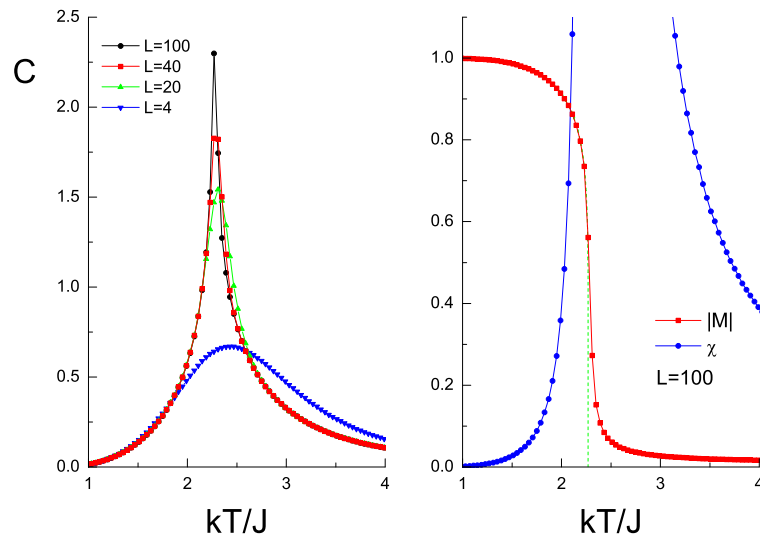
Figure 3.8 Left panel: Variation of specific heat curves as a function of temperature. Right panel: Magnetization and susceptibility versus temperature curves.

sizes *L*. Finite size effects can be clearly observed in this figure. Namely, as the system size increases then the curves converge to the results of exact calculations (Onsager, 1944). The situation can also be observed in left panel of Fig. 3.8 where the specific heat *C* curves are plotted as a function of temperature for various lattice sizes. As we approach to the thermodynamic limit then the divergent behavior of specific heat curves become apparent in the phase transition region. This divergent behavior can also be observed in the variation of magnetic susceptibility versus temperature curves (see the right panel in Fig. 3.8). An important deficiency of the method takes place at this point: As the linear dimension of the lattice increases then a better agreement with the exact results are obtained. However, this produces the need of a very large requirement of CPU time.

Up to now, we have investigated the thermal and magnetic properties of the model based on MC simulations. Now, let us discuss the critical properties of the system. The transition temperature of the system can not be precisely estimated from above discussion. In order to locate the transition temperature exactly, we can compute the fourth order cumulant of magnetization V_L with various lattice sizes. The fourth order cumulant of the magnetization, i.e. the Binder cumulant (Binder, 1981) for a spin

cluster is defined by

$$V_L(L,T) = 1 - \frac{\langle M^4 \rangle}{3\langle M^2 \rangle^2}, \tag{3.3.18}$$

where $\langle M^2 \rangle$ and $\langle M^4 \rangle$ denote the second and fourth moments of the magnetization in that cluster, respectively. The cumulant approaches the value 2/3 in the thermodynamic limit at temperatures $T < T_c$ while it tends to zero, reflecting a Gaussian distribution of the magnetization histogram, at $T > T_c$. At $T = T_c$ $V_L(L,T)$ acquires a nontrivial value, the critical Binder cumulant V_L^*.

Another method is to make use of the magnetization and correlation length critical exponents which are respectively given by

$$M \sim |T - T_c|^\beta, \tag{3.3.19}$$

$$\xi \sim |T - T_c|^\nu. \tag{3.3.20}$$

Combining these equations yields

$$M \sim \xi^{-\beta/\nu}. \tag{3.3.21}$$

In the thermodynamic limit, correlation length diverges at $T = T_c$. However, our system is a finite square lattice with linear size L. Hence, at the transition point the maximum correlation length equals to L. Therefore, for square lattices with linear sizes L_1 and L_2 we have

$$
\begin{aligned}
M_1 &= C_1 L_1^{-\beta/\nu}, \\
M_2 &= C_2 L_2^{-\beta/\nu}.
\end{aligned}
\tag{3.3.22}
$$

From Eq. (3.3.22) we get

$$\log\left(\frac{M_1}{M_2}\right) = \log\left(\frac{C_1}{C_2}\right) - \frac{\beta}{\nu}\log\left(\frac{L_1}{L_2}\right). \tag{3.3.23}$$

For $T = T_c$ we can write $C_1 = C_2$, and we finally obtain the following function

$$f(M,L) = \frac{\log(M_1/M_2)}{\log(L_1/L_2)} = -\frac{\beta}{\nu}. \tag{3.3.24}$$

If the left hand side of Eq. (3.3.24) is plotted for various L_1 and L_2 sets, these curves intersect each other at $T = T_c$. The $x-$ and $y-$ coordinates of the intersection point correspond to critical temperature T_c and critical exponent β/ν, respectively.
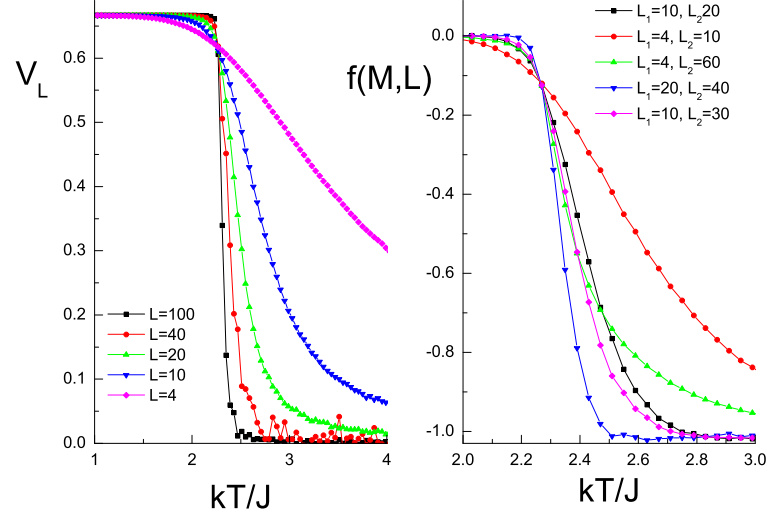
Figure 3.9 Left panel: Binder cumulant versus temperature curves of various lattice sizes. The projection of the intersection point of the curves on the x axis corresponds to T_c. Right panel: Determination of transition temperature T_c and the critical exponent β/ν according to Eq. (3.3.24).

The numerical data obtained from Eqs. (3.3.18) and (3.3.24) are depicted in Fig. 3.9. Variation of Binder cumulant $V_L(L,T)$ as a function of temperature for various lattice sizes is plotted in the left panel of Fig. 3.9 from which the transition temperature is obtained as $T_c = 2.27$ which agrees quite well with the exact value $T_c = 2/\log(1+\sqrt{2}) = 2.269$ (Onsager, 1944). On the other hand, according to the data based on Eq. (3.3.24) we have $T_c = 2.27$ and $\beta/\nu = 0.127$ (see the right panel in Fig. 3.9). The exact value of exponent is $\beta/\nu = 0.125$ (Stanley, 1971). The numerical precision can be improved by performing simulations for sufficiently narrow temperature intervals with quite large number of sample realizations.

There is also another alternative way to estimate the critical exponents from the computed data. Namely, at $T = T_c$ we can write

$$M \sim L^{-\beta/\nu}. \qquad (3.3.25)$$

Hence, at this temperature it is possible to extract the exponent β/ν from Eq. (3.3.25) by computing the magnetization for various lattice sizes. Consequently, the slope of log-log plot of Eq. (3.3.25) gives the desired value. The computed data is depicted in Fig.3.10 and it has been found that $\beta/\nu = 0.127$. As we noted before, the slight
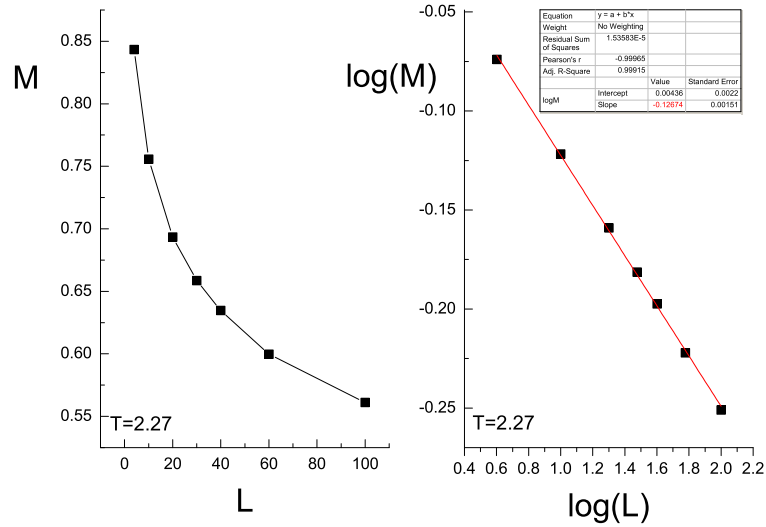
Figure 3.10 Left panel: Magnetization versus lattice size L at $T = T_c$ obtained from Eq. (3.3.25). Right panel: The same data but in a logarithmic scale. The exponent value is obtained as $\beta/\nu = 0.127$.

difference between the results of Eqs. (3.3.24) and (3.3.25) can be reduced by increasing the realization number or by generating longer Markov chains which means computing the statistical averages from longer time series of magnetization at a fixed temperature.

3.3.5 Application to a Classical Vector Model

In contrast to Ising-type models which have variables with discrete degrees of freedom, the models described by a Heisenberg Hamiltonian are characterized using variables which vary continuously. As we noted in Eq. (2.6.1), classical Heisenberg model and its various generalizations are commonly used to simulate the systems with continuous degrees of freedom. The anisotropic Heisenberg model can be represented by the following classical Hamiltonian

$$\mathcal{H} = -J \sum_{<ij>} \vec{S}_i . \vec{S}_j - D \sum_i \vec{S}_i^2, \ |\vec{S}_i| = 1. \tag{3.3.26}$$

The model described by Eq. (3.3.26) is a classical model since the spin variables are considered as three dimensional unit vectors with continuous degrees of freedom. The first term in Eq. (3.3.26) is the Heisenberg exchange constant and the second term is

the single ion anisotropy. Here anisotropy means that the three dimensional unitary spin vector $\vec{S}_i$ can favor a certain direction depending on the value of D. More clearly, we can modify Eq. (3.3.26) as

$$\mathcal{H} = -J \sum_{<ij>} \vec{S}_i . \vec{S}_j - D_x \sum_i \left(S_i^x\right)^2 - D_y \sum_i \left(S_i^y\right)^2 - D_z \sum_i \left(S_i^z\right)^2, \ |\vec{S}_i| = 1. \quad (3.3.27)$$

The model described by Eq. (3.3.27) corresponds to "anisotropic" Heisenberg model where the contribution of the components S_x, S_y, S_z to the length of the vector $\vec{S}_i$ depends on the anisotropy constants D_x, D_y, D_z.

Classical Heisenberg model is capable of verifying the experimental evidence of magnetic behavior of many materials such as RbMnF$_3$. MC simulation procedure of the model is very similar to Ising model. However, it is not possible to simply flip the spin variable since there are infinite number of trial states for the spin vector. The method of tracking the information about components of spin vector $\vec{S}_i$ constitutes a significant importance. A three dimensional classical spin vector can be defined as

$$\vec{S} = S_x \hat{i} + S_y \hat{j} + S_z \hat{k}. \quad (3.3.28)$$

This vector can be considered as a vector centered at origin of a unit sphere. The components S_x, S_y and S_z of vector $\vec{S}_i$ then can be defined in either cartesian or spherical coordinates. Now, the problem of generating an initial configuration with randomly oriented unit vectors becomes the problem of choosing a point randomly from the surface of a unit sphere. In spherical coordinates, the vector components are

$$
\begin{aligned}
S_x &= \sin\theta\cos\phi, \\
S_y &= \sin\theta\sin\phi, \\
S_z &= \cos\theta,
\end{aligned}
\quad (3.3.29)
$$

with $0 \le \theta \le \pi$, $0 \le \phi \le 2\pi$ and $|\vec{S}| = \sqrt{(S_x)^2 + (S_y)^2 + (S_z)^2} = 1$.

However, generating an initial configuration by using two random numbers θ and ϕ within the intervals $[0,\pi]$ and $[0,2\pi]$ cannot be sampled from a homogenous distribution, but the sample realizations may pile up around the northern and southern poles of the unit sphere. This situation can be clearly seen from Figs. 3.11a-c.
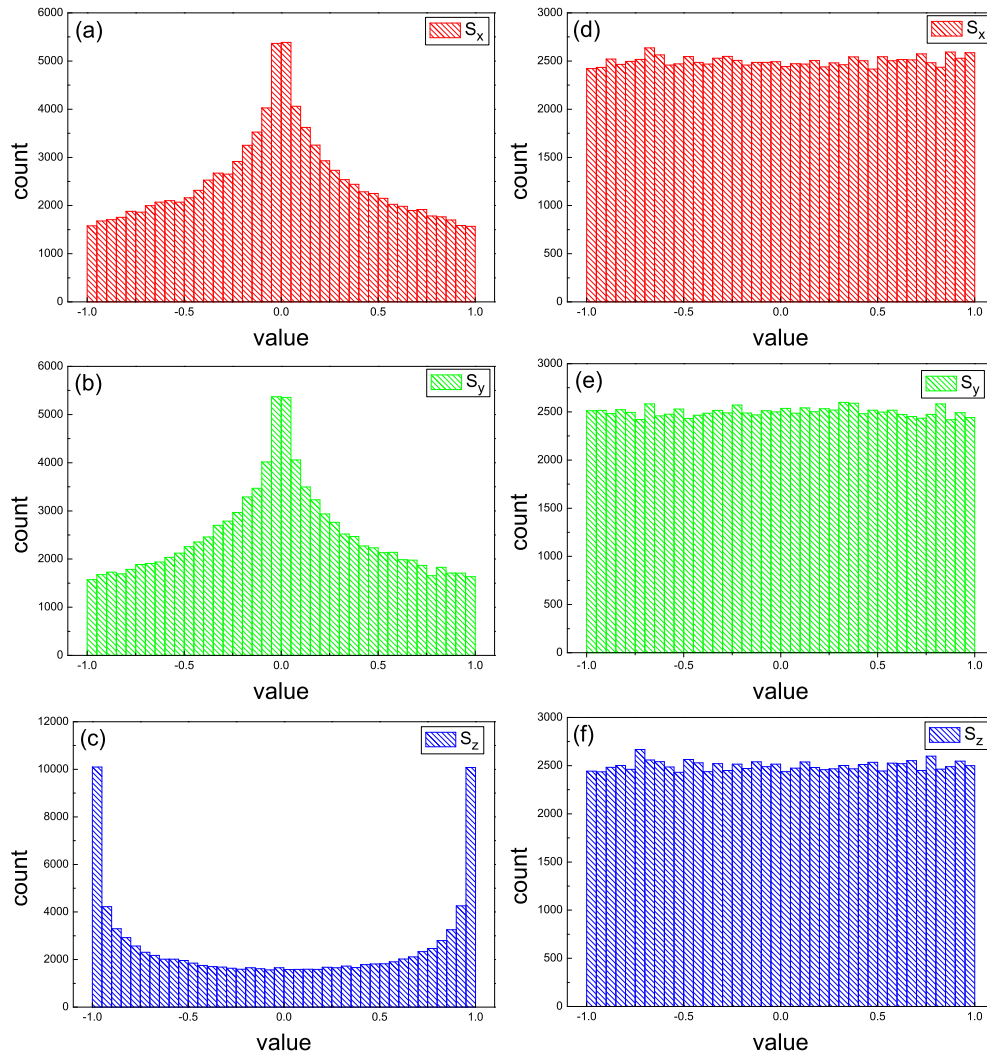
Figure 3.11 Distribution of randomly selected $N = 100000$ points corresponding to $x-$, $y-$ and $z-$ components of a classical unitary spin vector $\vec{S}$. Histograms (a)-(c) have been drawn from Eq. (3.3.29) whereas (d)-(f) have been generated from Marsaglia's method.

It is possible to overcome this problem by using a method known as Marsaglia algorithm (Marsaglia, 1972) which can be summarized as follows

- Generate two random numbers from a homogenous distribution within the interval $[0, 1]$

- Define a two dimensional ξ vector using the numbers r_1 and r_2

$$\xi_1 = 1 - 2r_1, \quad \xi_2 = 1 - 2r_2, \quad \xi^2 = \xi_1^2 + \xi_2^2.$$

- If the condition $\xi^2 < 1$ is satisfied then the components of the spin vector are

obtained as follows

$$S_x = 2S_0\xi_1(1-\xi^2)^{1/2}, \quad S_y = 2S_0\xi_2(1-\xi^2)^{1/2}, \quad S_z = S_0(1-2\xi^2),$$

where $S_0 = 1$ is the radius of the unit vector. The set of spin vectors produced in this way are part of a uniform distribution of directions. These conclusions have been depicted in Figs. 3.11d-f.
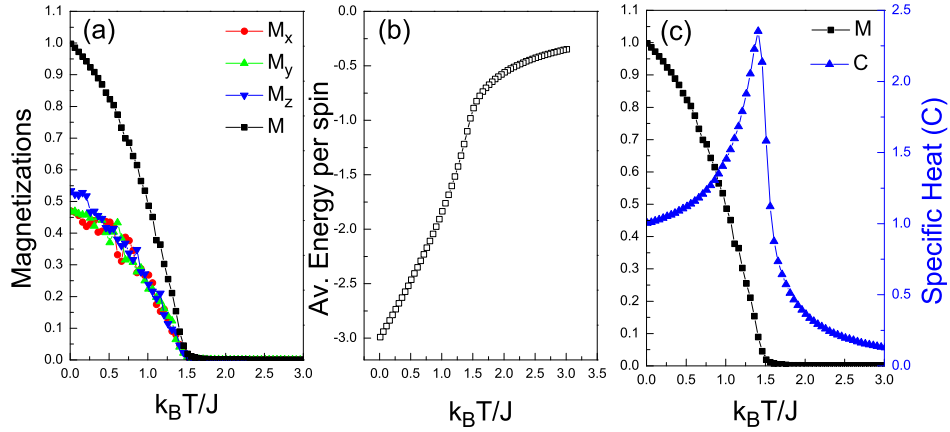
Figure 3.12 Simulation results for (a) magnetization components and (b) average energy per spin of isotropic ($D_x = D_y = D_z = 0$) classical Heisenberg model defined on a simple cubic lattice. Total magnetization and specific heat curves have also been depicted in (c).

The order parameter M of the classical Heisenberg model is determined by its multi-components, and the nature of the Hamiltonian determines which components are important. Namely, in the presence of single ion anisotropy (c.f. see Eq. (3.3.27)) ordering will occur only along the dominant directions depending on the values of the single ion anisotropy parameters D_x, D_y and D_z. In the isotropic case where $D_x = D_y = D_z$, all components are equivalent (Landau & Binder, 2001). In this context, the order parameter has the form

$$M = \sqrt{M_x^2 + M_y^2 + M_z^2}, \quad \text{where} \quad M_\alpha = \frac{1}{N}\sum_i S_{i\alpha}, \quad \alpha = x, y, z. \tag{3.3.30}$$

According to this detailed picture, we have performed MC simulations of classical Heisenberg model on a three dimensional simple cubic lattice. In simulations, we have generated Markov chains with 25000 steps and discarded the first 5000 of them for thermalization and we considered $N = 12^3$ spins. The calculated data (c.f Fig.

3.12) were compared with those of (Miyatake, Yamamoto, Kim, Toyonaga, & Nagai, 1986) for 50 different realizations and a good agreement have been found. Namely, the specific heat of the Heisenberg model on a simple cubic lattice has been depicted in Fig. 3.12c. We find that the critical temperature obtained from the maxima of specific heat curve for the Heisenberg model is $T_c \cong 1.45$ whereas the high temperature series expansion method predicts $T_c \cong 1.445$ (Ritchie & Fisher, 1972, Wood & Rushbrooke, 1966).

3.3.6 *Other Applications*

Apart from the models mentioned above, MC simulation technique was successfully applied to many variants and generalizations of Ising and Heisenberg Hamiltonians. These models have been briefly discussed below. For instance, behavior of kinetic Ising model described by the following Hamiltonian by imposing the PBCs

$$\mathcal{H} = -J \sum_{<ij>} S_i S_j - h(t) \sum_i S_i,$$ (3.3.31)

has been investigated by (Tomé & de Oliveira, 1990). The term $h(t)$ in Eq. (3.3.31) is a time-dependent external magnetic field which is defined as $h(t) = h_0 \cos(\omega t)$.

On the other hand, magnetization of thin films (Tucker, 2000, Zaim et al., 2008) by applying PBCs in the $x-$ and $y-$ directions, and free boundary conditions (FBCs) in $z-$ direction which is of finite thickness has been clarified. Moreover, magnetic properties of small particles have been simulated recently (Yüksel, Vatansever, & Polat, 2012b) by using free boundary conditions.

As shown in the simulations concerning the spin models mentioned above, PBCs or FBCs are often used. Implementation of the boundary conditions is very important in MC simulations and it is always determined according to the geometric features of the model.

MC simulations can also be easily adopted to investigate the effect of quenched disorder in spin models which is the main motivation of present report. An example

of this is the Ising model in the presence of random fields (or simply RFIM) which is described by the following Hamiltonian

$$\mathcal{H} = -J \sum_{<ij>} S_i S_j - \sum_i h_i S_i, \qquad (3.3.32)$$

where h_i is the random magnetic field acting on the lattice site i. Generally, random fields are distributed on the lattice sites according to a certain probability distribution function (PDF). The most general form of probability distribution is the triple Gaussian random magnetic field distribution which is defined as

$$
\begin{aligned}
P(h_i) \quad = \quad & \frac{(1-p)}{2} \left(\frac{1}{2\pi\sigma^2} \right)^{1/2} \left\{ \exp\left[-\frac{(h_i - h_0)^2}{2\sigma^2} \right] + \exp\left[-\frac{(h_i + h_0)^2}{2\sigma^2} \right] \right\} \\
& + p \left(\frac{1}{2\pi\sigma^2} \right)^{1/2} \exp\left[-\frac{h_i^2}{2\sigma^2} \right],
\end{aligned}
\qquad (3.3.33)
$$

which is just the superposition of three Gaussian distributions each having the same width σ and centered at $h = 0$ and $h = \pm h_0$ with probabilities p and $(1 - p)/2$, respectively. In the limit $\sigma \to 0$ trimodal PDF is recovered. MC simulation of such a problem for determining the phase transition characteristics in the presence of disorder is rather difficult to perform since in order to acquire statistically meaningful data one must generate realizations over many disorder configurations in addition to conventional configurational averaging. This is a rather time consuming process.

A detailed description of phase transition phenomena in magnetic systems in the presence of quenched disorder will be treated in the following chapters of this thesis report. However, as a final remark of this subsection let us explain the numerical method for generating random fields according to Eq. (3.3.33). In order to generate standard normal random numbers we often use the method called as polar form of the Box-Muller transformation (i.e. Marsaglia polar method) (Box & Muller, 1958). The algorithm can be briefly summarized as follows

1. Generate two random numbers r_1 and r_2 from a homogenous distribution within the interval [0,1]

2. Define the random variables $x_1 = 2r_1 - 1$, $x_2 = 2r_2 - 1$ and $w^2 = x_1^2 + x_2^2$

3. If the condition $w < 1$ is satisfied then define the new variable (else goto step 1)

$$y_1 = x_1 \sqrt{\frac{-2\log(x_1^2 + x_2^2)}{x_1^2 + x_2^2}}$$

4. Generate another random number r from uniform distribution within the interval [0,1]

5. if $r < (1-p)/2$ then $\xi = h_0 + \sigma y_1$

6. else if $r > (1-p)/2$ and $r < 1-p$ then $\xi = -h_0 + \sigma y_1$

7. else $\xi = \sigma y_1$

3.4   Mean Field and Effective Field Theories

We see from above discussions that there are very few systems characterized by a spin Hamiltonian that can be exactly solvable. Even the most powerful methods such as the transfer matrix technique, series expansion methods, and Monte Carlo simulations may fail as the complexity of the model system increases. Main adversities arise from mathematical difficulties or due to requirement of large amount of computational time. On the other hand, because of its simplicity, the mean-field theory (MFT) has been regarded as an important tool for the description of cooperative phenomena, however the method has some deficiencies due to neglecting the correlations.   Therefore we need improved methods for further and reliable treatment of magnetism as a cooperative phenomena.   The reliability of an approximation should be consistent with the experimental observations as much as possible or there should exist a good agreement between the results of rigorous theoretical calculations and that of the approximation method used. In this context, the key idea lies behind the consideration of correlations between spins located on the lattice sites throughout the calculations.

In this subsection, we will refer on various methods for obtaining approximate solutions in Ising systems and discuss the formulations in which the effects of

correlations are systematically taken into account which can be easily adopted to pure and disordered magnetic systems.

As noted by Kaneyoshi (Kaneyoshi, 1993), in the presence of extremely high anisotropic case, we can treat a spin model by considering only the $z-$ component of a spin. Hence, the Ising model of ferromagnetism is represented by the following Hamiltonian

$$\mathcal{H} = -J \sum_{<ij>} S_i^z S_j^z - h \sum_i S_i^z, \qquad (3.4.1)$$

where $S_i^z = \pm 1$ is the $z-$ component of the spin operator $\hat{S}$, J is the ferromagnetic exchange interaction between the nearest neighbor spins and h is the externally applied longitudinal magnetic field. Based on Eq. (2.4.3), the relation between the $z-$ component of spin operator (or spin angular momentum) S_i^z and the magnetic dipole moment μ_i^z associated with the ion localized at the site i can be established as $S_i^z = (1/2)\mu_i^z$. The order parameter (i.e. magnetization) which measures the ordering of the system is $m = \langle S_i^z \rangle$. In the ordered (ferromagnetic) phase $m \neq 0$ whereas in disordered (paramagnetic) phase we have $m = 0$.

The expectation value $\langle S_i^z \rangle$ of the spin variable at the site i is given by

$$m = \langle S_i^z \rangle = \frac{\text{Tr} S_i^z e^{-\beta H}}{\text{Tr} e^{-\beta H}}. \qquad (3.4.2)$$

Now by noticing that the spin variables commute with each other, i.e. $\left[S_i^z, S_j^z \right] = 0$, let us separate the Hamiltonian given by Eq. (3.4.1) into two parts as

$$\mathcal{H} = H_i + H', \qquad (3.4.3)$$

where H_i is associated with the contribution of site i to Eq. (3.4.1) and H' includes the interactions which do not depend on the site i. Therefore, the expectation value in Eq. (3.4.2) can be written as

$$m = \langle S_i^z \rangle = \frac{1}{Z} \left\{ \text{Tr} e^{-\beta H} \left[\frac{\text{tr}_i S_i^z \exp(-\beta H_i)}{\text{tr}_i \exp(-\beta H_i)} \right] \right\}. \qquad (3.4.4)$$

By performing the partial trace operations in Eq. (3.4.4) with $S_i^z = \pm 1$ we get

$$\begin{aligned} \langle S_i^z \rangle &= \frac{1}{Z} \text{Tr} \left[e^{-\beta H} \tanh(\beta E_i) \right], \\ \langle S_i^z \rangle &= \langle \tanh(\beta E_i) \rangle, \end{aligned} \qquad (3.4.5)$$

where $E_i = J \sum_j S_j^z + h$ is the local field acting on the lattice site i. The result (3.4.5) is known as the Callen identity in the literature (Callen, 1963).

At the mean field level, one ignores the whole correlations by considering the approximated local field $\tilde{E}_i = qJm + h$. Hence the mean field equation of state is obtained as follows

$$m = \tanh\left[\beta(qJm + h)\right], \qquad (3.4.6)$$

where q is the coordination number of the lattice. The solution of this transcendental function can be obtained graphically by letting

$$\begin{aligned} y_1 &= m, \\ y_2 &= \tanh\left(\frac{qm + h_0}{T}\right), \end{aligned} \qquad (3.4.7)$$

where $T = 1/\beta J$ is the reduced temperature and $h_0 = h/J$ is the normalized field amplitude.

The numerical solution of Eq. (3.4.6) can be obtained from the condition $y_1 = y_2$. Possible solutions are graphically represented in Fig. 3.13. In Figs. 3.13a and 3.13b, the intersection point of y_1 and y_2 correspond to the solution of Eq. (3.4.6). As seen from Fig. 3.13a, in the absence of magnetic field ($h_0 = 0.0$), for temperatures $T < T_c$, there are three formal solutions of m. The solution corresponding to $m = 0$ is not physically meaningful since the net magnetization should be different from zero for the temperatures less than T_c. Since the ground state is doubly degenerate, both positive and negative valued solutions satisfy Eq. (3.4.6). For $T > T_c$, there is only one intersection point which is located at $m = 0$ corresponding to the paramagnetic phase. On the other hand, at $T = T_c$ the intersection point simply shifts to the origin. The situation is also depicted for $h_0 > 0.0$ in Fig. 3.13b. For $h_0 > 0$, the magnetic moments tend to align in the external field direction. Therefore, the physical solution of Eq. (3.4.6) which minimizes the free energy for $h_0 > 0.0$ is the solution with $m > 0$ which decreases with increasing temperature due to the thermal effects. Finally, in Fig. 3.13c, we depict the magnetization spectrum for a wide range of reduced temperature with some selected values of h_0. We see from Fig. 3.13c that at low temperatures with $h_0 = 0.0$, all magnetic moments are aligned parallel with each other hence we have

$m = 1$. As the temperature increases then the thermal effects become dominant and the magnetization decreases continuously and reduces to zero at $T = T_c$. However, in the presence of external field ($h_0 \neq 0$), the system does not exhibit any phase transition.
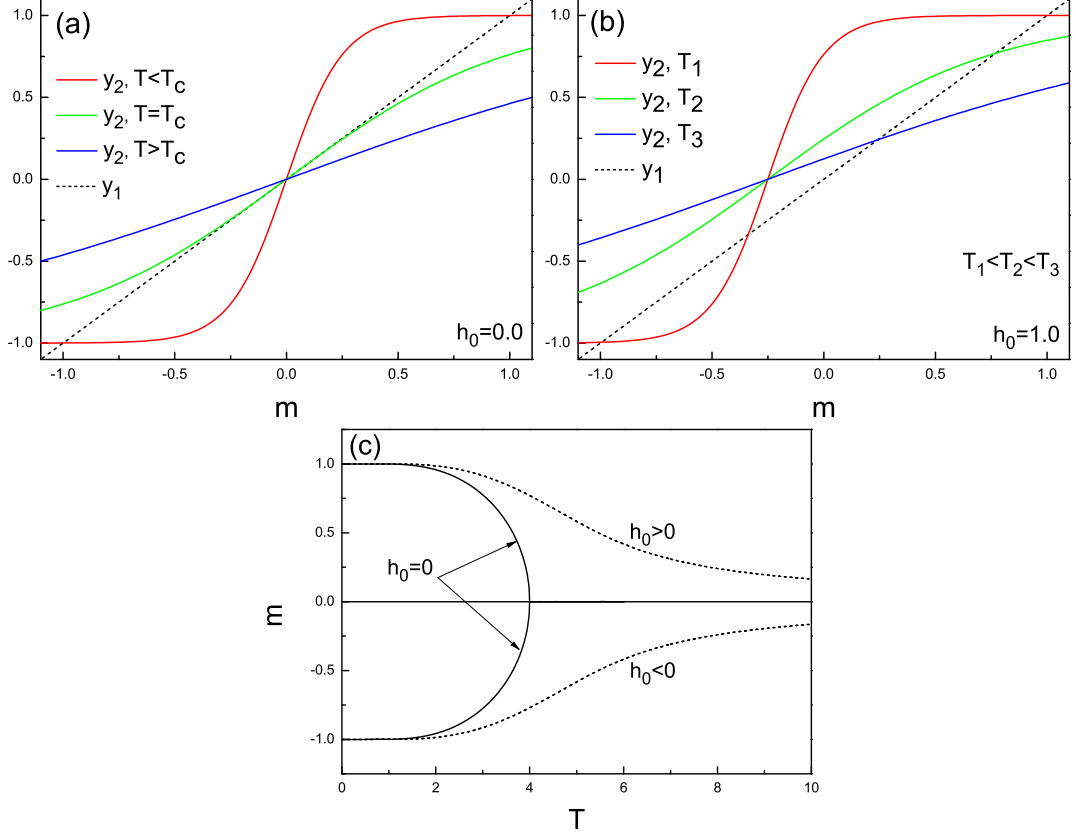
Figure 3.13 Graphical solution of Eq. (3.4.7) with $q = 4$ for (a) $h_0 = 0.0$ and (b) $h_0 > 0.0$. (c) Temperature dependence of mean field magnetization for a square lattice ($q = 4$).

In the absence of magnetic fields, it is easy to locate the transition temperature analytically by letting $\xi = \beta q J m$ and expanding Eq. (3.4.6) in terms of ξ since $m \rightarrow 0$ in the vicinity of transition temperature

$$m = \frac{e^\xi - e^{-\xi}}{e^\xi + e^{-\xi}} \cong \frac{1 + \xi - (1 - \xi)}{1 + \xi + 1 - \xi} = \xi, \tag{3.4.8}$$

from which we get

$$\frac{k_B T_c}{J} = q. \tag{3.4.9}$$

According to this result, critical temperature obtained by mean field formulation depends only on the coordination number q of the lattice. Therefore, the theory incorrectly predicts a phase transition even for a one dimensional lattice (Yeomans, 2000). This can be related to neglecting the entire correlations in calculations.

3.4.1 Decoupling (Zernike) Approximation

As seen in the preceding calculations, mean field theory promises a very naive picture concerning the phase transition characteristics of model systems represented by spin Hamiltonians. In order to introduce a more sophisticated technique we refer to a review paper written by Kaneyoshi (Kaneyoshi, 1993).

Now let us generalize the Callen identity (3.4.5) as

$$\langle \{f_i\} S_i^z \rangle = \langle \{f_i\} \tanh(\beta E_i) \rangle, \tag{3.4.10}$$

where $\{f_i\}$ can be any function as long as it is not a function of the site i. At this point the crucial step is to introduce the differential operator technique of Honmura and Kaneyoshi (Honmura & Kaneyoshi, 1979):

$$\tanh(\beta E_i) = \exp(E_i \nabla) \tanh(\beta x)|_{x=0}, \tag{3.4.11}$$

where $\nabla = \partial/\partial x$ is a differential operator. For $S_i^z = \pm 1$ we also have the following identity

$$e^{\alpha S_i^z} = \cosh(\alpha) + S_i^z \sinh(\alpha) \tag{3.4.12}$$

Using Eqs. (3.4.11) and (3.4.12) in Eq. (3.4.10) yields

$$
\begin{aligned}
\langle \{f_i\} S_i^z \rangle &= \langle \{f_i\} e^{E_i \nabla} \tanh(\beta x) \rangle, \\
&= \langle \{f_i\} e^{(J \sum_j S_j^z + h)\nabla} \tanh(\beta x) \rangle, \\
&= \langle \{f_i\} \prod_j e^{J S_j^z \nabla} \tanh[\beta(x+h)] \rangle,
\end{aligned} \tag{3.4.13}
$$

from which we finally obtain

$$\langle \{f_i\} S_i^z \rangle = \left\langle \{f_i\} \prod_{j=1}^{q} \left[\cos(J\nabla) + S_i^z \sinh(J\nabla) \right] \right\rangle f(x)|_{x=0}, \tag{3.4.14}$$

where

$$f(x) = \tanh[\beta(x+h)]. \tag{3.4.15}$$

Eq.(3.4.14) contains thermal averages of multiple correlation functions. If we attempt to treat all of the correlation functions which emerge when expanding the

right-hand side of Eq. (3.4.14) then the problem becomes mathematically intractable (as though !!). In order to overcome this problem one has to make an approximation. The simplest approximation, and one of the most frequently adopted, is to decouple these correlations according to

$$\left\langle S_j^z S_k^z ... S_l^z \right\rangle \approx \left\langle S_j^z \right\rangle \left\langle S_k^z \right\rangle ... \left\langle S_l^z \right\rangle. \tag{3.4.16}$$

Introducing the approximation (3.4.16) in Eq. (3.4.14) with $\{f_i\} = 1.0$ we get

$$m = [\cosh(J\nabla) + m\sinh(J\nabla)]^q f(x)|_{x=0}. \tag{3.4.17}$$

Eq. (3.4.17) can be written in a compact polynomial form by using the Binomial formula

$$m = \sum_{j=0}^{q} A_j m^j, \tag{3.4.18}$$

where the coefficients A_j are defined as

$$A_j = \begin{pmatrix} z \\ j \end{pmatrix} \cosh^{q-j}(J\nabla)\sinh^j(J\nabla)f(x)|_{x=0}, \tag{3.4.19}$$

which can be calculated numerically using the relation $e^{\alpha\nabla} f(x) = f(x + \alpha)$ where α is a constant variable. Following the same procedure and by using the exponential form of hyperbolic functions in Eq. (3.4.19) we get

$$\cosh^{q-j}(J\nabla)\sinh^j(J\nabla) = \sum_{k=0}^{q-j}\sum_{s=0}^{j} \frac{(-1)^s}{2^q} \begin{pmatrix} q-j \\ j \end{pmatrix} \begin{pmatrix} j \\ s \end{pmatrix} \exp\left[(q-2k-2s)J\nabla\right]. \tag{3.4.20}$$

With the help of Eqs. (3.4.19) and (3.4.20), magnetization of the system can be easily evaluated as a function of temperature for any coordination number q from Eq. (3.4.18). The numerical results are depicted in Fig. 3.14.

As seen in Fig. 3.14, magnetization of the system decreases with increasing temperature and vanishes at the transition temperature. Moreover, the transition temperature increases as the coordination number rises. Since the magnetization m is very small in the vicinity of critical temperature, we can linearize Eq. (3.4.18) to obtain the numerical value of the transition temperature. Hence, by expanding the right-hand side of Eq. (3.4.18) and taking only the linear terms we get

$$1 = q\cosh^{q-1}(J\nabla)\sinh(J\nabla)f(x)|_{x=0}, \tag{3.4.21}$$
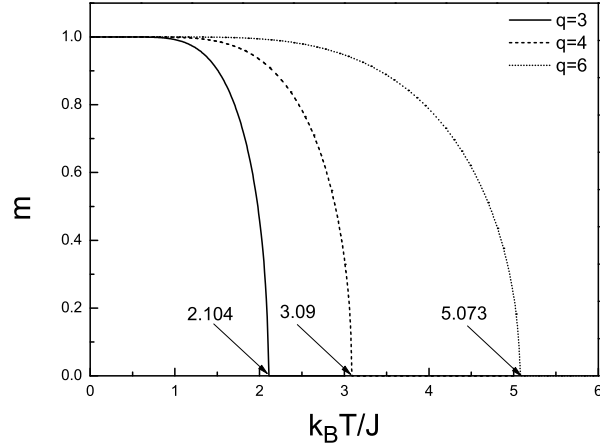
Figure 3.14 Magnetization versus temperature curves for lattices with coordination numbers $q = 3, 4, 6$. The numbers accompanying each curve denote the transition temperatures.

for any coordination number q. The numerical values of transition temperatures for various lattices obtained from Eq. (3.4.21) are also depicted in Fig. 3.14. These values are identical to those obtained from Zernike approximation (Zernike, 1940). We should also note that the inclusion of single-site correlations in the calculations apparently improves the MFT results.

Historically, the differential operator technique proposed in this subsection is also named as Matsudaira approximation (Matsudaira, 1973), functional integration method (Kaneyoshi, 1980) and finite cluster approximation (Boccara & Saber, 1985). Physical conclusions of all of these works are identical to that of the Zernike approximation, however due to its mathematical simplicity and relative easiness of the formulation for the extension to higher spin problems, the differential operator technique has been more favored than the other formalisms (Kaneyoshi, 1993).

So far we have dealt with the formulation of the differential operator technique for spin-1/2 Ising model. Now, in order to extend the formulation for higher spins, let us concentrate on the spin-1 Blume-Capel model (Blume, 1966, Capel, 1966) which is given by the following Hamiltonian

$$\mathcal{H} = -J \sum_{<ij>} S_i^z S_j^z - D \sum_i (S_i^z)^2, \qquad (3.4.22)$$

where the spin variable can take three possible values as $S_i^z = \pm 1, 0$ and term D in the second summation is crystal field interaction (i.e. single ion anisotropy) which simply corresponds to the energy difference between the magnetic ($S = \pm 1$) and non-magnetic ($S = 0$) states.

Now by following the same procedure as in the spin-1/2 problem and using the relation

$$e^{\alpha S_i^z} = (S_i^z)^2 \cosh(\alpha) + S_i^z \sinh(\alpha) + 1 - (S_i^z)^2, \quad S_i^z = \pm 1, 0, \qquad (3.4.23)$$

we obtain the thermal average of the magnetization

$$\left\langle \{f_i\} S_i^z \right\rangle = \left\langle \{f_i\} \prod_j \left[(S_j^z)^2 \cosh(J\nabla) + S_j^z \sinh(J\nabla) + 1 - (S_j^z)^2 \right] \right\rangle F(x)|_{x=0}. \qquad (3.4.24)$$

If we expand the right-hand side of Eq. (3.4.24) then the multi-spin correlation functions appear. At this point we use the decoupling approximation for the spin-1 system given by

$$\left\langle S_j^z (S_k^z)^2 ... S_l^z \right\rangle \cong \left\langle S_j^z \right\rangle \left\langle (S_k^z)^2 \right\rangle ... \left\langle S_l^z \right\rangle. \qquad (3.4.25)$$

Using the approximation (3.4.25) with $\{f_i\} = 1.0$ yields

$$\left\langle S_i^z \right\rangle = \prod_j \left[\left\langle (S_j^z)^2 \right\rangle \cosh(J\nabla) + \left\langle S_j^z \right\rangle \sinh(J\nabla) + 1 - \left\langle (S_j^z)^2 \right\rangle \right] F(x)|_{x=0}, \qquad (3.4.26)$$

where

$$F(x) = \frac{2 \sinh(\beta x)}{2 \cosh(\beta x) + e^{-\beta D}}. \qquad (3.4.27)$$

By using the approximation (3.4.25) in Eq. (3.4.24) we neglect the correlations between different sites, however the single-site correlations are exactly taken into account. As seen from Eq. (3.4.26) the magnetization depends on another parameter $\left\langle (S_i^z)^2 \right\rangle$.

The parameter $\left\langle (S_i^z)^2 \right\rangle$ can be easily obtained from

$$\left\langle (S_i^z)^2 \right\rangle = \frac{1}{Z} \left\{ \mathrm{Tr} e^{-\beta \mathcal{H}} \left[\frac{\mathrm{tr}_i (S_i^z)^2 e^{-\beta H_i}}{\mathrm{tr}_i e^{-\beta H_i}} \right] \right\}, \qquad (3.4.28)$$

and it is found as

$$\left\langle (S_i^z)^2 \right\rangle = \prod_j \left[\left\langle (S_j^z)^2 \right\rangle \cosh(J\nabla) + \left\langle S_j^z \right\rangle \sinh(J\nabla) + 1 - \left\langle (S_j^z)^2 \right\rangle \right] G(x)|_{x=0}, \qquad (3.4.29)$$

with

$$G(x) = \frac{2\cosh(\beta x)}{2\cosh(\beta x) + e^{-\beta D}}. \tag{3.4.30}$$

By assuming $m = \langle S_i^z \rangle$ and $y = \langle (S_i^z)^2 \rangle$, we obtain from Eqs. (3.4.26) and (3.4.29)

$$m = [y\cosh(J\nabla) + m\sinh(J\nabla) + 1 - y]^q F(x)|_{x=0}, \tag{3.4.31}$$

and

$$y = [y\cosh(J\nabla) + m\sinh(J\nabla) + 1 - y]^q G(x)|_{x=0}. \tag{3.4.32}$$

Magnetization m and quadrupolar moment y can be numerically evaluated by solving these coupled nonlinear equations. In addition, it is also possible to discuss the critical properties by expanding the right-hand sides of Eqs. (3.4.31) and (3.4.32) by assuming $m \to 0$ in the vicinity of critical temperature. Hence, in general we obtain

$$m = am + bm^3 + ..., \tag{3.4.33}$$

$$y = a' + b'm^2 + ..., \tag{3.4.34}$$

where

$$a = q[y\cosh(J\nabla) + 1 - y]^{q-1} \sinh(J\nabla)F(x)|_{x=0}, \tag{3.4.35}$$

$$b = \frac{q!}{3!(q-3)!}[y\cosh(J\nabla) + 1 - y]^{q-3} \sinh^3(J\nabla)F(x)|_{x=0}, \tag{3.4.36}$$

$$a' = [y\cosh(J\nabla) + 1 - y]^q G(x)|_{x=0}, \tag{3.4.37}$$

$$b' = \frac{q!}{2!(q-2)!}[y\cosh(J\nabla) + 1 - y]^{q-2} \sinh^2(J\nabla)G(x)|_{x=0}. \tag{3.4.38}$$

The second order phase transition line is determined from the condition

$$a = 1 \quad \text{and} \quad b < 0. \tag{3.4.39}$$

In the vicinity of the second-order transition temperature, the magnetization m is given by

$$m^2 = \frac{1-a}{b}. \tag{3.4.40}$$

The right-hand side of Eq. (3.4.40) must be positive. If it is not then the transition is of the first order. Hence the point at which

$$a = 1 \quad \text{and} \quad b = 0. \tag{3.4.41}$$

is the tricritical point (Kaneyoshi, 1993, 1986).

In this context, the phase diagrams in $(k_B T_c / J - D / J)$ plane obtained within the framework of differential operator technique based on decoupling approximation for various coordination numbers are depicted in Fig. 3.15. In Fig. 3.15, the solid (dashed) lines correspond to second (first) order phase transition lines and the tricritical points are shown by hollow circles. In the highly anisotropic case $(D \to \infty)$, we have $y = 1$ for the whole range of temperature and the spin-1 Blume Capel model reduces to spin-1/2 Ising model.
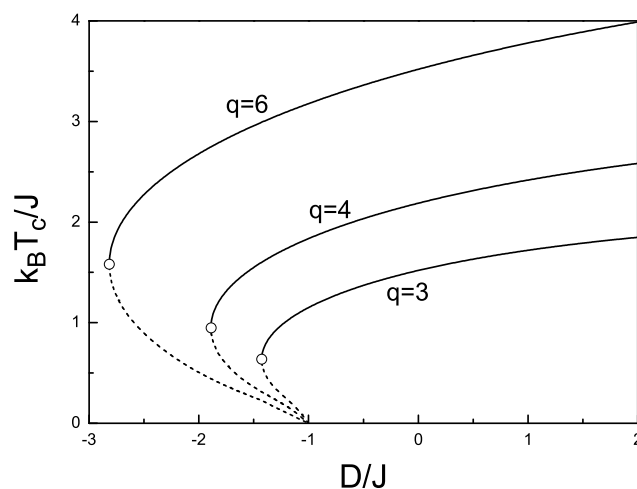
Figure 3.15 Phase diagrams of spin-1 Blume-Capel model obtained from differential operator technique in a $(k_B T_c / J - D / J)$ plane for lattices with $q = 3, 4$ and 6. The solid (dashed) lines correspond to second (first) order phase transition lines whereas hollow circles denote the tricritical points.

Finally, we note that the structures of the functions $F(x)$ and $G(x)$ defined in Eqs. (3.4.27) and (3.4.30) depend on the types of interactions defined in the Hamiltonian but they are independent of the lattice geometry. In a simple and practical manner, it is possible to determine these functions from the local Hamiltonian H_i of the site i. For instance, let us consider the spin-1 Blume Capel model where the local Hamiltonian

H_i is given by

$$H_i = -\left(J \sum_j S_j^z\right) S_i^z - D(S_i^z)^2 = -E_i S_i^z - D(S_i^z)^2. \qquad (3.4.42)$$

By inserting the $z-$ component of Pauli spin operator S_i^z for spin-1 in Eq. (3.4.42), we can get the matrix form of $-H_i$ as follows

$$-H_i = \begin{pmatrix} -E_i - D & 0 & 0 \\ 0 & 0 & 0 \\ 0 & 0 & E_i - D \end{pmatrix}, \qquad (3.4.43)$$

then the functions $F(x)$ and $G(x)$ are defined as follows

$$F(x) = \frac{1}{\sum_{n=1}^{d} \exp(\beta\lambda_n)} \sum_{n=1}^{d} \left\langle \phi_n | S_i^z | \phi_n \right\rangle \exp(\beta\lambda_n), \qquad (3.4.44)$$

$$G(x) = \frac{1}{\sum_{n=1}^{d} \exp(\beta\lambda_n)} \sum_{n=1}^{d} \left\langle \phi_n | (S_i^z)^2 | \phi_n \right\rangle \exp(\beta\lambda_n), \qquad (3.4.45)$$

where d is the dimensionality, λ_n represents the eigenvalues and ϕ_n denotes the normalized eigenvectors corresponding to the eigenvalues λ_n of the matrix $-H_i$, respectively. This formalism is also valid for a general spin-S model.

3.4.2 Correlated Effective Field (Bethe-Peierls) Approximation

In order to improve the formalism of decoupling approximation depicted above, (Kaneyoshi et al., 1981) have attempted to describe a formulation for the consideration of multi-site correlations in their calculations by introducing the concept of a correlated effective field into the many-body correlation functions of neighboring spins of a particular site instead of decoupling approximation. Their formalism can be briefly described as follows:

For simplicity let us discuss the problem for a square lattice with $q = 4$ and define a cluster of $q + 1$ spins as shown in Fig. 3.16 where the spin variables located at the central and perimeter lattice sites are denoted as S_0 and S_j, $(j = 1, ..., 4)$, respectively. In the absence of magnetic field ($h = 0$), the Hamiltonian (3.4.1) which has been defined
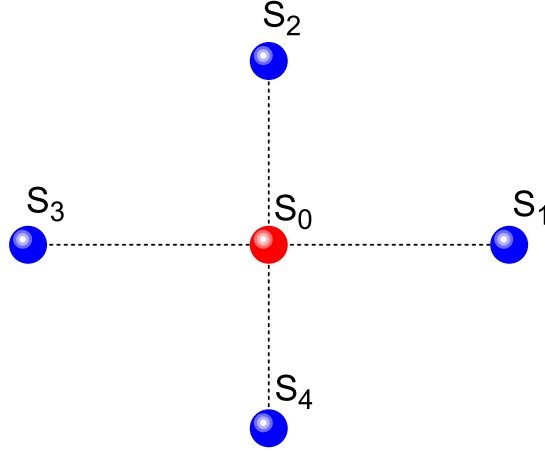
Figure 3.16 A cluster of $q + 1$ spins defined on a square lattice where the spin variables S_i are located on each lattice site.

for a spin-1/2 system yields

$$\langle \{f_i\} S_0 \rangle = \left\langle \{f_i\} \prod_{j=1}^{q} \left[\cosh(J\nabla) + S_j \sinh(J\nabla) \right] \right\rangle f(x)|_{x=0}, \qquad (3.4.46)$$

where $f(x) = \tanh(\beta x)$ and the superscript z of the spin variable is omitted for simplicity. By expanding the right-hand side of Eq. (3.4.46) for $q = 4$ with $\{f_i\} = 1.0$ we get

$$\langle S_0 \rangle = K_1 (S_1 + S_2 + S_3 + S_4) + K_2 (S_1 S_2 S_3 + S_2 S_3 S_4 + S_1 S_2 S_4 + S_1 S_3 S_4), \quad (3.4.47)$$

where

$$
\begin{aligned}
K_1 &= \frac{1}{8} \tanh(4\beta J) + \frac{1}{4} \tanh(2\beta J), \\
K_2 &= \frac{1}{8} \tanh(4\beta J) - \frac{1}{4} \tanh(2\beta J).
\end{aligned}
\qquad (3.4.48)
$$

Now, instead of using decoupling approximation (3.4.16), let us introduce the concept of correlated effective field for a particular perimeter site;

$$
\begin{aligned}
S_j &= \langle S_j \rangle + \lambda(S_0 - \langle S_0 \rangle), \quad j = 1, ..., 4 \\
&= m + \lambda(S_0 - m),
\end{aligned}
\qquad (3.4.49)
$$

where λ is a temperature-dependent static correlation parameter (Kaneyoshi et al., 1981).

In order to treat the three-site correlations in Eq. (3.4.47) we use Eq. (3.4.49) by taking into account the translational symmetry of the system as follows

$$S_j S_k S_l = [m + \lambda(S_0 - m)]^3, \quad j \neq k \neq l \tag{3.4.50}$$

hence with $\langle S_0^2 \rangle = 1$ and $\langle S_0^3 \rangle = \langle S_0 \rangle = m$ we get

$$\langle S_1 S_2 S_3 \rangle = m^3 + \lambda^2(3m - 3m^3) + \lambda^3(-2m + 2m^3). \tag{3.4.51}$$

By inserting Eqs. (3.4.49) and (3.4.51) in Eq. (3.4.47) we have

$$m = Am + Bm^3, \tag{3.4.52}$$

with

$$A = 4K_1 + 12K_2\lambda^2 - 8K_2\lambda^3, \tag{3.4.53}$$

and

$$B = 4K_2(1 - 3\lambda^2 + 3\lambda^3), \tag{3.4.54}$$

from which the magnetization m is given by

$$m = \sqrt{\frac{1-A}{B}}. \tag{3.4.55}$$

In order to get a numerical solution for m and λ concerning the critical properties of the system we need another equation. Namely, for $\{f_i\} = S_1$ in Eq. (3.4.46) and using the relations $\langle S_i^2 \rangle = 1$ and $\langle S_i^3 \rangle = \langle S_i \rangle$

$$
\begin{aligned}
\langle S_0 S_1 \rangle =\ & K_1 + K_1\left[\langle S_1 S_2 \rangle + \langle S_1 S_3 \rangle + \langle S_2 S_4 \rangle\right] \\
& + K_2\left[\langle S_2 S_3 \rangle + \langle S_2 S_4 \rangle + \langle S_3 S_4 \rangle\right] \\
& + K_2\langle S_1 S_2 S_3 S_4 \rangle,
\end{aligned} \tag{3.4.56}
$$

where the two-site and four-site correlations can be obtained from Eq. (3.4.49) and they are found as

$$
\begin{aligned}
\langle S_0 S_1 \rangle &= m^2 + \lambda(1 - m^2), \\
\langle S_1 S_2 \rangle &= m^2 + \lambda^2 - m^2\lambda^2, \\
\langle S_1 S_2 S_3 S_4 \rangle &= \lambda^4 + (6\lambda^2 - 8\lambda^3 + 2\lambda^4)m^2 + (1 - 6\lambda^2 + 8\lambda^3 - 3\lambda^4)m^4.
\end{aligned}
$$

$$\tag{3.4.57}$$

As a result, combining Eqs. (3.4.56) and (3.4.57) yields

$$
\begin{aligned}
m^2 + \lambda(1-m^2) \;=\;& K_1 + 3(K_1+K_2)m^2 + K_2 m^4 + 3(K_1+K_2+2K_2 m^2)(1-m^2)\lambda^2 \\
& -8K_2 m^2(1-m^2)\lambda^3 + K_2(1+3m^2)(1-m^2)\lambda^4.
\end{aligned}
\tag{3.4.58}
$$

Thus, magnetization and the correlated-effective field parameter can be determined by solving the coupled Eqs. (3.4.55) and (3.4.58). Moreover, the transition temperature T_c and the correlated-effective field parameter λ_c at T_c can be numerically evaluated by linearizing Eqs. (3.4.52) and (3.4.58).
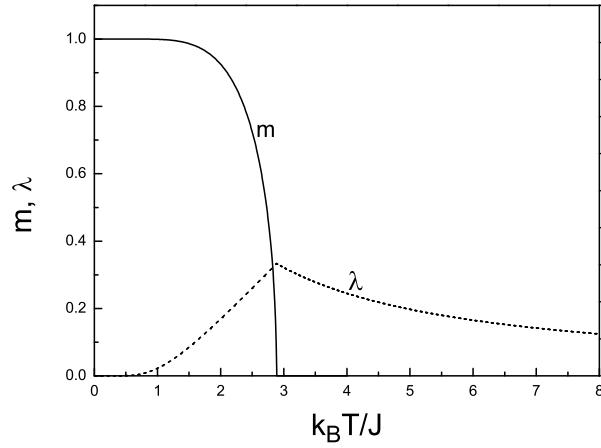
Figure 3.17 Temperature dependence of m and λ for a square lattice, (Kaneyoshi et al., 1981).

Hence, in the vicinity of the transition point we have

$$
4K_1 + 12K_2\lambda^2 - 8K_2\lambda^3 = 1,
\tag{3.4.59}
$$

and

$$
\lambda = K_1 + 3(K_1+K_2)\lambda^2 + K_2\lambda^4.
\tag{3.4.60}
$$

The numerical solution of Eqs. (3.4.59) and (3.4.60) yields

$$
k_B T_c/J = 2.8854, \quad \lambda_c = 1/3,
\tag{3.4.61}
$$

which improves the result of decoupling approximation. Variation of m and λ is depicted in Fig. 3.17. The results given in Eq. (3.4.61) can also be generalized for an arbitrary coordination number q (Kaneyoshi et al., 1981)

$$
k_B T_c/J = \frac{2}{\ln[q/(q-2)]}, \quad \lambda_c = \frac{1}{q-1}.
\tag{3.4.62}
$$

CHAPTER FOUR
IMPROVED EFFECTIVE FIELD THEORY WITH MULTI-SITE
CORRELATIONS

It is clear from previous discussions that a formalism in which the multi-site correlations are particularly considered certainly improves the results concerning the critical properties of the model systems. However, there are several possible ways of counting these multi-site correlation functions in the calculations and there exist various approximation techniques in the literature. Hence, in this chapter, our purpose is to present a detailed picture about the methods which have already been proposed in the literature, and clarify the advantages and disadvantages of these methods in a heuristic manner by comparing the qualitative and quantitative aspects of the numerical results.

For this aim, firstly we will describe the formulation of a recently introduced cluster theory (Kaneyoshi, 1999a,b) for spin-1/2 system and then treat the problem by performing the possible modifications introduced by us. As we shall see in the following discussions, our approximation scheme predicts very good results, especially for the numerical values of transition temperatures, and can be applicable to a wide variety of extensions of standard Ising model including the Blume-Capel model and the systems in the presence of transverse fields, as well as quenched disordered models. However, a detailed discussion of the applications of the method proposed by us will be the subject of the further discussions.

4.1   The Cluster Theory in Ising Systems with Differential Operator Technique

4.1.1   *Formulation for Spin-1/2 Ising System*

The model system is represented by the conventional spin-1/2 Hamiltonian in the presence of longitudinal magnetic field h with nearest-neighbor interactions

$$\mathcal{H} = -J \sum_{<ij>} S_i S_j - h \sum_i S_i. \tag{4.1.1}$$

Now, in order to proceed further, let us consider a regular lattice which has N identical spins arranged. We define a cluster on the lattice which consists of a central spin labeled S_0, and q perimeter spins being the nearest neighbors of the central spin. As shown in Fig. 4.1, the cluster consists of $q+1$ spins being independent from the spin operator $\hat{S}$. The nearest-neighbor spins are in an effective field produced by the outer spins, which can be determined by the condition that the thermal average of the central spin is equal to that of its nearest-neighbor spins. The main superiority of this method against the correlated effective-field theory is basically to approach the problem by considering a larger cluster (i.e. compare Figs. 3.16 and 4.1).
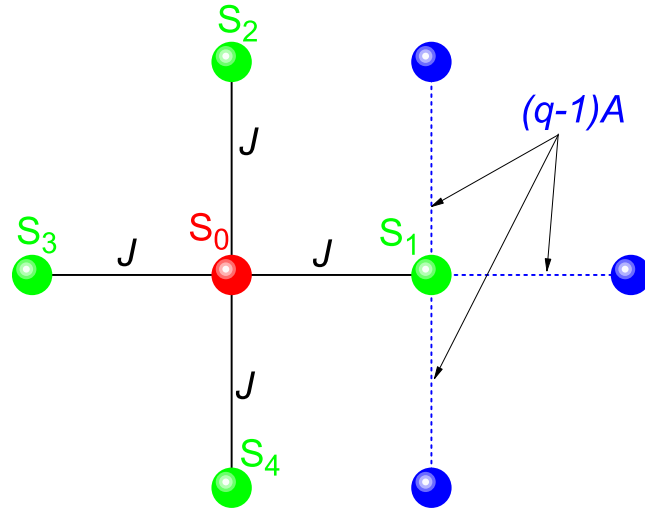
Figure 4.1 Schematic representation of the cluster model which consists of a central spin S_0 and q perimeter spins as the nearest neighbors of S_0. The interactions remaining out of the cluster are shown as dashed lines and they are represented by an effective field $\gamma = (q-1)A$.

Now, recall from Eq. (3.4.4) that the thermal average of central spin $\langle S_0 \rangle$ and a perimeter spin $\langle S_\delta \rangle$ can be evaluated using the local fields θ_0 and θ_δ as follows

$$\langle \{f_i\} S_0 \rangle = \langle \{f_i\} \tanh(\beta \theta_0) \rangle, \tag{4.1.2}$$

and

$$\langle \{g_i\} S_\delta \rangle = \langle \{g_i\} \tanh(\beta \theta_\delta) \rangle, \tag{4.1.3}$$

where $\theta_0 = J \sum_\delta S_\delta + h$ and $\theta_\delta = JS_0 + h + (q-1)A$, and A is an unknown parameter to

be determined self consistently. Applying differential operator technique (3.4.11) in Eqs. (4.1.2) and (4.1.3) yields

$$\langle \{f_i\} S_0 \rangle = \left\langle \{f_i\} \prod_{\delta=1}^{q} \cosh(J\nabla) + S_\delta \sinh(J\nabla) \right\rangle \tanh[\beta(x+h)]|_{x=0}, \qquad (4.1.4)$$

and

$$\langle \{g_i\} S_\delta \rangle = [\cosh(J\nabla) + S_0 \sinh(J\nabla)] \tanh[\beta(x+h+\gamma)], \qquad (4.1.5)$$

where $\gamma = (q-1)A$ is the effective field produced by the spins out of the cluster. Due to the translational symmetry of the system, we have

$$\langle S_1 \rangle = \langle S_2 \rangle = ... = \langle S_q \rangle. \qquad (4.1.6)$$

By remembering this property we can easily obtain the thermal average of central and perimeter spins by expanding the right-hand sides of Eqs. (4.1.4) and (4.1.5) with $\{f_i\} = \{g_i\} = 1.0$. For instance, for a square lattice ($q = 4$) we have

$$
\begin{aligned}
\langle S_0 \rangle &= K_0 + K_1 \sum_{\delta=1}^{q=4} \langle S_\delta \rangle + K_2 \sum_{\delta \neq \delta'} \langle S_\delta S_{\delta'} \rangle + K_3 \sum_{\delta \neq \delta' \neq \delta''} \langle S_\delta S_{\delta'} S_{\delta''} \rangle \\
&\quad + K_4 \sum_{\delta \neq \delta' \neq \delta'' \neq \delta'''} \langle S_\delta S_{\delta'} S_{\delta''} S_{\delta'''} \rangle, \\
&= K_0 + 4K_1 \langle S_1 \rangle + 6K_2 \langle S_1 S_2 \rangle + 4K_3 \langle S_1 S_2 S_3 \rangle + K_4 \langle S_1 S_2 S_3 S_4 \rangle \\
\langle S_1 \rangle &= a_1 + a_2 \langle S_0 \rangle, \qquad (4.1.7)
\end{aligned}
$$

where the coefficients are defined as

$$
\begin{aligned}
K_0 &= \frac{3}{8}\tanh(\beta h) + \frac{1}{16}\tanh[\beta(-4J+h)] + \frac{1}{4}\tanh[\beta(-2J+h)] \\
&\quad + \frac{1}{4}\tanh[\beta(2J+h)] + \frac{1}{16}\tanh[\beta(4J+h)], \\
K_1 &= -\frac{1}{16}\tanh[\beta(-4J+h)] - \frac{1}{8}\tanh[\beta(-2J+h)] \\
&\quad + \frac{1}{8}\tanh[\beta(2J+h)] + \frac{1}{16}\tanh[\beta(4J+h)], \\
K_2 &= -\frac{1}{8}\tanh[\beta h] + \frac{1}{16}\tanh[\beta(-4J+h)] + \frac{1}{16}\tanh[\beta(4J+h)], \\
K_3 &= -\frac{1}{16}\tanh[\beta(-4J+h)] + \frac{1}{8}\tanh[\beta(-2J+h)] \\
&\quad - \frac{1}{8}\tanh[\beta(2J+h)] + \frac{1}{16}\tanh[\beta(4J+h)], \\
K_4 &= \frac{3}{8}\tanh(\beta h) + \frac{1}{16}\tanh[\beta(-4J+h)] - \frac{1}{4}\tanh[\beta(-2J+h)] \\
&\quad - \frac{1}{4}\tanh[\beta(2J+h)] + \frac{1}{16}\tanh[\beta(4J+h)], \qquad (4.1.8)
\end{aligned}
$$

and

$$a_1 = \frac{1}{2}\tanh[\beta(-J+h+\gamma)] + \frac{1}{2}\tanh[\beta(J+h+\gamma)],$$

$$a_2 = -\frac{1}{2}\tanh[\beta(-J+h+\gamma)] + \frac{1}{2}\tanh[\beta(J+h+\gamma)]. \tag{4.1.9}$$

The single-site correlation functions $\langle S_0 \rangle$ and $\langle S_1 \rangle$ obtained in Eq. (4.1.7) are the fundamental correlation functions of the system. In a recent work (Kaneyoshi, 1999a), a method has been proposed which accounts the multi-site correlation functions systematically. Namely, the two-site correlation functions $\langle S_0 S_1 \rangle$ and $\langle S_1 S_2 \rangle$ are simply obtained from perimeter spin correlation $\langle S_1 \rangle$ in Eq. (4.1.7) and they are found as

$$\langle S_0 S_1 \rangle = a_1 \langle S_0 \rangle + a_2, \tag{4.1.10}$$

and

$$\langle S_1 S_2 \rangle = a_1 \langle S_1 \rangle + a_2 \langle S_0 S_1 \rangle. \tag{4.1.11}$$

Similarly, the three-site correlation functions $\langle S_0 S_1 S_2 \rangle$ and $\langle S_1 S_2 S_3 \rangle$ are obtained from Eqs. (4.1.10) and (4.1.11), respectively and they are given as follows

$$\langle S_0 S_1 S_2 \rangle = a_1 \langle S_0 S_1 \rangle + a_2 \langle S_1 \rangle, \tag{4.1.12}$$

and

$$\langle S_1 S_2 S_3 \rangle = a_1 \langle S_1 S_2 \rangle + a_2 \langle S_0 S_1 S_2 \rangle. \tag{4.1.13}$$

One of the remaining two correlation functions, namely the four-site correlation function $\langle S_1 S_2 S_3 S_4 \rangle$ can be obtained from Eq. (4.1.13);

$$\langle S_1 S_2 S_3 S_4 \rangle = a_1 \langle S_1 S_2 S_3 \rangle + a_2 \langle S_0 S_1 S_2 S_3 \rangle. \tag{4.1.14}$$

Finally, for $\langle S_0 S_1 S_2 S_3 \rangle$ we use Eq. (4.1.12) and we get

$$\langle S_0 S_1 S_2 S_3 \rangle = a_1 \langle S_0 S_1 S_2 \rangle + a_2 \langle S_1 S_2 \rangle. \tag{4.1.15}$$

In evaluating Eqs. (4.1.10)-(4.1.15), we use the fact $\langle S_i^2 \rangle = 1$ which is due to the property of the z component of spin operator $\hat{S}$. At this stage, in order to determine the numerical value of A, let us introduce the condition

$$\langle S_0 \rangle = \langle S_1 \rangle. \tag{4.1.16}$$

Eqs. (4.1.10)-(4.1.15) with (4.1.7) constitute a system of linear equations and can be represented in a matrix form

$$M = \begin{pmatrix} 1 & -4K_1 & 0 & 0 & 0 & -6K_2 & -4K_3 & -K_4 \\ -a_2 & 1 & 0 & 0 & 0 & 0 & 0 & 0 \\ -a_1 & 0 & 1 & 0 & 0 & 0 & 0 & 0 \\ 0 & -a_2 & -a_1 & 1 & 0 & 0 & 0 & 0 \\ 0 & 0 & 0 & -a_1 & 1 & -a_2 & 0 & 0 \\ 0 & -a_1 & -a_2 & 0 & 0 & 1 & 0 & 0 \\ 0 & 0 & 0 & -a_2 & 0 & -a_1 & 1 & 0 \\ 0 & 0 & 0 & 0 & -a_2 & 0 & -a_1 & 1 \end{pmatrix}, Y = \begin{pmatrix} K_0 \\ a_1 \\ a_2 \\ 0 \\ 0 \\ 0 \\ 0 \\ 0 \end{pmatrix}, \quad (4.1.17)$$

with unknowns

$$
\begin{aligned}
x_1 &= \langle S_0 \rangle, \\
x_2 &= \langle S_1 \rangle, \\
x_3 &= \langle S_0 S_1 \rangle, \\
x_4 &= \langle S_0 S_1 S_2 \rangle, \\
x_5 &= \langle S_0 S_1 S_2 S_3 \rangle, \\
x_6 &= \langle S_1 S_2 \rangle, \\
x_7 &= \langle S_1 S_2 S_3 \rangle, \\
x_8 &= \langle S_1 S_2 S_3 S_4 \rangle.
\end{aligned}
\qquad (4.1.18)
$$

By solving Eq. (4.1.17) with the help of Eq. (4.1.16) we can obtain the temperature dependence of correlation functions listed in Eq. (4.1.18). In the absence of external field, ($h = 0$) the transition temperature $k_B T_c / J$ can be obtained by assuming $\gamma \to 0$ in the vicinity of $k_B T_c / J$ which leads to the result

$$k_B T_c / J = 2.8854, \qquad (4.1.19)$$

for a square lattice ($q = 4$). Surprisingly, this result is completely the same as that of correlated effective field-theory (Kaneyoshi, Fittipaldi, Honmura, & Manabe, 1981), although we consider a relatively larger cluster within the latter approach.

However, there is not a unique process to obtain the correlation identities within the present formulation, and this is the most vital point in the calculations. For instance, the two site correlation function $\langle S_0 S_1 \rangle$ can also be obtained from $\langle S_0 \rangle$, instead of $\langle S_1 \rangle$ in Eq. (4.1.7). Consequently, the correlation functions x_3, x_4 and x_5 in Eq. (4.1.18) can be derived on the basis of x_1, instead of x_2. The most useful advantage of this method can be clarified as follows: From Eqs. (4.1.7) and (4.1.10)-(4.1.15) we see that the whole set of the correlation identities except $x_1 = \langle S_0 \rangle$ have been obtained as a function of the coefficients a_1 and a_2 which contain the effect of the spins out of the cluster as an approximated effective field. It possible to improve the method by reducing the number of correlation identities containing the effective field parameter γ which means that we should derive the correlation functions $\langle S_0 S_1 \rangle$, $\langle S_0 S_1 S_2 \rangle$ and $\langle S_0 S_1 S_2 S_3 \rangle$ on the basis of $\langle S_0 \rangle$. By following this procedure we get the following set of the correlation functions

$$
\begin{aligned}
\langle S_0 \rangle &= K_0 + 4K_1 \langle S_1 \rangle + 6K_2 \langle S_1 S_2 \rangle + 4K_3 \langle S_1 S_2 S_3 \rangle + K_4 \langle S_1 S_2 S_3 S_4 \rangle, \\
\langle S_1 \rangle &= a_1 + a_2 \langle S_0 \rangle, \\
\langle S_0 S_1 \rangle &= 4K_1 + (K_0 + 6K_2) \langle S_1 \rangle + 4K_3 \langle S_1 S_2 \rangle + K_4 \langle S_1 S_2 S_3 \rangle, \\
\langle S_0 S_1 S_2 \rangle &= (K_0 + 6K_2 + K_4) \langle S_1 S_2 \rangle + 4(K_1 + K_3) \langle S_1 \rangle, \\
\langle S_0 S_1 S_2 S_3 \rangle &= (K_0 + 6K_2 + K_4) \langle S_1 S_2 S_3 \rangle + 4(K_1 + K_3) \langle S_1 S_2 \rangle, \\
\langle S_1 S_2 \rangle &= a_1 \langle S_1 \rangle + a_2 \langle S_0 S_1 \rangle, \\
\langle S_1 S_2 S_3 \rangle &= a_1 \langle S_1 S_2 \rangle + a_2 \langle S_0 S_1 S_2 \rangle, \\
\langle S_1 S_2 S_3 S_4 \rangle &= a_1 \langle S_1 S_2 S_3 \rangle + a_2 \langle S_0 S_1 S_2 S_3 \rangle, \quad\quad\quad\quad (4.1.20)
\end{aligned}
$$

Solution of Eq. (4.1.20) with the help of Eq. (4.1.16) yields

$$
k_B T_c / J = 2.536, \quad\quad\quad\quad (4.1.21)
$$

which certainly improves the numerical results based on decoupling approximation (DA) (Kaneyoshi, 1993), as well the correlated effective field theory (CEFT) (Kaneyoshi et al., 1981) and the cluster theory (EFT) of (Kaneyoshi, 1999a). Our formulation has recently been extended to an arbitrary coordination number q (Akinci, 2011). In Table 4.1, we compare the critical temperature $k_B T_c / J$ of the system obtained

within the present approach with those of the other methods in the literature for various coordination numbers. As seen in Table 4.1, our formulation gives the best approximated values for the numerical values of the critical temperatures when compared with other methods. Note that the results obtained by series expansion method (Fisher, 1967) are regarded as exact values. Moreover, the superiority of the present approximation is also quite evident from Fig. 4.2 where the magnetization versus reduced temperature curves are plotted for a square lattice within the framework of several approximation schemes, as well as exact treatment.

Table 4.1 The critical temperatures of a spin-1/2 system obtained by several approximations as well as exact results and the results of the present work.

Lattice	MFA	DA	CEFT	EFT	Present Work	Exact
3	3.0	2.104	1.821	1.821	1.504	1.519
4	4.0	3.090	2.885	2.885	2.536	2.269
6	6.0	5.073	4.933	4.933	4.527	4.511
8	8.0	7.061	6.952	6.952	6.516	6.353
12	12.0	11.045	10.970	10.970	10.499	9.795
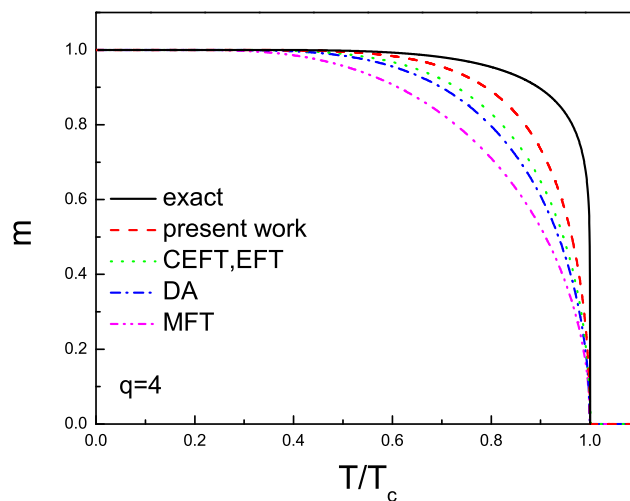
Figure 4.2 Variation of magnetization $m = \langle S_0 \rangle$ of a square lattice ($q = 4$) with temperature obtained by several methods in comparison with the exact result and the present work.

4.1.2 *Formulation for Spin-1 Blume-Capel Model*

Now, we are in a position of extending our formulation to more complicated models by considering a spin-1 system with a single-ion anisotropy D, i.e. Blume-Capel model (Blume, 1966, Capel, 1966). For simplicity, let us consider the problem on a honeycomb lattice ($q = 3$). However, a generalized formulation for an arbitrary coordination number can be found in (Akinci, 2012). As we mentioned in preceding discussions, the Hamiltonian of a spin-1 Blume-Capel model is given by

$$\mathcal{H} = -J \sum_{<ij>} S_i^z S_j^z - D \sum_i (S_i^z)^2, \tag{4.1.22}$$

where the first summation is taken over the nearest-neighbor spins with $S_i^z = \pm 1, 0$. Within the differential operator technique (Kaneyoshi, 1993), and using Eq. (3.4.23) with $\{f_i\} = 1.0$, the average value of the central spin S_0, namely the longitudinal magnetization $m_z = \langle S_0 \rangle$ and quadrupolar moment $q_z = \langle (S_0)^2 \rangle$ in the cluster of $q + 1$ spins (c.f. see Fig. 4.1) can be obtained as follows

$$m = \langle S_0 \rangle = \left\langle \prod_{j=1}^{3} \left[(S_j)^2 \cosh(J\nabla) + S_j \sinh(J\nabla) + 1 - (S_j)^2 \right] \right\rangle F(x)|_{x=0}, \tag{4.1.23}$$

and

$$q_z = \langle (S_0)^2 \rangle = \left\langle \prod_{j=1}^{3} \left[(S_j)^2 \cosh(J\nabla) + S_j \sinh(J\nabla) + 1 - (S_j)^2 \right] \right\rangle G(x)|_{x=0}, \tag{4.1.24}$$

where the functions $F(x)$ and $G(x)$ can be easily obtained from Eqs. (3.4.44) and (3.4.45). Note that the superscript z is omitted for simplicity.

Corresponding to Eqs. (4.1.23) and (4.1.24), magnetization and quadrupolar moment of a perimeter spin are defined by

$$\langle S_1 \rangle = \left\langle (S_0)^2 \cosh(J\nabla) + S_0 \sinh(J\nabla) + 1 - (S_0)^2 \right\rangle F(x + \gamma)|_{x=0}, \tag{4.1.25}$$

and

$$\langle (S_1)^2 \rangle = \left\langle (S_0)^2 \cosh(J\nabla) + S_0 \sinh(J\nabla) + 1 - (S_0)^2 \right\rangle G(x + \gamma)|_{x=0}, \tag{4.1.26}$$

where $\gamma = (q - 1)A$ is the effective field produced by the spins out of the cluster of $q + 1$ spins.

The next step is to expand the right-hand sides of Eqs. (4.1.23) and (4.1.24) which yields

$$\langle S_0 \rangle = 3k_1 \langle S_1 \rangle + 6(k_2 - k_1)\langle S_1 S_2^2 \rangle + k_3 \langle S_1 S_2 S_3 \rangle$$

$$+3(k_1 - 2k_2 + k_4)\langle S_1 S_2^2 S_3^2 \rangle, \tag{4.1.27}$$

and

$$\langle (S_0)^2 \rangle = r_0 + 3(r_1 - r_0)\langle S_1^2 \rangle + 3r_2 \langle S_1 S_2 \rangle$$

$$+3(r_0 - 2r_1 + r_3)\langle S_1^2 S_2^2 \rangle + 3(r_4 - r_2)\langle S_1 S_2 S_3^2 \rangle$$

$$+(-r_0 + 3r_1 - 3r_3 + r_5)\langle S_1^2 S_2^2 S_3^2 \rangle, \tag{4.1.28}$$

where

$$r_0 = G(0),$$

$$k_1 = \sinh(J\nabla)F(x)|_{x=0}, \qquad r_1 = \cosh(J\nabla)G(x)|_{x=0},$$

$$k_2 = \cosh(J\nabla)\sinh(J\nabla)F(x)|_{x=0}, \qquad r_2 = \sinh^2(J\nabla)G(x)|_{x=0},$$

$$k_3 = \sinh^3(J\nabla)F(x)|_{x=0}, \qquad r_3 = \cosh^2(J\nabla)G(x)|_{x=0},$$

$$k_4 = \cosh^2(J\nabla)\sinh(J\nabla)F(x)|_{x=0}, \qquad r_4 = \cosh(J\nabla)\sinh^2(J\nabla)G(x)|_{x=0},$$

$$r_5 = \cosh^3(J\nabla)G(x)|_{x=0}, \tag{4.1.29}$$

by noticing that due to the symmetry properties of the functions $F(x)$ and $G(x)$, some of the coefficients simply drop out in the absence of external magnetic field.

Similarly, corresponding to Eqs. (4.1.27) and (4.1.28), for the perimeter spin correlation functions we have

$$\langle S_1 \rangle = a_1(1 - \langle S_0^2 \rangle) + a_2 \langle S_0 \rangle + a_3 \langle S_0^2 \rangle, \tag{4.1.30}$$

and

$$\langle (S_1)^2 \rangle = b_1(1 - \langle S_0^2 \rangle) + b_2 \langle S_0 \rangle + b_3 \langle S_0^2 \rangle, \tag{4.1.31}$$

with

$$a_1 = F(\gamma), \qquad b_1 = G(\gamma),$$

$$a_2 = \sinh(J\nabla)F(x+\gamma)|_{x=0}, \qquad b_2 = \sinh(J\nabla)G(x+\gamma)|_{x=0},$$

$$a_3 = \cosh(J\nabla)F(x+\gamma)|_{x=0}, \qquad b_3 = \cosh(J\nabla)G(x+\gamma)|_{x=0}. \tag{4.1.32}$$

The coefficients in Eqs. (4.1.29) and (4.1.32) can be numerically evaluated as a function of system parameters from the relation $e^{\alpha\nabla}f(x) = f(x+\alpha)|_{x=0}$. Moreover, if we apply decoupling approximation

$$
\begin{aligned}
\langle S_1 S_2^2 \rangle &= \langle S_1 \rangle \langle S_2^2 \rangle = my, \\
\langle S_1 S_2^2 S_3^2 \rangle &= \langle S_1 \rangle \langle S_2^2 \rangle \langle S_3^2 \rangle = my^2, \\
\langle S_1 S_2 S_3 \rangle &= \langle S_1 \rangle \langle S_2 \rangle \langle S_3 \rangle = m^3,
\end{aligned}
\tag{4.1.33}
$$

then Eqs. (4.1.27) and (4.1.28) reduce to Eqs. (3.4.31) and (3.4.32) with $q = 3$, respectively. Hence, one advantage of the present approximation method proposed within this thesis report is that no uncontrolled decoupling procedure is used for the higher-order correlation functions.

Eqs. (4.1.27), (4.1.28), (4.1.30) and (4.1.31) are fundamental correlation functions of the system. For spin-1 Ising system with $q = 3$, taking these equations as a basis we derive a set of linear equations of the spin correlation functions which interact in the system. Throughout the derivations (including the expansions of Eqs. (4.1.23) and (4.1.24)), we use the properties $(\hat{S}_\delta)^4 = (\hat{S}_\delta)^2$ and $(\hat{S}_\delta)^3 = \hat{S}_\delta$ for $z-$ component of operator $\hat{S}$ for spin-1. In addition, by taking into account the translational symmetry of the system, we make the following assumptions

$$
\begin{aligned}
\langle S_1^n \rangle &= \langle S_\delta^n \rangle;\ n = 1,2 \text{ and } \delta = 2,..,q \\
\langle S_1 S_2^n \rangle &= \langle S_\delta S_{\delta'}^n \rangle;\ n = 1,2 \text{ and } \delta = 1,..,q \text{ and } \delta \neq \delta' \\
\langle S_1 S_2^n S_3^m \rangle &= \langle S_\delta S_{\delta'}^n S_{\delta''}^m \rangle;\ n,m = 1,2 \text{ and } \delta = 1,..,q \text{ and } \delta \neq \delta' \neq \delta'' \\
\langle S_0 S_1^n \rangle &= \langle S_0 S_\delta^n \rangle;\ n = 1,2 \text{ and } \delta = 2,..,q \\
\langle S_0 S_1^n S_2^m \rangle &= \langle S_0 S_\delta^n S_{\delta'}^m \rangle;\ n,m = 1,2 \text{ and } \delta = 1,..,q \text{ and } \delta \neq \delta'
\end{aligned}
$$
$$
\begin{aligned}
&. \\
&. \\
&.
\end{aligned}
\tag{4.1.34}
$$

Thus, the number of the set of linear equations obtained for the spin-1 Ising system with $q = 3$ reduces to 21 and the complete set is given in Eq. (4.1.35).

$$\langle S_0 \rangle = 3k_1 \langle S_1 \rangle + 6(k_2 - k_1)\langle S_1 S_2^2 \rangle + k_3 \langle S_1 S_2 S_3 \rangle$$
$$+ 3(k_1 - 2k_2 + k_4)\langle S_1 S_2^2 S_3^2 \rangle$$

$$\langle S_1 S_0 \rangle = 3k_1 \langle S_1^2 \rangle + 6(k_2 - k_1)\langle S_1^2 S_2^2 \rangle + k_3 \langle S_1 S_2 S_3^2 \rangle$$
$$+ 3(k_1 - 2k_2 + k_4)\langle S_1^2 S_2^2 S_3^2 \rangle$$

$$\langle S_1 S_2 S_0 \rangle = (6k_2 - 3k_1)\langle S_1 S_2^2 \rangle + (3k_1 - 6k_2 + k_3 + 3k_4)\langle S_1 S_2^2 S_3^2 \rangle$$

$$\langle S_1 \rangle = a_1(1 - \langle (S_0^z)^2 \rangle) + a_2 \langle S_0^z \rangle + a_3 \langle (S_0^z)^2 \rangle$$

$$\langle S_1 S_2 \rangle = a_1 \langle S_1 \rangle + a_2 \langle S_0 S_1 \rangle + (a_3 - a_1)\langle S_1 S_0^2 \rangle$$

$$\langle S_1 S_2 S_3 \rangle = a_1 \langle S_1 S_2 \rangle + a_2 \langle S_0 S_1 S_2 \rangle + (a_3 - a_1)\langle S_1 S_2 S_0^2 \rangle$$

$$\langle S_1^2 \rangle = b_1(1 - \langle (S_0^z)^2 \rangle) + b_2 \langle S_0^z \rangle + b_3 \langle (S_0^z)^2 \rangle$$

$$\langle S_1 S_2^2 \rangle = b_1 \langle S_1 \rangle + b_2 \langle S_0 S_1 \rangle + (b_3 - b_1)\langle S_1 S_0^2 \rangle$$

$$\langle S_1^2 S_2^2 \rangle = b_1 \langle S_1^2 \rangle + b_2 \langle S_0 S_1^2 \rangle + (b_3 - b_1)\langle S_1^2 S_0^2 \rangle$$

$$\langle S_0 S_1^2 \rangle = b_3 \langle S_0 \rangle + b_2 \langle S_0^2 \rangle$$

$$\langle S_0 S_1 S_2^2 \rangle = b_3 \langle S_0 S_1 \rangle + b_2 \langle S_1 S_0^2 \rangle$$

$$\langle S_0 S_1^2 S_2^2 \rangle = b_3 \langle S_0 S_1^2 \rangle + b_2 \langle S_1^2 S_0^2 \rangle$$

$$\langle S_1 S_2 S_3^2 \rangle = b_1 \langle S_1 S_2 \rangle + b_2 \langle S_0 S_1 S_2 \rangle + (b_3 - b_1)\langle S_1 S_2 S_0^2 \rangle$$

$$\langle S_1 S_2^2 S_3^2 \rangle = b_1 \langle S_1 S_2^2 \rangle + b_2 \langle S_0 S_1 S_2^2 \rangle + (b_3 - b_1)\langle S_1 S_2^2 S_0^2 \rangle$$

$$\langle S_1^2 S_2^2 S_3^2 \rangle = b_1 \langle S_1^2 S_2^2 \rangle + b_2 \langle S_0 S_1^2 S_2^2 \rangle + (b_3 - b_1)\langle S_1^2 S_2^2 S_0^2 \rangle$$

$$\langle (S_0)^2 \rangle = r_0 + 3(r_1 - r_0)\langle S_1^2 \rangle + 3r_2 \langle S_1 S_2 \rangle + 3(r_0 - 2r_1 + r_3)\langle S_1^2 S_2^2 \rangle$$
$$+ 3(r_4 - r_2)\langle S_1 S_2 S_3^2 \rangle + (-r_0 + 3r_1 - 3r_3 + r_5)\langle S_1^2 S_2^2 S_3^2 \rangle$$

$$\langle S_1 S_0^2 \rangle = (3r_1 - 2r_0)\langle S_1 \rangle + (3r_2 + 3r_0 - 6r_1 + 3r_3)\langle S_1 S_2^2 \rangle$$
$$+ (-r_0 + 3r_1 - 3r_2 - 3r_3 + 3r_4 + r_5)\langle S_1 S_2^2 S_3^2 \rangle$$

$$\langle S_1^2 S_0^2 \rangle = (3r_1 - 2r_0)\langle S_1^2 \rangle + (3r_2 + 3r_0 - 6r_1 + 3r_3)\langle S_1^2 S_2^2 \rangle$$
$$+ (-r_0 + 3r_1 - 3r_2 - 3r_3 + 3r_4 + r_5)\langle S_1^2 S_2^2 S_3^2 \rangle$$

$$\langle S_1 S_2 S_0^2 \rangle = (r_0 - 3r_1 + 3r_2 + 3r_3)\langle S_1 S_2 \rangle$$
$$(-r_0 + 3r_1 - 3r_2 - 3r_3 + 3r_4 + r_5)\langle S_1 S_2 S_3^2 \rangle$$

$$\langle S_1 S_2^2 S_0^2 \rangle = (r_0 - 3r_1 + 3r_2 + 3r_3)\langle S_1 S_2^2 \rangle$$
$$(-r_0 + 3r_1 - 3r_2 - 3r_3 + 3r_4 + r_5)\langle S_1 S_2^2 S_3^2 \rangle$$

$$\langle S_1^2 S_2^2 S_0^2 \rangle = (r_0 - 3r_1 + 3r_2 + 3r_3)\langle S_1^2 S_2^2 \rangle$$
$$+ (-r_0 + 3r_1 - 3r_2 - 3r_3 + 3r_4 + r_5)\langle S_1^2 S_2^2 S_3^2 \rangle \qquad (4.1.35)$$

We can write Eq. (4.1.35) in the form of a 21×21 matrix and solve in terms of the variables x_i [$(i = 1, 2, ..., 21)$ ($e.g., x_1 = \langle S_0 \rangle, x_2 = \langle S_1 S_0 \rangle, ..., x_{21} = \langle S_1^2 S_2^2 S_0^2 \rangle$)] of the linear equations. Consequently, all of the spin correlation functions can be easily determined as functions of the temperature, effective field and crystal field. Since the thermal average of the central spin is equal to that of its nearest-neighbor spins within the present method then the unknown parameter A can be numerically determined by the relation

$$\langle S_0 \rangle = \langle S_1 \rangle \qquad \text{or} \qquad x_1 = x_4. \qquad (4.1.36)$$

By solving Eq. (4.1.36) numerically at a given fixed set of Hamiltonian parameters we obtain the parameter A. Then we use the numerical values of A to obtain the spin correlation functions given in Eq. (4.1.35). Note that $A = 0$ is always the root of Eq. (4.1.36) corresponding to the disordered state of the system. The nonzero root of A in Eq. (4.1.36) corresponds to the long-range ordered state of the system. The transition temperature $k_B T_c / J$ can also be numerically evaluated by letting $\gamma \to 0$ in the vicinity of $k_B T_c / J$. The phase diagrams in a $(k_B T_c / J - D/J)$ plane has been depicted in Fig. 4.3a for honeycomb ($q = 3$), square ($q = 4$) and triangular, as well as for simple cubic ($q = 6$) lattices. Although the above formulation is performed for a honeycomb lattice, calculation details for $q = 4$ and $q = 6$ can be found in (Yüksel, Akinci, & Polat, 2009, Akinci, 2012).
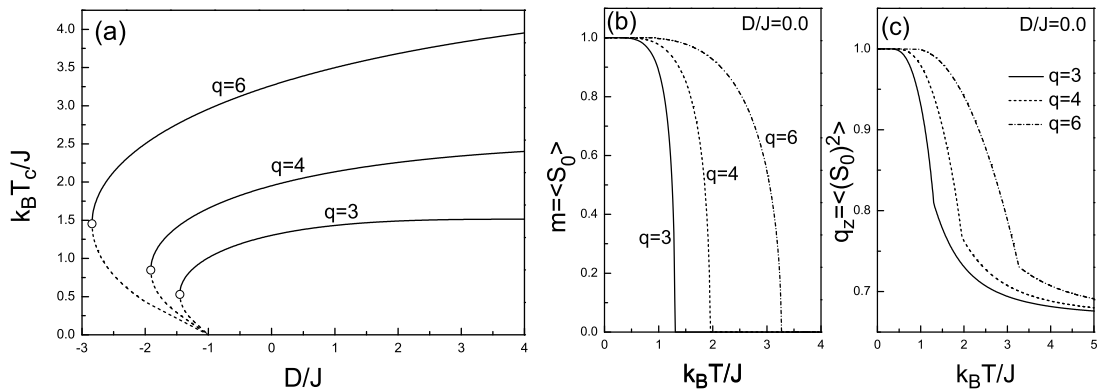

Figure 4.3 (a) Phase diagrams of honeycomb, square and simple cubic (or triangular) lattices in a $(k_B T_c / J - D/J)$ plane. (b) Magnetization, and (c) quadrupolar moment curves corresponding to Fig. 4.3a with $D/J = 0.0$.

As seen from Fig. 4.3a, the phase diagrams exhibit both second and first order phase transitions with a tricritical point. In the highly anisotropic limit ($D/J \rightarrow \infty$) the energy is minimized when the spins align parallel with each other in the $z-$ direction which means that a magnetic configuration with $S_i^z = \pm 1$ is favored. In this limit, the system reduces to spin-1/2 for any coordination number. In the isotropic limit ($D/J = 0$), the second order transition temperature values $k_B T_c / J = 1.302, 1.952, 3.265$ obtained for $q = 3, 4$ and 6 can be compared with those of DA (Kaneyoshi, 1993) $k_B T_c / J = 1.519, 2.188, 3.519$ and EFT (Kaneyoshi, 1999b) which yields $k_B T_c / J = 1.428, 2.114, 3.466$. We see from these results that the calculations are more accurate than the traditional DA and EFT techniques. For instance, the reduced transition temperature of isotropic spin-1 Blume-Capel model on a square lattice has the value $k_B T_c / J = 2.188$ and 2.114 within the traditional DA and EFT whereas our result $k_B T_c / J = 1.952$ can be compared with the result $k_B T_c / J = 1.690$ of accurate Monte Carlo simulations (Silva, Caparica, & Plascak, 2006). On the other hand, if D/J increases in negative direction then the ground state energy tends to increase. As a result, the transition temperature decreases due to the manifestation of spins aligned perpendicular to $z-$ direction (i.e. $S_i^z = 0$). In this case, nonmagnetic state is favored. For sufficiently large negative values of D/J, population of nonmagnetic lattice sites increases drastically against the magnetic sites. Consequently, critical frontier in ($k_B T_c / J - D/J$) plane exhibits a double valued region which is called reentrant phenomena where the system exhibits two successive phase transitions.

In Figs. 4.3b and 4.3c, we have depicted the variation of magnetization ($\langle S_0 \rangle$) and quadrupolar moment ($\langle (S_0^2) \rangle$) curves with reduced temperature for coordination numbers $q = 3, 4$ and 6 corresponding to the phase diagrams in Fig. 4.3a with $D = 0$. It is clear from these figures that the magnetization of the system gradually decreases and reduces to zero at the transition temperature whereas the longitudinal quadrupolar moment q_z decreases as the temperature increases and changes abruptly at the second-order transition temperature. For the completeness and consistence of discussion, temperature dependence of several multi-spin correlation functions are depicted in Fig. 4.4 in the isotropic limit ($D/J = 0$) for a honeycomb lattice ($q = 3$).
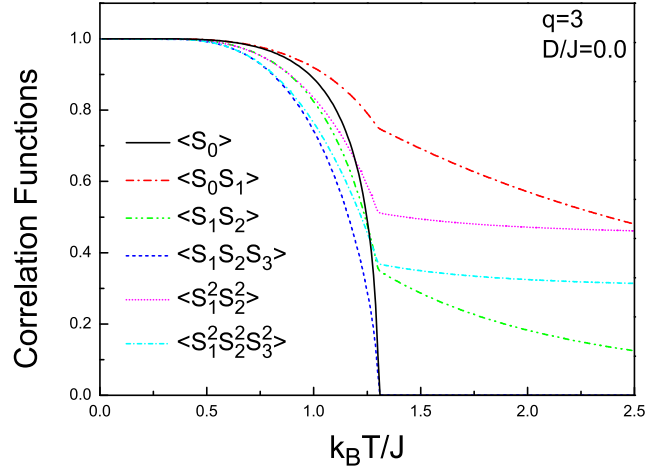
Figure 4.4 Temperature dependence of several spin
correlation functions of a spin-1 isotropic ($D/J = 0.0$)
Blume-Capel model on a honeycomb lattice ($q = 3$).

We should stress that there is not a unique formalism to derive the set of the correlation functions listed in Eq. (4.1.35). An alternative procedure has recently been proposed by (Kaneyoshi, 1999b) within the framework of EFT, but by using the approximated van der Waerden identity (i.e. approximated form of Eq. (3.4.23)). Indeed, there may exist several treatment methods for the derivation process. However, in a "heuristic" manner, by comparing the results obtained from several alternative sets of linear equations corresponding to Eq. (4.1.35), we find that the results obtained within the framework of the present formalism improve those of the various approximation schemes (c.f. see the discussions concerning a previous section). Although the method seems mathematically simple, it requires to do tedious calculations. On the other hand, as wee shall see soon after, present formalism can be easily adopted to much more complicated problems such as the models in the presence of quenched disorder, and produces results which fit quite well with many of the distinguished techniques.

4.1.3 Spin-1 Blume Capel Model in the Presence of Longitudinal and Transverse Magnetic Fields

As an application of the proposed formalism let us introduce the spin-1 Blume-Capel model in the presence of both longitudinal and transverse fields which can be represented by the following Hamiltonian

$$\mathcal{H} = -J \sum_{<i,j>} S_i^z S_j^z - D \sum_i (S_i^z)^2 - \Omega \sum_i S_i^x - h \sum_i S_i^z, \qquad (4.1.37)$$

where S_i^z and S_i^x denote the $z-$ and $x-$ components of the spin operator, respectively. The first summation in Eq. (4.1.37) is over the nearest-neighbor pairs of spins and the operator S_i^z takes the values $S_i^z = 0, \pm 1$. J, D, Ω and h terms stand for the exchange interaction, single-ion anisotropy (i.e. crystal field) and transverse and longitudinal magnetic fields, respectively.

Since there exist two kinds of external field sources, namely h and Ω, there are two directions in which we can observe a spontaneous magnetization. In other words, due to the presence of a longitudinal field h, a spontaneous magnetization m_z will be induced in the $z-$ direction whereas in the presence of transverse component Ω, we will also have a magnetization m_x which will be induced along the $x-$ direction.

Although the Hamiltonian in Eq. (4.1.37) is defined for a magnetic system, Ising model in a transverse field was originally introduced by de Gennes (Gennes, 1963) to describe the collective motions of hydrogen bonds in a ferroelectric crystal such as potassium dihydrogen phosphate (KH_2PO_4) by assuming the Hamiltonian of the form

$$\mathcal{H} = -J \sum_{<ij>} S_i^z S_j^z - \Omega \sum_i S_i^x, \qquad (4.1.38)$$

where S_i^z and S_i^x denote the $z-$ and $x-$ components of proton spin operator, respectively. The model represented by Eq. (4.1.38) can be briefly summarized as follows: In a three dimensional lattice, the pair of oxygen ions on the lattice site i produces a symmetric double well potential, and the hydrogen ion (i.e. proton) in the $O-H-O$ bond is under the influence of this potential. $S_i^z = \pm 1$ states of proton simply correspond to the two minima of the potential well. However, since the width

and height of this double well potential is finite, a quantum tunneling of the proton can take place with probability associated with the parameter Ω which is determined by the mass of the proton and the well structure or lattice constant. In the absence of transverse field Ω, the system exhibits an ordered ferroelectric phase whereas as Ω increases then it becomes dominant against the proton-proton interactions between the nearest-neighbor sites. If the value of Ω exceeds a threshold value then we observe disordered para-electric phase (Dutta, Divakaran, Sen, Chakrabarti, Rosenbaum, & Aeppli, 2012).

Ferroelectric system defined in Eq. (4.1.38) can also be written in magnetic language by direct analogy. In this context, Eq. (4.1.37) can be regarded as an extended and generalized form of transverse Ising model (TIM) for higher spins in magnitude. This model has been widely examined in statistical mechanics and condensed matter physics since the pioneering work of de Gennes (Gennes, 1963). The model in Eq. (4.1.37) can be considered as a semi quantum mechanical model due to the non-commuting transverse field. A detailed literature review concerning the theoretical investigation of thermal and magnetic properties of TIM can be found in (Yüksel & Polat, 2010).

Mathematical formulation of the model is simply based on the cluster defined in Fig. 4.1, and as we have discussed in the previous section, our aim is to obtain a a set of spin correlation functions which depend on the temperature and Hamiltonian parameters. The procedure is the same as that introduced for spin-1 Blume-Capel model, but this time the form of the functions $F(x)$, $G(x)$, etc. will be derived by taking the Hamiltonian in Eq. (4.1.37) as a basis.

At first, we start constructing the mathematical background of our model by using the approximated spin correlation identities introduced by Sá Barreto et al. (Barreto, Fittipaldi, & Zeks, 1981, Kaneyoshi, 1993)

$$\langle \{f_i\} S_i^{\alpha} \rangle = \left\langle \{f_i\} \frac{Tr_i S_i^{\alpha} \exp(-\beta H_i)}{Tr_i \exp(-\beta H_i)} \right\rangle, \tag{4.1.39}$$

$$\langle \{f_i\} (S_i^{\alpha})^2 \rangle = \left\langle \{f_i\} \frac{Tr_i (S_i^{\alpha})^2 \exp(-\beta H_i)}{Tr_i \exp(-\beta H_i)} \right\rangle, \tag{4.1.40}$$

where $\beta = 1/k_B T$ and $\alpha = z$ or x.

In order to apply the differential operator technique (Kaneyoshi, 1993, Honmura & Kaneyoshi, 1979), we should separate the Hamiltonian (4.1.37) into two parts as $H = H_i + H'$. Here, one part denoted by H_i includes all contributions associated with the site i, and the other part H' does not depend on the site i. At this point, one should notice that the spin operators S_i^z and S_i^x do not commute with each other which reflects the quantum mechanical origin of the model. Although this situation requires to handle the problem in a fully quantum mechanical point of view, a classical treatment is also capable of explaining various magnetic phenomena.

By following the standard procedure discussed in Chapter 3, we can write $-H_i$ as

$$-H_i = E_i S_i^z + D\left(S_i^z\right)^2 + \Omega S_i^x + h S_i^z, \tag{4.1.41}$$

where $E_i = J \sum_j S_j^z$ is the local field on the site i. If we use the matrix representations of the operators S_i^z and S_i^x for the spin-1 system then we can obtain the matrix form of Eq. (4.1.41)

$$-H_i = \begin{pmatrix} E_i + D + h & \Omega/\sqrt{2} & 0 \\ \Omega/\sqrt{2} & 0 & \Omega/\sqrt{2} \\ 0 & \Omega/\sqrt{2} & -E_i + D - h \end{pmatrix}. \tag{4.1.42}$$

In order to proceed further, we have to diagonalize $-H_i$ matrix in Eq. (4.1.42). The three eigenvalues are

$$
\begin{aligned}
\lambda_1 &= \frac{2D}{3} + \frac{2p}{3}\cos\left(\frac{\theta}{3}\right), \\
\lambda_2 &= \frac{2D}{3} - \frac{2p}{3}\cos\left(\frac{\pi - \theta}{3}\right), \\
\lambda_3 &= \frac{2D}{3} - \frac{2p}{3}\cos\left(\frac{\pi + \theta}{3}\right),
\end{aligned}
\tag{4.1.43}
$$

where

$$
\begin{aligned}
\theta &= \arccos\left(\frac{\zeta}{p^3}\right), \\
\zeta &= D\left(9E_i^2 - \frac{9}{2}\Omega^2 - D^2 + 18E_i h + 9h^2\right), \\
p^2 &= 3E_i^2 + 3\Omega^2 + D^2 + 6E_i h + 3h^2,
\end{aligned}
$$

and the eigenvectors φ_k of $-H_i$ corresponding to the eigenvalues in Eq. (4.1.43) are calculated as follows

$$\alpha_k = \pm\sqrt{1-\beta_k^2-\gamma_k^2},$$

$$\beta_k = -\frac{[E_i+(D+h-\lambda_k)]}{\Omega/\sqrt{2}}\alpha_k,$$

$$\gamma_k = -\frac{[E_i+(D+h-\lambda_k)]}{[E_i-(D-h-\lambda_k)]}\alpha_k,$$

$$\varphi_k = \begin{pmatrix} \alpha_k \\ \beta_k \\ \gamma_k \end{pmatrix}, \qquad k=1,2,3. \tag{4.1.44}$$

Hereafter, we apply the differential operator technique in Eqs. (4.1.39) and (4.1.40) with $\{f_i\}=1$. From Eq. (4.1.39) we obtain the following spin correlations for the thermal average of a central spin for honeycomb lattice ($q=3$) as

$$\langle S_0^z\rangle = \left\langle \prod_{j=1}^{q=3}\left[1+S_j^z\sinh(J\nabla)+(S_j^z)^2\{\cosh(J\nabla)-1\}\right]\right\rangle F(x)|_{x=0}, \tag{4.1.45}$$

and

$$\langle S_0^x\rangle = \left\langle \prod_{j=1}^{q=3}\left[1+S_j^z\sinh(J\nabla)+(S_j^z)^2\{\cosh(J\nabla)-1\}\right]\right\rangle H(x)|_{x=0}. \tag{4.1.46}$$

By expanding the right-hand sides of Eqs. (4.1.46) and (4.1.47) we get the longitudinal and transverse spin correlations as

$$\begin{aligned}
m_z = \langle S_0^z\rangle =\ & l_0 + 3k_1\langle S_1\rangle + 3(l_1-l_0)\langle S_1^2\rangle + 3l_2\langle S_1 S_2\rangle \\
& + 6(k_2-k_1)\langle S_1 S_2^2\rangle + 3(l_0-2l_1+l_3)\langle S_1^2 S_2^2\rangle \\
& + k_3\langle S_1 S_2 S_3\rangle + 3(l_4-l_2)\langle S_1 S_2 S_3^2\rangle \\
& + 3(k_1-2k_2+k_4)\langle S_1 S_2^2 S_3^2\rangle \\
& + (-l_0+3l_1-3l_3+l_5)\langle S_1^2 S_2^2 S_3^2\rangle, \tag{4.1.47}
\end{aligned}$$

and

$$\begin{aligned}
m_x = \langle S_0^x\rangle =\ & p_0 + 3c_1\langle S_1\rangle + 3(p_1-p_0)\langle S_1^2\rangle + 3p_2\langle S_1 S_2\rangle \\
& + 6(c_2-c_1)\langle S_1 S_2^2\rangle + 3(p_0-2p_1+p_3)\langle S_1^2 S_2^2\rangle \\
& + c_3\langle S_1 S_2 S_3\rangle + 3(p_4-p_2)\langle S_1 S_2 S_3^2\rangle \\
& + 3(c_1-2c_2+c_4)\langle S_1 S_2^2 S_3^2\rangle \\
& + (-p_0+3p_1-3p_3+p_5)\langle S_1^2 S_2^2 S_3^2\rangle, \tag{4.1.48}
\end{aligned}$$

with the coefficients

$$l_0 = F(0)$$

$$l_1 = \cosh(J\nabla)F(x)|_{x=0} \qquad\qquad k_1 = \sinh(J\nabla)F(x)|_{x=0}$$

$$l_2 = \sinh^2(J\nabla)F(x)|_{x=0} \qquad\qquad k_2 = \cosh(J\nabla)\sinh(J\nabla)F(x)|_{x=0}$$

$$l_3 = \cosh^2(J\nabla)F(x)|_{x=0} \qquad\qquad k_3 = \sinh^3(J\nabla)F(x)|_{x=0}$$

$$l_4 = \cosh(J\nabla)\sinh^2(J\nabla)F(x)|_{x=0} \qquad k_4 = \cosh^2(J\nabla)\sinh(J\nabla)F(x)|_{x=0}$$

$$l_5 = \cosh^3(J\nabla)F(x)|_{x=0}$$

and

$$p_0 = H(0)$$

$$p_1 = \cosh(J\nabla)H(x)|_{x=0} \qquad\qquad c_1 = \sinh(J\nabla)H(x)|_{x=0}$$

$$p_2 = \sinh^2(J\nabla)H(x)|_{x=0} \qquad\qquad c_2 = \cosh(J\nabla)\sinh(J\nabla)H(x)|_{x=0}$$

$$p_3 = \cosh^2(J\nabla)H(x)|_{x=0} \qquad\qquad c_3 = \sinh^3(J\nabla)H(x)|_{x=0}$$

$$p_4 = \cosh(J\nabla)\sinh^2(J\nabla)H(x)|_{x=0} \qquad c_4 = \cosh^2(J\nabla)\sinh(J\nabla)H(x)|_{x=0}$$

$$p_5 = \cosh^3(J\nabla)H(x)|_{x=0}$$

Next, the average value of a perimeter spin in the system can be written as follows and it is found as

$$m_1 = \langle S_\delta^z \rangle = \langle 1 + S_0^z \sinh(J\nabla) + (S_0^z)^2 \{\cosh(J\nabla) - 1\} \rangle F(x+\gamma)|_{x=0}, \qquad (4.1.49)$$

$$\langle S_1 \rangle = a_1 \left(1 - \langle (S_0^z)^2 \rangle \right) + a_2 \langle S_0^z \rangle + a_3 \langle (S_0^z)^2 \rangle, \qquad (4.1.50)$$

where $\gamma = (q-1)A$ is the effective field produced by the $(q-1)$ spins outside of the cluster depicted in Fig. 4.1 and A is an unknown parameter to be determined self-consistently. The coefficients in Eq. (4.1.50) are then given by

$$a_1 = F(\gamma),$$

$$a_2 = \sinh(J\nabla)F(x+\gamma)|_{x=0},$$

$$a_3 = \cosh(J\nabla)F(x+\gamma)|_{x=0}.$$

As a result of the usage of van der Waerden identity (3.4.23) for spin-1 systems, we have to introduce the additional parameters $\langle (S_0^z)^2 \rangle$, $\langle (S_0^x)^2 \rangle$ and $\langle (S_\delta^z)^2 \rangle$ to obtain the

quadrupolar moments. With the help of Eq. (4.1.40), we have

$$q_z = \langle (S_0^z)^2 \rangle = \left\langle \prod_{j=1}^{q} \left[1 + S_j^z \sinh(J\nabla) + (S_j^z)^2 \{\cosh(J\nabla) - 1\} \right] \right\rangle G(x)|_{x=0}, \qquad (4.1.51)$$

$$q_x = \langle (S_0^x)^2 \rangle = \left\langle \prod_{j=1}^{q} \left[1 + S_j^z \sinh(J\nabla) + (S_j^z)^2 \{\cosh(J\nabla) - 1\} \right] \right\rangle K(x)|_{x=0}. \qquad (4.1.52)$$

Hence, we get the longitudinal and transverse components of the quadrupolar moment of central spin by expanding the right-hand sides of Eqs. (4.1.51) and (4.1.52)

$$\begin{aligned}
\langle (S_0^z)^2 \rangle &= r_0 + 3n_1 \langle S_1 \rangle + 3(r_1 - r_0) \langle S_1^2 \rangle + 3r_2 \langle S_1 S_2 \rangle \\
&\quad + 6(n_2 - n_1) \langle S_1 S_2^2 \rangle + 3(r_0 - 2r_1 + r_3) \langle S_1^2 S_2^2 \rangle + n_3 \langle S_1 S_2 S_3 \rangle \\
&\quad + 3(r_4 - r_2) \langle S_1 S_2 S_3^2 \rangle + 3(n_1 - 2n_2 + n_4) \langle S_1 S_2^2 S_3^2 \rangle \\
&\quad + (-r_0 + 3r_1 - 3r_3 + r_5) \langle S_1^2 S_2^2 S_3^2 \rangle,
\end{aligned} \qquad (4.1.53)$$

and

$$\begin{aligned}
\langle (S_0^x)^2 \rangle &= v_0 + 3\mu_1 \langle S_1 \rangle + 3(v_1 - v_0) \langle S_1^2 \rangle + 3v_2 \langle S_1 S_2 \rangle \\
&\quad + 6(\mu_2 - \mu_1) \langle S_1 S_2^2 \rangle + 3(v_0 - 2v_1 + v_3) \langle S_1^2 S_2^2 \rangle + \mu_3 \langle S_1 S_2 S_3 \rangle \\
&\quad + 3(v_4 - v_2) \langle S_1 S_2 S_3^2 \rangle + 3(\mu_1 - 2\mu_2 + \mu_4) \langle S_1 S_2^2 S_3^2 \rangle \\
&\quad + (-v_0 + 3v_1 - 3v_3 + v_5) \langle S_1^2 S_2^2 S_3^2 \rangle.
\end{aligned} \qquad (4.1.54)$$

The coefficients in Eqs. (4.1.53) and (4.1.54) are respectively given by

$$r_0 = G(0)$$

$$r_1 = \cosh(J\nabla)G(x)|_{x=0} \qquad\qquad n_1 = \sinh(J\nabla)G(x)|_{x=0}$$

$$r_2 = \sinh^2(J\nabla)G(x)|_{x=0} \qquad\qquad n_2 = \cosh(J\nabla)\sinh(J\nabla)G(x)|_{x=0}$$

$$r_3 = \cosh^2(J\nabla)G(x)|_{x=0} \qquad\qquad n_3 = \sinh^3(J\nabla)G(x)|_{x=0}$$

$$r_4 = \cosh(J\nabla)\sinh^2(J\nabla)G(x)|_{x=0} \qquad n_4 = \cosh^2(J\nabla)\sinh(J\nabla)G(x)|_{x=0}$$

$$r_5 = \cosh^3(J\nabla)G(x)|_{x=0}$$

and

$$v_0 = K(0)$$

$$v_1 = \cosh(J\nabla)K(x)|_{x=0} \qquad \mu_1 = \sinh(J\nabla)K(x)|_{x=0}$$

$$v_2 = \sinh^2(J\nabla)K(x)|_{x=0} \qquad \mu_2 = \cosh(J\nabla)\sinh(J\nabla)K(x)|_{x=0}$$

$$v_3 = \cosh^2(J\nabla)K(x)|_{x=0} \qquad \mu_3 = \sinh^3(J\nabla)K(x)|_{x=0}$$

$$v_4 = \cosh(J\nabla)\sinh^2(J\nabla)K(x)|_{x=0} \qquad \mu_4 = \cosh^2(J\nabla)\sinh(J\nabla)K(x)|_{x=0}$$

$$v_5 = \cosh^3(J\nabla)K(x)|_{x=0}$$

Corresponding to Eq. (4.1.49), quadrupolar moment of the perimeter spin can be written as follows

$$\langle (S_\delta^z)^2 \rangle = \langle 1 + S_0^z \sinh(J\nabla) + (S_0^z)^2 \{\cosh(J\nabla) - 1\} \rangle G(x+\gamma), \qquad (4.1.55)$$

$$\langle S_1^2 \rangle = b_1 \left(1 - \langle (S_0^z)^2 \rangle\right) + b_2 \langle S_0^z \rangle + b_3 \langle (S_0^z)^2 \rangle. \qquad (4.1.56)$$

with

$$b_1 = G(\gamma)$$

$$b_2 = \sinh(J\nabla)G(x+\gamma)|_{x=0}$$

$$b_3 = \cosh(J\nabla)G(x+\gamma)|_{x=0}$$

With the help of Eqs. (4.1.43) and (4.1.44), the functions $F(x)$, $G(x)$, $H(x)$ and $K(x)$ in Eqs. (4.1.45), (4.1.46), (4.1.51) and (4.1.52) can be calculated numerically from the relations

$$F(x) = \frac{1}{\sum_{n=1}^{d} \exp(\beta\lambda_n)} \sum_{n=1}^{d} \langle \varphi_n | S_i^z | \varphi_n \rangle \exp(\beta\lambda_n), \qquad (4.1.57)$$

$$H(x) = \frac{1}{\sum_{n=1}^{d} \exp(\beta\lambda_n)} \sum_{n=1}^{d} \langle \varphi_n | S_i^x | \varphi_n \rangle \exp(\beta\lambda_n), \qquad (4.1.58)$$

$$G(x) = \frac{1}{\sum_{n=1}^{d} \exp(\beta\lambda_n)} \sum_{n=1}^{d} \langle \varphi_n | (S_i^z)^2 | \varphi_n \rangle \exp(\beta\lambda_n), \qquad (4.1.59)$$

$$K(x) = \frac{1}{\sum_{n=1}^{d} \exp(\beta\lambda_n)} \sum_{n=1}^{d} \langle \varphi_n | (S_i^x)^2 | \varphi_n \rangle \exp(\beta\lambda_n), \qquad (4.1.60)$$

where $d = 3$ is the dimensionality of the matrix $-H_i$ in Eq. (4.1.42).

Eqs. (4.1.47), (4.1.48), (4.1.50), (4.1.53), (4.1.54) and (4.1.56) are fundamental correlation functions of the system. When the right-hand sides of Eqs. (4.1.45), (4.1.46), (4.1.51) and (4.1.52) are expanded, the multi-spin correlation functions can be easily obtained. The simplest approximation, and one of the most frequently adopted is to decouple these equations according to

$$\left\langle S_j^z (S_k^z)^2 ... S_l^z \right\rangle \cong \left\langle S_j^z \right\rangle \left\langle (S_k^z)^2 \right\rangle ... \left\langle S_l^z \right\rangle, \tag{4.1.61}$$

for $i \neq j \neq ... \neq l$ (Kaneyoshi, 1993). The main difference of the method used in this study from the other approximations in the literature emerges in comparison with any decoupling approximation (DA) when expanding the right-hand sides of equations (4.1.45), (4.1.46), (4.1.51) and (4.1.52). In other words, one advantage of the approximation method proposed by this study is that no uncontrolled decoupling procedure is used for the higher-order correlation functions.

For spin-1 Ising system with $q = 3$, taking equations (4.1.47), (4.1.48), (4.1.50) , (4.1.53), (4.1.54) and (4.1.56) as basis relations, we derive a set of linear equations of the spin correlation functions which interact in the system. By taking into account the translational symmetry properties (c.f. refer to Eq .(4.1.34)) of the system with $(\hat{S}_\delta)^4 = (\hat{S}_\delta)^2$ and $(\hat{S}_\delta)^3 = \hat{S}_\delta$ for spin-1, we have 23 linear equations (i.e. correlation functions) in total for spin-1 system on a honeycomb lattice ($q = 3$), and the complete set can be found in (Yüksel & Polat, 2010). Since the thermal average of the central spin is equal to that of its nearest-neighbor spins within the present method then the unknown parameter A can be numerically determined by the relation

$$\langle S_0^z \rangle = \langle S_1 \rangle. \tag{4.1.62}$$

Once the set of linear equations is numerically solved, all of the spin correlation functions can be easily determined as functions of the temperature, effective field, crystal field and longitudinal magnetic field as well as transverse magnetic field which the other studies in the literature do not include. For instance, using the single-spin and multi-spin correlation functions, the internal energy can be numerically evaluated from

$$-\frac{U}{NJ} = \frac{q}{2} \langle S_0 S_1 \rangle + D \langle (S_0^z)^2 \rangle + \Omega \langle S_0^x \rangle + h \langle S_0^z \rangle. \tag{4.1.63}$$

With the use of Eq. (4.1.63), the specific heat at constant magnetic field h of the system can be numerically determined from the relation

$$C_h = \left(\frac{\partial U}{\partial T}\right)_h. \tag{4.1.64}$$

Once the spin correlation functions have been evaluated then we can examine the ferromagnetic properties of the spin-1 TIM with crystal field under an applied longitudinal magnetic field on a honeycomb lattice using the proposed formulation.
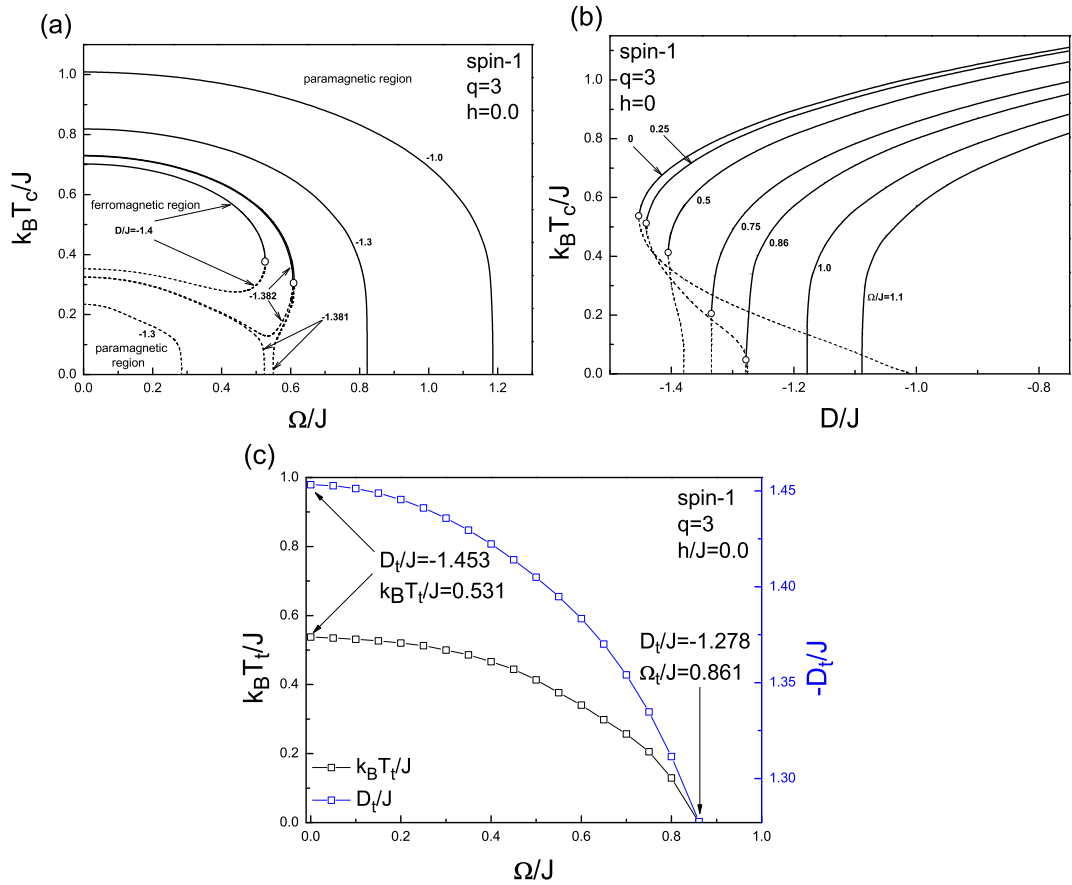
Figure 4.5 Phase diagrams of the spin-1 system with $h/J = 0$ in (a) ($k_B T_c/J$-Ω/J), (b) ($k_B T_c/J$-D/J) planes. The numbers on the curves denote the values of the crystal field D/J and transverse field Ω/J, respectively. (c) Transverse field dependencies of the tricritical temperature $k_B T_t/J$ and tricritical crystal field $-D_t/J$.

Let us focus our attention on the phase diagrams of the system in ($k_B T_c/J - \Omega/J$) and ($k_B T_c/J - D/J$) planes and investigate the whole phase diagrams by examining the numerical results for the thermal and magnetic properties. In order to plot the

phase diagrams, we assume $\langle S_0^z \rangle = \langle S_1 \rangle$ and the effective field γ is very small in the vicinity of $k_B T_c/J$ and solve the set of linear equations in (Yüksel & Polat, 2010) numerically using the self-consistent relation corresponding to equation (4.1.62). In Figs. 4.5a and 4.5b, we plot the variation of the critical temperature with transverse field Ω/J and crystal field D/J, respectively. Fig. 4.5a shows the phase diagram in the $(k_B T_c/J - \Omega/J)$ plane with $h/J = 0$ and for selected values of D/J, namely $-1.0, -1.3, -1.381, -1.382$ and -1.4. In this figure, we can call attention to the signs of an interesting behavior known as reentrant phenomena. In other words, when the crystal field strength is positive valued, the type of the transition in the system is invariably second order which is independent from transverse field value. On the other hand, if the crystal field value is sufficiently negative then we can expect to see two successive phase transitions. Solid and dashed lines in Fig. 4.5a correspond to the second and first order phase transition lines, respectively. Tricritical end points at which first and second order transition points meet are shown as white circles. In our calculations, we realized that one can observe reentrant behavior in the system for the values of $\Omega/J < 0.861$ and $-1.453 < D/J < -1.02$. For the values of $D/J \leq -1.382$ the transition lines exhibit a bulge which gets smaller as the value of D/J approaches the value of -1.453 which means that ferromagnetic phase region gets narrower. We have also examined the phase diagram of the present system in $(k_B T_c/J - D/J)$ plane with $h/J = 0$ and for selected values of Ω/J such as $0, 0.25, 0.5, 0.75, 0.86, 1.0$ and 1.1. The numerical results are shown in Fig. 4.5b. Solid and dashed lines in Fig. 4.5b correspond to the second and first order phase transition lines, respectively. White circles denote tricritical points. As we can see from this figure, as the value of transverse field Ω/J increases starting from zero then the value of tricritical point decreases gradually and disappears for $\Omega/J > 0.86$. If the transverse field value is greater than this value then we have only second order transitions in the system. These results show that the reentrant phenomenon originates from the competition between the crystal field D/J and transverse field Ω/J. Furthermore, the variation of the coordinates of the tricritical points $k_B T_t/J$ and D_t/J as a function of transverse field Ω/J is illustrated in Fig. 4.5c. As seen in this figure, value of $k_B T_t/J$ and the absolute value of D_t/J decreases as the value of transverse field increases and the

tricritical temperature disappears at the critical value of the transverse field Ω_t/J. In addition, this figure shows that the tricritical points exist for $1.278 < -D_t/J < 1.453$ and $\Omega/J < \Omega_t/J = 0.861$. These new results are not reported before. Hence, it would be worthwhile to compare these results with the other works in literature. For instance Jiang et al. (Jiang, Li, Zhong, & Yang, 1993) obtained $1.235 < -D_t/J < 1.427$ and $\Omega_t/J = 0.934$ while Miao et al. (Miao, Wei, Liu, & Geng, 2009) reported the values $1.229 < -D_t/J < 1.427$ and $\Omega_t/J = 0.945$. We believe our results are physically more reasonable and accurate in comparison with these works based on DA given in Eq. (4.1.61), since it neglects the multi-spin correlations and introducing this approximation affects the accuracy and reliability of numerical results. Furthermore, we note that the reentrant behavior is not observed in (Miao, Wei, Liu, & Geng, 2009). Consequently, all of the results mentioned above are qualitatively in a good agreement with the other works (Bouziane & Saber, 2009, Jiang, Li, Zhong, & Yang, 1993, Htoutou, Oubelkacem, Ainane, & Saber, 2005b, Jiang, 1994, Htoutou, Benaboud, Ainane, & Saber, 2004, Htoutou, Ainane, Saber, & de Miguel, 2005a), but not with (Miao, Wei, Liu, & Geng, 2009).

For the calculation details and further investigation of the effects of the single-ion anisotropy and longitudinal as well as transverse components of the external field on the temperature dependence of the order parameters m_z, m_x, q_z, q_x, Helmholtz free energy F, the entropy S, and the specific heat C curves, we refer the reader to (Yüksel & Polat, 2010).

CHAPTER FIVE

APPLICATIONS OF THE PROPOSED FORMALISM FOR THE MODELS WITH QUENCHED DISORDER EFFECTS

So far, we have limited our discussion on the approximation techniques concerning the study of the collective behavior of ideally pure magnetic systems such as prefect crystals, and we have proposed an EFT formulation being inspired by a cluster of Ising spins. We have presented the results obtained within the introduced method for spin-1/2 Ising and spin-1 Blume-Capel models with longitudinal and transverse fields. Based on the discussions of preceding sections, we have concluded that our method which have been successfully applied to pure systems is superior to conventional MFT and EFT methods.

On the other hand, until the recent past, effects of quenched disorder and random impurities on the thermal and magnetic properties of magnetic materials were usually considered as undesired ingredients in experimental studies. As stated by Fisher et al. (Fisher, Grinsrein, & Khurana, 1988), "experimentalists were often driven to elaborate lengths to reduce the randomness in their samples to negligible levels". However, owing to the recent advances in experimental techniques, the research on magnetism has mainly directed to the investigation of magnetic systems with quenched randomness and competing interactions. Eventually, the phenomena has become one of the most actively studied problems in statistical mechanics and condensed matter physics.

In the theoretical investigation of phase transitions and critical phenomena in magnetism, we basically consider two kinds of disorder in model systems. The first one is called "annealed" disorder in which the configuration of disorder or impurities may change in time which means that the disorder at a particular lattice site i is not localized but may move around the sample medium. The other type is known as "quenched" disorder in which the disorder is localized within a given configuration which can be imagined as structurally frozen in (Feng, 1996). Theoretically, the former case can be achieved by generating a new configuration of random variables uniformly at each

time step whereas for the latter type, the random effects can be taken into account by a given probability distribution function, and this is the main motivation of the present thesis report.

On the basis of Ising model and its generalizations, a general Hamiltonian containing the most frequently encountered disorder types can be written as

$$\mathcal{H} = -\sum_{<ij>} J_{ij} c_i c_j S_i^z S_j^z - \sum_i D_i (S_i^z)^2 - \sum_i h_i S_i^z.$$

According to the first term in Hamiltonian given above, a disorder may originate as a consequence of impurities in a perfect crystal. Namely, if the lattice site i is occupied by a magnetic atom, we have $c_i = 1$ otherwise $c_i = 0$. Moreover, again from the first summation we see that the nearest neighbor interactions may be ferromagnetic but vary in strength ($0 < J_{ij} < 1$), or we can model a bond diluted system in which some of the ferromagnetic couplings are broken. Another interesting behavior can be observed when the distribution of the variables J_{ij} includes both positive (ferromagnetic) and negative (antiferromagnetic) interactions (Fisher et al., 1988) which leads to a phenomenon called "frustration", due to the competing interactions. Apart from these, the second term in above Hamiltonian characterizes a disorder in single-ion anisotropy for spin-S ($S > 1/2$) Ising systems. Finally, the last term represents the famous random field Ising model where the magnetic fields h_i are random variables sampled from a particular distribution function with no correlations between their values at different sites (Fisher et al., 1988).

In the following sections, we will apply our method introduced in Chapter 4 on a wide variety of magnetic systems in the presence of several types of quenched disorder, and we intent to discuss the obtained results in detail. For this purpose, at first we will apply our formulation for diluted Ising ferromagnets. Next, we will discuss the bond dilution problem, and we will also consider a model in the presence of random crystal fields. Finally, we will give a detailed picture concerning the random field Ising model, and discuss the results obtained in the present formalism in detail. We should also note that the formulation of the aforementioned model systems will be briefly discussed, however we will particularly focus our attention on the numerical results.

For calculation details, we will refer the readers to our published papers when needed.

5.1   Site-Diluted Ising Ferromagnets

Site diluted ferromagnets constitute an example of magnetic systems with quenched disorder such as a compound $A_xB_{1-x}C$ where magnetic A atoms in a pure magnet AC are replaced by non-magnetic B impurities. Formerly, Sato et al. (Sato, Arrott, & Kikuchi, 1959) have shown that in a dilute lattice a Curie or a Néel temperature does not appear until a finite concentration of magnetic atoms is obtained if the atomic distribution is random. They have also found that this concentration depends on the coordination number of the lattice. For a detailed literature review of problem, see (Akinci, Yuksel, & Polat, 2011c).

Mean field theory (MFT) of site dilution problem predicts that the system always has a finite critical temperature and stays in a ferromagnetic state at lower temperatures, except that $c = 0$ where c denotes the magnetic atom concentration. Therefore, it is not capable of locating a critical site concentration at which the transition temperature reduces to zero. The reason is due to the fact that MFT neglects single-site and multi-site correlations. On the other hand, decoupling approximation (DA) accounts all the single site correlations, but it also neglects multi-site correlations between different sites. Hence, DA provides results that are superior to those obtained within the traditional MFT. Furthermore, CEFT which is an extension of DA partially takes into account the effects of multi-spin correlations and improves the results of conventional DA in many cases. Based on the physical aspects of the problem, whether in DA or CEFT formalism, evaluation of configurational averages emerging in definition of spin identities plays a critical role. However, as mentioned by Tucker (Tucker, 1991), the conventional configurational averaging technique applied in Refs. (Taggart, 1982, Kaneyoshi, Tamura, & Honmura, 1984, Boccara, 1983, Yang & Zhong, 1989, Kaneyoshi & Jaščur, 1992, Kaneyoshi, 1995b,a) is based on a procedure that decouples the site occupation variable from the thermal average of spin variables, even when both quantities referred to the same site while in Refs. (Balcerzak, Bobák, Mielnicki,

& Truong, 1985, Tucker, 1991, Saber & Tucker, 1991, Bobák & Jaščur, 1991, Tucker, 1992, Sarmento & Kaneyoshi, 1993, Bobák, Mockovčiak, & Sivulka, 1993), the authors used an improved configurational averaging method in which only the correlations between quantities pertaining to different sites are neglected (decoupled). However, it is possible to improve the accuracy of these methods by including multi-site, as well as single site correlations with a new type of improved configurational averaging technique.

As a site diluted spin-1/2 Ising model, we consider the following Hamiltonian

$$H = -J \sum_{<i,j>} c_i c_j S_i^z S_j^z, \tag{5.1.1}$$

where the summation is over the nearest-neighbor pairs of spins and the operator S_i^z takes the values $S_i^z = \pm 1$. We assume that the lattice sites are randomly diluted and c_i denotes a site occupation variable which equals to 1 if the site is occupied by a magnetic atom or to 0 if it is empty.

According to the Callen identity (Callen, 1963) for the spin-1/2 Ising system, the thermal average of the identity $c_i S_i^z$ at the site i is given by

$$c_i \left\langle \{f_i\} S_i^z \right\rangle = c_i \left\langle \{f_i\} \tanh \left[\beta c_i \left(J \sum_j c_j S_j^z \right) \right] \right\rangle, \tag{5.1.2}$$

where $\beta = 1/k_B T$, j expresses the nearest-neighbor sites of the central spin and $\{f_i\}$ can be any function of the Ising variables as long as it is not a function of the site i. Applying the differential operator technique (Honmura & Kaneyoshi, 1979, Kaneyoshi, 1993) in Eq. (5.1.2) and using the relation

$$\exp(\alpha c_i) = c_i \exp(\alpha) + 1 - c_i, \tag{5.1.3}$$

with the fact that $c_i^n = c_i$, we get

$$c_i \left\langle \{f_i\} S_i^z \right\rangle = c_i \left\langle \{f_i\} \prod_{j=1}^q \exp\left(J c_j S_j^z \nabla \right) \right\rangle \tanh(\beta x)|_{x=0}. \tag{5.1.4}$$

By putting Eq. (5.1.3) into Eq. (5.1.4) we obtain

$$c_i \left\langle \{f_i\} S_i^z \right\rangle = c_i \left\langle \{f_i\} \prod_{j=1}^q \left\{ c_j \cosh(J\nabla) + c_j S_j^z \sinh(J\nabla) + 1 - c_j \right\} \right\rangle \tanh(\beta x)|_{x=0}, \tag{5.1.5}$$

where ∇ is a differential operator, q is the coordination number of the lattice, and $\langle ... \rangle$ represents the thermal average. Eq. (5.1.5) is valid only for a given specific magnetic atom configuration. Hence, if we consider configurational averages then we may rewrite Eq. (5.1.5) as

$$\left\langle c_i \left\langle \{f_i\} S_i^z \right\rangle \right\rangle_r = \left\langle c_i \left\langle \{f_i\} \prod_{j=1}^{q} \left\{ c_j \cosh(J\nabla) + c_j S_j^z \sinh(J\nabla) + 1 - c_j \right\} \right\rangle \right\rangle_r \tanh(\beta x)|_{x=0},$$

(5.1.6)

where $\langle ... \rangle_r$ represents random configurational averages. When the right-hand side of Eq. (5.1.6) is expanded, the multi-site correlation functions appear. The simplest approximation, and one of the most frequently adopted is to decouple these correlations which is called decoupling approximation (DA). In conventional manner, eliminating the term c_i from both sides of Eq. (5.1.5) then performing the configurational average with $\{f_i\} = 1$ leads to the following equation,

$$\left\langle \left\langle S_i^z \right\rangle \right\rangle_r = \left\langle \left\langle \prod_{j=1}^{q} \left\{ c_j \cosh(J\nabla) + c_j S_j^z \sinh(J\nabla) + 1 - c_j \right\} \right\rangle \right\rangle_r \tanh(\beta x)|_{x=0}. \qquad (5.1.7)$$

In conventional DA one expands the right-hand side of Eq. (5.1.7) then decouples the multi-site correlations according to

$$\left\langle \left\langle c_i ... c_j c_k S_k^z c_l S_l^z ... c_m S_m^z \right\rangle \right\rangle_r \cong \langle c_i \rangle_r ... \left\langle c_j \right\rangle_r \langle c_k \rangle_r \left\langle \left\langle S_k^z \right\rangle \right\rangle_r \times \langle c_l \rangle_r \left\langle \left\langle S_l^z \right\rangle \right\rangle_r ... \langle c_m \rangle_r \left\langle \left\langle S_m^z \right\rangle \right\rangle_r$$

(5.1.8)

with

$$\langle c_\alpha \rangle_r = c \quad \text{and} \quad \left\langle \left\langle S_\alpha^z \right\rangle \right\rangle_r = m \qquad \alpha = i, ... j, k, l, ..., m.$$

However, this approximation decouples the site occupation variable from the thermal and configurational averages of spin variable, even when both quantities referred to the same site.

On the other hand, an improved version of decoupling approximation deals with the quantity $\left\langle c_i \left\langle S_i^z \right\rangle \right\rangle_r$. In other words, in an improved decoupling procedure, one expands the right-hand side of Eq. (5.1.6) instead of Eq. (5.1.7) and decouples the multi-site correlations according to

$$\left\langle \left\langle c_i ... c_j c_k S_k^z c_l S_l^z ... c_m S_m^z \right\rangle \right\rangle_r \cong \langle c_i \rangle_r ... \langle c_j \rangle_r \left\langle c_k \left\langle S_k^z \right\rangle \right\rangle_r \times \left\langle c_l \left\langle S_l^z \right\rangle \right\rangle_r ... \langle c_m \left\langle S_m^z \right\rangle \rangle_r, \quad (5.1.9)$$

with

$$\langle c_i \rangle_r = \left\langle c_j \right\rangle_r = c \quad \text{and} \quad \langle c_\alpha \langle S^z_\alpha \rangle \rangle_r = m, \quad \alpha = k, l, ..., m.$$

In this approximation, only the correlations between quantities pertaining to different sites are neglected. A detailed discussion about these configurational averaging techniques is also given by (Tucker, 1991).

We state that hereafter, we will carry on the formulation of the dilute spin-1/2 system for a honeycomb lattice ($q = 3$), however a brief explanation of the method for a square lattice ($q = 4$) can be found in (Akinci, Yuksel, & Polat, 2011c). Now, if we expand the right-hand side of Eq. (5.1.6) for $q = 3$ *without using DA*, we get some certain identities in the form

$$\left\langle \left\langle c_i...c_j c_k S^z_k c_l S^z_l...c_m S^z_m \right\rangle \right\rangle_r = \left\langle c_i...c_j \right\rangle_r \times \left\langle \left\langle c_k S^z_k c_l S^z_l...c_m S^z_m \right\rangle \right\rangle_r. \tag{5.1.10}$$

In Eq. (5.1.10), we use the fact that occupation number c_i of a given site i is independent from the thermal average, as long as the correlation function does not contain a spin variable S^z_i, and the site occupation numbers pertaining to different sites are assumed to be statistically independent from each other. Hence, we may rearrange Eq. (5.1.10) as

$$\left\langle \left\langle c_i...c_j c_k S^z_k c_l S^z_l...c_m S^z_m \right\rangle \right\rangle_r = \langle c_i \rangle_r ... \left\langle c_j \right\rangle_r \times \left\langle \left\langle c_k S^z_k c_l S^z_l...c_m S^z_m \right\rangle \right\rangle_r, \tag{5.1.11}$$

where $\langle c_i \rangle_r = \left\langle c_j \right\rangle_r = c$. In the present formulation, it is clear that Eq. (5.1.11) improves DA based on Eqs. (5.1.8) and (5.1.9) by taking into account the multi-site correlations. With the help of Eq. (5.1.11), and by expanding the right-hand side of Eq. (5.1.6) for the central site $c_0 S^z_0$ with $\{f_i\} = 1$ we have

$$m = \langle \langle c_0 S_0 \rangle \rangle_r = x_1 = (3c - 6c^2 + 3c^3) x_4 K_1 + (6c^2 - 6c^3) x_4 K_2 + 3c^3 x_4 K_3 + c x_6 K_4,$$
$$\tag{5.1.12}$$

where the terms x_i in Eq. (5.1.12) are defined as

$$x_1 = \langle \langle c_0 S_0 \rangle \rangle_r, \quad x_4 = \langle \langle c_1 S_1 \rangle \rangle_r, \quad x_6 = \langle \langle c_1 S_1 c_2 S_2 c_3 S_3 \rangle \rangle_r.$$

In obtaining Eq. (5.1.12) we use the fact that $\tanh(\beta x)$ is an odd function. Hence, only

the odd coefficients give non-zero contribution which can be given as follows:

$$
\begin{aligned}
K_1 &= \sinh(J\nabla)\tanh(\beta x)|_{x=0}, \\
K_2 &= \cosh(J\nabla)\sinh(J\nabla)\tanh(\beta x)|_{x=0}, \\
K_3 &= \cosh^2(J\nabla)\sinh(J\nabla)\tanh(\beta x)|_{x=0}, \\
K_4 &= \sinh^3(J\nabla)\tanh(\beta x)|_{x=0}.
\end{aligned}
\tag{5.1.13}
$$

For comparison, if we apply the improved decoupling approximation given in Eq. (5.1.9) then Eq. (5.1.12) reduces to

$$
m = (3c - 6c^2 + 3c^3)mK_1 + (6c^2 - 6c^3)mK_2 + 3c^3 mK_3 + cm^3 K_4,
\tag{5.1.14}
$$

which is identical to those obtained in Refs. (Balcerzak, Bobák, Mielnicki, & Truong, 1985, Tucker, 1991, Bobák & Jaščur, 1991). Additionally, applying the conventional method given in Eq. (5.1.8) gives the following result

$$
m = (3c - 6c^2 + 3c^3)mK_1 + (6c^2 - 6c^3)mK_2 + 3c^3 mK_3 + c^3 m^3 K_4.
\tag{5.1.15}
$$

It seems like it is fortuitous that although, the equations of states of approximations (5.1.8) and (5.1.9) are differ from each other in the last term, they give the same phase diagram in $(k_B T_c / J - c)$ plane. The reason comes from the fact that in Eqs. (5.1.14) and (5.1.15) both approximations ignore the term m^3 in the limit $T \to T_c$. Hence, it should be emphasized that the importance and distinction of our method becomes evident by expansion of Eq. (5.1.6) without using any kind of DA.

The next step is to carry out the configurational and thermal averages of the perimeter site in the system, and it is found as

$$
\langle\langle\{f_\delta\}c_\delta S_\delta\rangle\rangle_r = \langle c_\delta \langle\{f_\delta\}(c_0\cosh(J\nabla) + c_0 S_0 \sinh(J\nabla) + 1 - c_0)\rangle\rangle_r \tanh(\beta(x+\gamma)).
$$
$$
\tag{5.1.16}
$$

From Eq. (5.1.16) with $\delta = \{f_\delta\} = 1$ we get the following identity

$$
\langle\langle c_1 S_1 \rangle\rangle_r = x_4 = (c - c^2)A_1 + c^2 A_2 + c x_1 A_3.
\tag{5.1.17}
$$

For the sake of simplicity, the superscript z is omitted from the left- and right-hand

sides of Eqs. (5.1.12) and (5.1.17). The coefficients in Eq. (5.1.17) are given as

$$
\begin{aligned}
A_1 &= \tanh(\beta(x+\gamma))|_{x=0}, \\
A_2 &= \cosh(J\nabla)\tanh(\beta(x+\gamma))|_{x=0}, \\
A_3 &= \sinh(J\nabla)\tanh(\beta(x+\gamma))|_{x=0}.
\end{aligned}
\tag{5.1.18}
$$

The coefficients in Eqs. (5.1.13) and (5.1.18) can be easily calculated by applying a mathematical relation, $e^{\alpha\nabla}f(x) = f(x+\alpha)$. In Eq. (5.1.18), $\gamma = (q-1)A$ is the effective field produced by the $(q-1)$ spins outside of the cluster, and A is an unknown parameter to be determined self-consistently (c.f. see Fig. 4.1).

Eqs. (5.1.12) and (5.1.17) are the fundamental correlation functions of the system. On the other hand, for a honeycomb lattice, taking Eqs. (5.1.12) and (5.1.17) as basis, we derive a set of linear equations of the site correlation functions in the system. Recalling the rules given in Chapter 4, we get a system of linear equations with 6 unknowns for $q = 3$ (for a detailed explanation of derivation process of correlation functions, see (Akinci, Yuksel, & Polat, 2011c)):

$$
\begin{aligned}
x_1 &= (3c - 6c^2 + 3c^3)x_4 K_1 + (6c^2 - 6c^3)x_4 K_2 + 3c^3 x_4 K_3 + cx_6 K_4, \\
x_2 &= (3c^2 - 6c^3 + 3c^4)K_1 + (6c^3 - 6c^4)K_2 + 3c^4 K_3 + c^2 x_5 K_4, \\
x_3 &= (-3c^2 + 3c^3)x_4 K_1 + (6c^2 - 6c^3)x_4 K_2 + 3c^3 x_4 K_3 + c^3 x_4 K_4, \\
x_4 &= (c - c^2)A_1 + c^2 A_2 + cx_1 A_3, \\
x_5 &= cA_3 x_2 + (c - c^2)A_1 x_4 + c^2 A_2 x_4, \\
x_6 &= cA_3 x_3 + (c - c^2)A_1 x_5 + c^2 A_2 x_5,
\end{aligned}
\tag{5.1.19}
$$

where

$$
\begin{aligned}
x_1 &= \langle\langle c_0 S_0 \rangle\rangle_r, \\
x_2 &= \langle\langle c_0 S_0 c_1 S_1 \rangle\rangle_r, \\
x_3 &= \langle\langle c_0 S_0 c_1 S_1 c_2 S_2 \rangle\rangle_r, \\
x_4 &= \langle\langle c_1 S_1 \rangle\rangle_r, \\
x_5 &= \langle\langle c_1 S_1 c_2 S_2 \rangle\rangle_r, \\
x_6 &= \langle\langle c_1 S_1 c_2 S_2 c_3 S_3 \rangle\rangle_r.
\end{aligned}
\tag{5.1.20}
$$

Since the thermal and configurational average of the central site is equal to that of its nearest-neighbor sites within the present method, the unknown parameter A can be numerically determined by the relation

$$x_1 = x_4. \tag{5.1.21}$$

Desired critical properties of the system can be obtained by numerical solution of Eqs. (5.1.20) and Eq. (5.1.21). In the following, we will present the results for a spin-1/2 dilute ferromagnetic system defined on honeycomb and square lattices. However, the formulation and numerical results concerning a spin-1 model can also be found in (Akinci, Yuksel, & Polat, 2011c).

In Fig. 5.1 we show the phase diagrams and magnetization, as well as specific heat curves for honeycomb ($q = 3$) and square ($q = 4$) lattices which can be obtained by solving Eqs. (5.1.19) and (5.1.21) numerically. In Fig. 5.1a variations of magnetization curves are depicted as a function of temperature $k_B T / J$ with typical values of site concentration c. As expected, we see in Fig. 5.1a that as the temperature increases starting from zero, the magnetization of the system decreases continuously, and it falls rapidly to zero at the critical temperature $k_B T_c / J$ for selected c values. The number of interacting sites on the lattice decreases as c decreases and hence, $k_B T_c / J$ value of the system and the saturation value of magnetization curves also decrease as c decreases. In particular, the ground state saturation value of magnetization for $q = 3$ linearly decreases with decreasing value of c up to $c = 0.71$. For $c = 0.7$, the site concentration gets closer to its critical value (i.e. percolation threshold) c^* and the magnetization saturates at $m = 0.616$ at low temperatures. In Fig. 5.1b we examine the effect of site concentration c on the temperature dependence of specific heat of the system. We see that as the temperature increases starting from zero, then the specific heat curves exhibit a sharp peak at a second-order phase transition temperature which decreases with decreasing c. As c approaches its critical value c^* at which critical temperature reduces to zero then an additional broad Schottky-type maximum appears and below c^* phase transition disappears. For $c > c^*$ the system forms an infinite cluster of lattice sites. However, as c gets closer to c^* then isolated finite clusters appear and for $c < c^*$ the system cannot exhibit long range

ferromagnetic order even at zero temperature which causes a broad round maximum in specific heat vs temperature curves. These observations are qualitatively agree with those of Refs. (Bobák & Jaščur, 1994, Bonfim & Fittipaldi, 1983, Balcerzak, Bobák, Mielnicki, & Truong, 1985, Wiatrowski, Balcerzak, & Mielnicki, 1988) and show the proper thermodynamic behavior over the whole range of temperatures, including the ground-state behavior ($C/Nk_B \to 0$ as $k_B T/J \to 0$) and the thermal stability condition ($C/Nk_B \geq 0$). Next, Fig. 5.1c represents the variation of the saturation magnetization with site concentration. In this figure, we also compare our results (blue line) with those of EFT based on conventional DA (C-DA, black line) and improved DA (I-DA, red line) methods. It is clearly evident that site dilution lowers down the saturation magnetization. According to C-DA saturation magnetization of the system continuously decreases as c decreases then falls rapidly to zero at c^*. On the other hand, I-DA predicts a linear decrease at high magnetic atom concentrations, but as c decreases gradually then a monotonic decline is observed in the saturation magnetization value. According to our results we observe a linear decrement trend up to the vicinity of c^* which originates as a result of consideration of the multi-site correlations. We also observe that as the coordination number q of the lattice increases then the critical site concentration value c^* decreases which means that destructing the ferromagnetic order of the system will be harder as more atoms interact with each other, even at lower magnetic atom concentrations. Finally, we represent the phase diagram of the system in ($k_B T_c/J - c$) plane which separates the ferromagnetic and paramagnetic phases and we compare our results with those of the other methods in the literature. According to this figure, critical temperature $k_B T_c/J$ of system decreases gradually, and ferromagnetic region gets narrower as c decreases, and $k_B T_c/J$ value depresses to zero at $c = c^*$. Such a behavior is an expected fact in dilution problems. Numerical values of critical concentration c^* for honeycomb ($q = 3$) and square ($q = 4$) lattices are given in Table 5.1, and compared with the other works in the literature. It is well known that the series expansion (SE) method gives the best approximate values to the known exact results (Stauffer & Aharony, 1991). Therefore, we see in Table 5.1 that the present work improves the results of finite cluster approximation (OSCA and TSCA), as well as the other works based on EFT with DA. The reason is due to

the fact that, in contrast to the previously published works mentioned above, there is no uncontrolled decoupling procedure used for the higher-order correlation functions within the present approximation.

Table 5.1 Numerical values of critical site concentration c^* for spin-1/2 system obtained within the present work for $q = 3, 4$ and comparison with various approximations in the literature: Average coordination number approximation $2/q$ and Bethe approximation $(q-1)^{-1}$ (Sato et al., 1959), renormalization group (RG) (Yeomans & Stinchcombe, 1978, 1979), CEFT (Taggart, 1982), DA (Balcerzak et al., 1985, Li & Yang, 1985, Bobák & Jaščur, 1991, Saber, 1997), OSCA (Wiatrowski et al., 1988, Bobák et al., 1993), TSCA (Bobák & Karaba, 1987, Bobák et al., 1993), CVM (Balcerzak, 2001), MC (Néda, 1994), SE (Sykes & Essam, 1964, Sykes et al., 1976).

q	MFT	$2/q$	$(q-1)^{-1}$	RG	CEFT	DA,OSCA	TSCA	CVM	MC	SE	Present Work
3	0	0.667	0.5		0.711	0.5575	0.5706	0.768		0.698	0.6727
4	0	0.5	0.333	0.602	0.558	0.4284	0.4303	0.640	0.413	0.593	0.4594

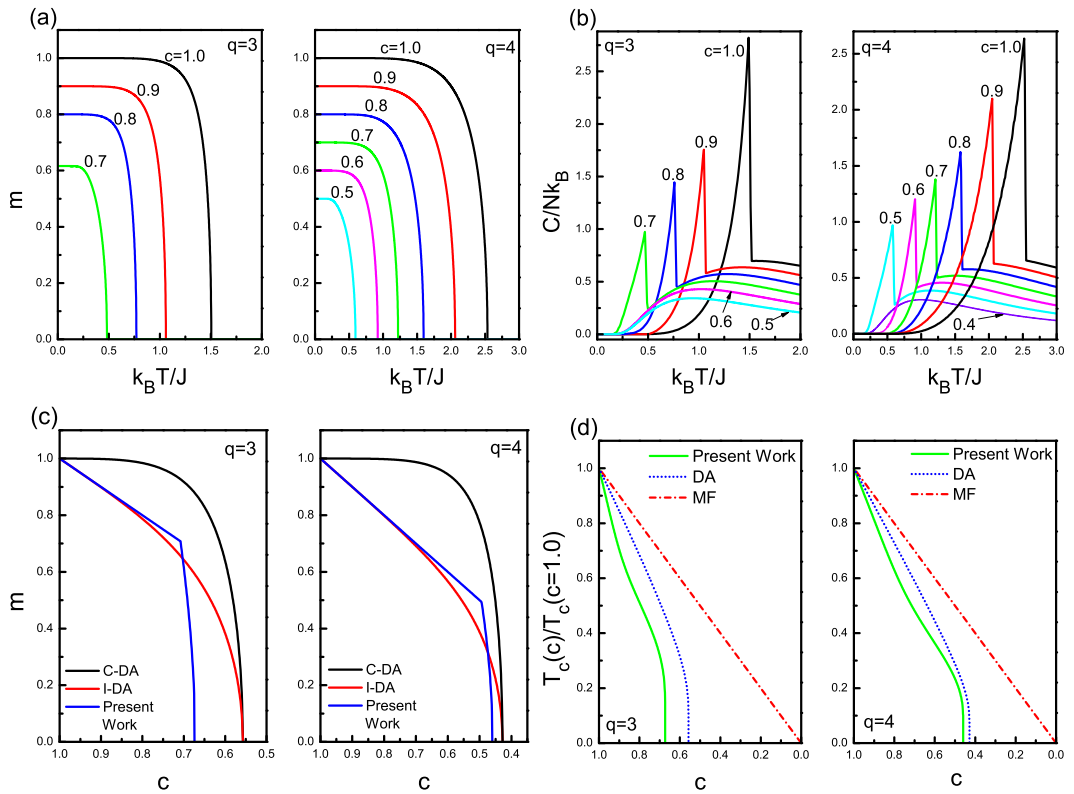Figure 5.1 Temperature dependence of (a) magnetization, (b) specific heat curves of dilute ferromagnetic system for honeycomb ($q = 3$) and square ($q = 4$) lattices with some selected values of site concentration c. (c) Ground state magnetizations as a function of temperature for $q = 3$, and $q = 4$. (d) Phase diagrams of the system in ($k_B T_c/J - c$) plane obtained by MFT (dash-dotted), DA (dotted), and present work (solid).

5.2 Bond-Diluted Spin-1 Blume-Capel Model with Transverse and Crystal Field Interactions

After the observation of reentrant magnetism by Maletta and Felsch (Maletta & Felsch, 1979), the interest has also been directed to investigation of the disorder effects on the thermal and magnetic properties of TIM where the type of the bond interactions is chosen at random according to a given probability distribution. For a detailed literature review of problem see (Akinci, Yuksel, & Polat, 2011b). The most simple model concerning the quenched randomness in nearest-neighbor interactions can be represented by the following Hamiltonian

$$\mathcal{H} = -\sum_{<ij>} J_{ij} S_i^z S_j^z, \tag{5.2.1}$$

where the type of the exchange interactions between the nearest-neighbor sites are distributed according to a given probability distribution. For instance, the exchange couplings between the neighboring spins can be generated according to distribution

$$P(J_{ij}) = \left[2\pi(\Delta J_{ij})^2\right]^{-1/2} \exp[-(J_{ij} - J)^2 / 2\Delta J_{ij}^2], \tag{5.2.2}$$

which is called Edwards-Anderson model. On the other hand, a simplified form of the model can also be written as

$$P(J_{ij}) = (1 - p)\delta(J_{ij} - \alpha J_1) + p\delta(J_{ij} - J_2), \tag{5.2.3}$$

where $J_2 > 0$, $\alpha = J_1/J_2$ with $|\alpha| \leq 1$. For $\alpha > 0$, we have the ordered ferromagnetic phase but the strength of the ferromagnetic couplings may not be uniformly distributed. For $\alpha = 0$ we have a bond-diluted model, and for $\alpha < 0$ there are competing ferromagnetic and anti-ferromagnetic interactions and thus frustrations (Tóth & Tóthová, 1994). Note that the model reduces to pure system for $p = 1$.

Now, let us introduce the bond diluted spin-1 system with both crystal and transverse fields within the framework of our EFT formalism. The Hamiltonian describing our model is

$$\mathcal{H} = -\sum_{<i,j>} J_{ij} S_i^z S_j^z - D\sum_i (S_i^z)^2 - \Omega\sum_i S_i^x, \tag{5.2.4}$$

where S_i^z and S_i^x denote the z and x components of the spin operator, respectively. The first summation in Eq. (5.2.4) is over the nearest-neighbor pairs of spins and the operator S_i^z takes the values $S_i^z = 0, \pm 1$. J_{ij}, D and Ω terms stand for the exchange interaction, single-ion anisotropy (i.e. crystal field) and transverse field, respectively. We assume that the nearest neighbor interactions are randomly distributed on the lattice according to the probability distribution function

$$P(J_{ij}) = (1-p)\delta(J_{ij}) + p\delta(J_{ij} - J), \qquad (5.2.5)$$

where $0 < p \le 1$ and it denotes the concentration of closed bonds. We construct the mathematical background of our model by using the approximated spin correlation identities (Barreto et al., 1981) by taking into account random configurational averages

$$\langle\langle\{f_i\}S_i^\alpha\rangle\rangle_r = \left\langle\left\langle\{f_i\}\frac{\mathrm{Tr}_i S_i^\alpha \exp(-\beta H_i)}{\mathrm{Tr}_i \exp(-\beta H_i)}\right\rangle\right\rangle_r, \qquad (5.2.6)$$

$$\langle\langle\{f_i\}(S_i^\alpha)^2\rangle\rangle_r = \left\langle\left\langle\{f_i\}\frac{\mathrm{Tr}_i (S_i^\alpha)^2 \exp(-\beta H_i)}{\mathrm{Tr}_i \exp(-\beta H_i)}\right\rangle\right\rangle_r, \qquad (5.2.7)$$

where $\beta = 1/k_B T$, $\alpha = z$ or x, $\{f_i\}$ is an arbitrary function which is independent of the central spin S_i and the inner $\langle...\rangle$ and the outer $\langle...\rangle_r$ products represents the thermal and random configurational averages, respectively. Now, our aim is to derive the fundamental correlation functions $\langle\langle S_0^\alpha\rangle\rangle_r$, $\langle\langle (S_0^\alpha)^2\rangle\rangle_r$, $\langle\langle S_1^z\rangle\rangle_r$ and $\langle\langle (S_1^z)^2\rangle\rangle_r$. The $z-$ components of these correlation functions are the fundamental relations in determining the complete set of correlation functions. Again we consider a honeycomb lattice for simplicity, since the number of linear equations increases gradually for larger coordination number q.

In the next step, we separate the Hamiltonian (5.2.4) into two parts as $\mathcal{H} = H_i + H'$. Here, the effective Hamiltonian H_i includes all the contributions associated with the site i, and the other part H' does not depend on the site i. We can write $-H_i$ as

$$-H_i = E_i S_i^z + D\left(S_i^z\right)^2 + \Omega S_i^x, \qquad (5.2.8)$$

where $E_i = \sum_j J_{ij} S_j^z$ is the local field on the site i. As we noted before, in order to proceed further we have to diagonalize $-H_i$ matrix in Eq. (5.2.8). For a spin-1 system, eigenvalues λ_n and corresponding eigenvectors φ_n of $-H_i$ are given in Eqs. (4.1.43) and (4.1.44), respectively.

By applying the differential operator technique in Eqs. (5.2.6) and (5.2.7) with $\{f_i\} = 1$, we obtain the following spin correlations for the thermal and configurational averages of a central spin, as well as its perimeter spin for a honeycomb lattice ($q = 3$) as follows

$$\langle\langle S_0^z\rangle\rangle_r = \left\langle\left\langle\left[\prod_{j=1}^{q=3}\left[1 + S_j^z\sinh(J_{ij}\nabla) + (S_j^z)^2\{\cosh(J_{ij}\nabla) - 1\}\right]\right]\right\rangle\right\rangle_r F(x)|_{x=0}, \qquad (5.2.9)$$

$$\langle\langle S_0^x\rangle\rangle_r = \left\langle\left\langle\left[\prod_{j=1}^{q=3}\left[1 + S_j^z\sinh(J_{ij}\nabla) + (S_j^z)^2\{\cosh(J_{ij}\nabla) - 1\}\right]\right]\right\rangle\right\rangle_r H(x)|_{x=0}. \qquad (5.2.10)$$

$$\langle\langle (S_0^z)^2\rangle\rangle_r = \left\langle\left\langle\left[\prod_{j=1}^{q=3}\left[1 + S_j^z\sinh(J_{ij}\nabla) + (S_j^z)^2\{\cosh(J_{ij}\nabla) - 1\}\right]\right]\right\rangle\right\rangle_r G(x)|_{x=0}, \qquad (5.2.11)$$

$$\langle\langle (S_0^x)^2\rangle\rangle_r = \left\langle\left\langle\left[\prod_{j=1}^{q=3}\left[1 + S_j^z\sinh(J_{ij}\nabla) + (S_j^z)^2\{\cosh(J_{ij}\nabla) - 1\}\right]\right]\right\rangle\right\rangle_r K(x)|_{x=0}, \qquad (5.2.12)$$

and

$$\langle\langle S_\delta^z\rangle\rangle_r = \langle\langle 1 + S_0^z\sinh(J_{ij}\nabla) + (S_0^z)^2\{\cosh(J_{ij}\nabla) - 1\}\rangle\rangle_r F(x+\gamma)|_{x=0}, \qquad (5.2.13)$$

$$\langle\langle (S_\delta^z)^2\rangle\rangle_r = \langle\langle 1 + S_0^z\sinh(J_{ij}\nabla) + (S_0^z)^2\{\cosh(J_{ij}\nabla) - 1\}\rangle\rangle_r G(x+\gamma). \qquad (5.2.14)$$

Note that the functions $F(x)$, $H(x)$, $G(x)$ and $K(x)$ in above relations can be calculated using Eqs. (4.1.57)-(4.1.60), respectively. By expanding the right-hand sides of Eqs. (5.2.9)-(5.2.14) we can get the explicit forms of the longitudinal and transverse spin correlations. Since we have already given a detailed formulation for a spin-1 system (c.f. Sections 4.1.2 and 4.1.3), we will not deal with the tedious calculation details for the present problem. However, in order to depict the configurational averaging procedure explicitly, for instance, let us expand the right-hand side of Eq.(5.2.9) as

$$
\begin{aligned}
m_z = \langle\langle S_0^z\rangle\rangle_r ={} & l_0 + 3k_1\langle\langle S_1\rangle\rangle_r + 3(l_1 - l_0)\langle\langle S_1^2\rangle\rangle_r + 3l_2\langle\langle S_1 S_2\rangle\rangle_r \\
& + 6(k_2 - k_1)\langle\langle S_1 S_2^2\rangle\rangle_r + 3(l_0 - 2l_1 + l_3)\langle\langle S_1^2 S_2^2\rangle\rangle_r \\
& + k_3\langle\langle S_1 S_2 S_3\rangle\rangle_r + 3(l_4 - l_2)\langle\langle S_1 S_2 S_3^2\rangle\rangle_r \\
& + 3(k_1 - 2k_2 + k_4)\langle\langle S_1 S_2^2 S_3^2\rangle\rangle_r \\
& + (-l_0 + 3l_1 - 3l_3 + l_5)\langle\langle S_1^2 S_2^2 S_3^2\rangle\rangle_r,
\end{aligned} \qquad (5.2.15)
$$

where

$l_0 = F(0),$

$l_1 = \left\langle \cosh(J_{ij}\nabla) \right\rangle_r F(x)|_{x=0},$ $\qquad$ $k_1 = \left\langle \sinh(J_{ij}\nabla) \right\rangle_r F(x)|_{x=0},$

$l_2 = \left\langle \sinh(J_{ij}\nabla) \right\rangle_r^2 F(x)|_{x=0},$ $\qquad$ $k_2 = \left\langle \cosh(J_{ij}\nabla) \right\rangle_r \left\langle \sinh(J_{ij}\nabla) \right\rangle_r F(x)|_{x=0},$

$l_3 = \left\langle \cosh(J_{ij}\nabla) \right\rangle_r^2 F(x)|_{x=0},$ $\qquad$ $k_3 = \left\langle \sinh(J_{ij}\nabla) \right\rangle_r^3 F(x)|_{x=0},$

$l_4 = \left\langle \cosh(J_{ij}\nabla) \right\rangle_r \left\langle \sinh(J_{ij}\nabla) \right\rangle_r^2 F(x)|_{x=0},$ $\quad$ $k_4 = \left\langle \cosh(J_{ij}\nabla) \right\rangle_r^2 \left\langle \sinh(J_{ij}\nabla) \right\rangle_r F(x)|_{x=0},$

$l_5 = \left\langle \cosh(J_{ij}\nabla) \right\rangle_r^3 F(x)|_{x=0}.$ $\qquad\qquad\qquad\qquad\qquad\qquad\qquad$ (5.2.16)

We note that, for the sake of simplicity, the superscript z is omitted from the correlation functions on the right-hand side of Eq. (5.2.15). The random configurational averages in Eq. (5.2.16) can be obtained by using the probability distribution in Eq. (5.2.3) and they are found as

$$
\begin{aligned}
\left\langle \cosh(J_{ij}\nabla) \right\rangle_r &= \int dJ_{ij}P(J_{ij})\cosh(J_{ij}\nabla) \\
&= (1-p)+p\cosh(J\nabla), \\
\left\langle \sinh(J_{ij}\nabla) \right\rangle_r &= \int dJ_{ij}P(J_{ij})\sinh(J_{ij}\nabla) \\
&= p\sinh(J\nabla). \qquad\qquad\qquad (5.2.17)
\end{aligned}
$$

It is quite clear from above discussion that as long as the form of the probability distribution of the quenched bond disorder is given, the present formulation can be easily adopted to any disorder problem including the disordered systems with competing ferromagnetic and anti-ferromagnetic interactions.

As in conventional process, we also expand the right-hand sides of Eqs. (5.2.10)-(5.2.14) by following the above procedure and we obtain the explicit forms of basis relations of a bond diluted spin-1 system (Akinci, Yuksel, & Polat, 2011b) from which we derive a set of 21 linear equations for $z-$ components, in addition to transverse spin correlations $\langle \langle S_0^x \rangle \rangle_r$ and $\langle \langle (S_0^x)^2 \rangle \rangle_r$ which in total yields 23 linear equations. The complete set can be found in (Akinci et al., 2011b).

Now, we are able to discuss the numerical results concerning the phase diagrams of the system. In Fig. 5.2, we plot the dependence of the bond percolation threshold

Table 5.2 Bond percolation threshold value p_c for $D/J = 0$ and $\Omega/J = 0$ obtained by several methods including EFT with single site kinematic relations (Tucker, 1994), DA (Yan & Deng, 2002), finite cluster approximation FCA (Benayad, Benyoussef, & Boccara, 1985, Kerouad & Saber, 1991), two-spin cluster approximation TSCA (Tóth & Tóthová, 1994), MC simulations (Vyssotsky, Gordon, Frisch, & Hammersley, 1961) and series expansions (SE) (Domb & Sykes, 1961) and present work for a honeycomb lattice.

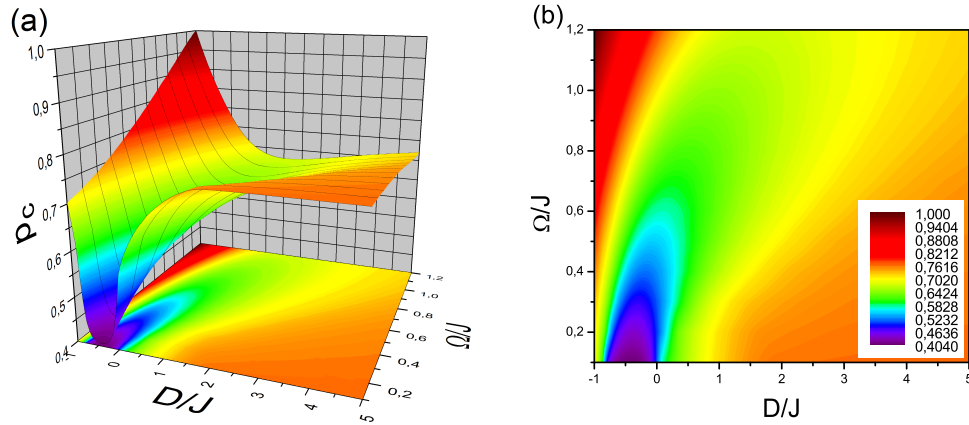| EFT	DA	FCA	FCA	TSCA	MC	SE	Present Work
0.5158	0.5364	0.5158	0.5160	0.5449	0.64	0.66	0.5397

Figure 5.2 Variation of the bond percolation threshold p_c with crystal field D/J and transverse field Ω/J. (a) 3D contour plot surface, (b) projection on (Ω/J-D/J) plane.

surface with $-1.0 < D/J < 5$ and $0.1 < \Omega < 1.2$. As we can see from Fig. 5.2a, the effect of the transverse field Ω/J on the percolation threshold value clearly depends on the value of the crystal field D/J and vice versa. Namely, for the values of $-1.0 < D/J < 0.32$, as Ω/J increases then the p_c increases and reaches its maximum value. On the other hand, for the other D/J values, p_c decreases for a while and then tends to increase with increasing Ω/J. If the value of D/J is sufficiently positive then p_c value remains more or less constant being independent from the value of Ω/J. We think that the mechanism underlying this behavior completely originates from a collective effect of both Ω/J and D/J or strictly speaking, we can mention about a competition between D/J and Ω/J on the system. One should notice that, for the values of $D/J = -1.0$ and $\Omega/J = 1.2$ the system can not exhibit a long range ordering since $p_c = 1.0$. In the limit

$D/J \to \infty$, single-ion anisotropy is dominant against Ω/J, and $p_c = 0.7622$ value below which the system can not exhibit a long range ferromagnetic order is the percolation threshold of corresponding spin-1/2 system (Akinci, 2011). Moreover, in the absence of crystal and transverse field interactions, numerical value of percolation threshold p_c is given in Table 5.2 and it is compared with the other works in the literature. As seen from Table 5.2, we improve the results of the other works based on EFT approximation (Tucker, 1994, Yan & Deng, 2002, Benayad, Benyoussef, & Boccara, 1985, Kerouad & Saber, 1991). For the further detailed discussions regarding the tricritical properties, refer to (Akinci et al., 2011b).

5.3 Spin-1 Blume-Capel Model with Random Crystal Field Interactions

Ordinary spin-1 Blume-Capel (and also Blume-Emery-Griffiths) model has been widely used over three decades in literature to give a theoretical explanation for a wide variety of physical observations, including essentially superfluid transitions in ^{3}He $-^4$He mixtures (Graf, Lee, & Reppy, 1967). The general Hamiltonian of a spin-1 Blume-Emery-Griffiths model (Blume, Emery, & Griffiths, 1971)

$$\mathcal{H} = -J \sum_{<ij>} S_i S_j - K \sum_{<ij>} S_i^2 S_j^2 - D \sum_i S_i^2, \qquad (5.3.1)$$

was introduced to describe the phase separation in ^{3}He $-^4$He mixtures where $S_i = \pm 1, 0$ and $K = K_{33} + K_{44} - 2K_{34}$ with $K_{\alpha\beta}$ being the interaction energy between $^\alpha$He $-^\beta$He atoms ($\alpha, \beta = 3, 4$). Since $K_{\alpha\beta}$ is almost independent of α and β, we generally have $K \approx 0$.

According to former experimental measurements (Graf, Lee, & Reppy, 1967) and theoretical investigations (Blume, Emery, & Griffiths, 1971), phase diagrams depicted in temperature versus ^{3}He concentration was shown to exhibit a λ line with a tricritical point which separates the normal and superfluid phases from a mixed phase where ^{4}He rich and ^{3}He rich phases coexist. On the other hand, phase transition properties of such a system can be drastically changed by introducing a disorder due to the presence of a porous medium. From the experimental point of view, critical properties of

^{3}He $-^4$He mixtures in porous aerogel medium with various porosity values have been investigated in detail and it was reported that as a consequence of presence of disorder due to aerogel medium, the coexistence boundary is detached, the tricritical point is removed and a superfluid ^{3}He phase is originated at sufficiently low temperatures and high concentration of ^{3}He mixtures on the phase diagram (Mulders, Ma, Kim, Yoon, & Chan, 1995, Kim, Ma, & Chan, 1993, Paetkau & Beamish, 1998).

On the theoretical side, in order to characterize the effect of quenched disorder originating from the aerogel medium on the phase transition properties in superfluid systems, a random anisotropy Blume-Capel model has been proposed (Buzano, Maritan, & Pelizzola, 1994, Maritan, Cieplak, Swift, & Toigo, 1992). The presence of aerogel was modeled as a random external field that selects which of the two types of helium to have nearby (Buzano, Maritan, & Pelizzola, 1994) by the following Hamiltonian

$$\mathcal{H} = -J \sum_{<ij>} S_i S_j + \sum_i \Delta_i S_i^2, \qquad (5.3.2)$$

where S_i is a fictitious spin variable which can take the values $S_i = \pm 1, 0$ and Δ_i is a site-dependent random variable distributed according to a probability distribution function $P(\Delta_i)$ on the lattice sites. The spin states $S_i = \pm 1$ and $S_i = 0$ denote ^{4}He and ^{3}He atoms located on a particular lattice site i, respectively. The probability density is often chosen as

$$P(\Delta_i) = p\delta(\Delta_i - \Delta_0) + (1-p)\delta(\Delta_i - \Delta_1) \qquad (5.3.3)$$

in the literature (Buzano, Maritan, & Pelizzola, 1994, Maritan, Cieplak, Swift, & Toigo, 1992). According to Eq. (5.3.3), fraction p of the lattice sites with $\Delta_0 < 0$ is occupied by ^{4}He atoms since $S_i = \pm 1$ minimizes the Hamiltonian (5.3.2) whereas the remaining lattice sites with $\Delta_1 > 0$ are occupied by ^{3}He atoms with $S_i = 0$. Hence, it can be deduced that the fully magnetized state of the system corresponds to pure ^{4}He superfluid. As the magnetization reduces towards zero then the number of ^{3}He atoms filling the aerogel pores increases.

However, there is not a unique form of distribution (5.3.3). Namely, different probability distributions correspond to different physical systems and may lead to

different phase transition characteristics. In this context, from the theoretical point of view, the Blume-Capel (BC) model with a random crystal field (RCF) has been studied by a variety of techniques (for a detailed literature review see (Yüksel, Akinci, & Polat, 2012a)). Other than this, it is well known that magnetic systems with dilute crystal fields exhibit qualitatively similar characteristics when compared to the site dilution problem of magnetic atoms. From this point of view, for a BC model with diluted crystal fields, MFT predicts that the phase transition temperature of the system will remain at a finite value until zero concentration is reached which can be regarded as a limitation of the mean field predictions. On the other hand, the results obtained by conventional EFT based on DA are limited to second-order phase transitions and tricritical points, and a detailed description of first-order transitions has not been reported. In this context, we believe that the BC model with RCF still deserves particular attention for investigating the proper phase diagrams, especially the first-order transition lines that include reentrant phase transition regions. Therefore, taking the multi-site correlations into consideration will improve the results of conventional EFT approximations. Consequently, we intend to investigate the effects of RCF distributions on the phase diagrams of spin-1 BC model on several 2D lattices with various coordination numbers.

For this aim let us consider the following Hamiltonian equation

$$\mathcal{H} = -J \sum_{<ij>} S_i^z S_j^z - \sum_i D_i (S_i^z)^2, \qquad (5.3.4)$$

where the first term is a summation over the nearest-neighbor spins with $S_i^z = \pm 1, 0$ and the term D_i on the second summation represents a random crystal field, distributed according to a given probability distribution. In this work, we primarily deal with two kinds of probability distributions, namely, a quenched diluted crystal field distribution and a double peaked delta distribution which are given by Eqs. (5.3.5) and (5.3.6), respectively as follows

$$P(D_i) = p\delta(D_i - D) + (1 - p)\delta(D_i), \qquad (5.3.5)$$

$$P(D_i) = \frac{1}{2} \{ \delta[D_i - (D - \Delta)] + \delta[D_i - (D + \Delta)] \}, \qquad (5.3.6)$$

where the parameter p in Eq. (5.3.5) denotes the concentration of the spins on the lattice which are influenced by a crystal field D. Using the conventional form of approximated spin correlation identities defined in Eqs. (5.2.6) and (5.2.7), we obtain the following spin identity with thermal and configurational averages of a central spin for a lattice with a coordination number q as

$$\langle\langle S_0^z \rangle\rangle_r = \left\langle \left\langle \left[\prod_{j=1}^{q} \left[1 + S_j^z \sinh(J\nabla) + (S_j^z)^2 \{\cosh(J\nabla) - 1\} \right] \right] \right\rangle \right\rangle_r F(x)|_{x=0}. \tag{5.3.7}$$

The function $F(x)$ in Eq. (5.3.7) is defined by

$$F(x) = \int dD_i P(D_i) f(x, D_i), \tag{5.3.8}$$

where

$$\begin{aligned} f(x, D_i) &= \frac{1}{\sum_{n=1}^{3} \exp(\beta\lambda_n)} \sum_{n=1}^{3} \langle\varphi_n|S_i^z|\varphi_n\rangle \exp(\beta\lambda_n), \\ &= \frac{2\sinh(\beta x)}{2\cosh(\beta x) + e^{-\beta D_i}}. \end{aligned} \tag{5.3.9}$$

In Eq. (5.3.9), λ_n denotes the eigenvalues of $-H_i$ matrix, and φ_n represents the eigenvectors corresponding to the eigenvalues λ_n of $-H_i$ matrix. With the help of Eq. (5.3.9), and by using the distribution functions defined in Eqs. (5.3.5) and (5.3.6), the function $F(x)$ in Eq. (5.3.8) can be easily calculated by numerical integration. Hereafter, we will focus our attention on the construction of the correlation functions, as well as magnetization and quadrupole moment identities of a honeycomb lattice with $q = 3$. A brief formulation of the fundamental spin identities for a square lattice with $q = 4$ can be found in (Yüksel et al., 2012a).

By expanding the right-hand side of Eq. (5.3.7) for a honeycomb lattice with $q = 3$, we get the longitudinal magnetization as

$$\begin{aligned} m_z = \langle\langle S_0^z \rangle\rangle_r &= l_0 + 3k_1\langle\langle S_1 \rangle\rangle_r + 3(l_1 - l_0)\langle\langle S_1^2 \rangle\rangle_r + 3l_2\langle\langle S_1 S_2 \rangle\rangle_r \\ &\quad + 6(k_2 - k_1)\langle\langle S_1 S_2^2 \rangle\rangle_r + 3(l_0 - 2l_1 + l_3)\langle\langle S_1^2 S_2^2 \rangle\rangle_r \\ &\quad + k_3\langle\langle S_1 S_2 S_3 \rangle\rangle_r + 3(l_4 - l_2)\langle\langle S_1 S_2 S_3^2 \rangle\rangle_r \\ &\quad + 3(k_1 - 2k_2 + k_4)\langle\langle S_1 S_2^2 S_3^2 \rangle\rangle_r \\ &\quad + (-l_0 + 3l_1 - 3l_3 + l_5)\langle\langle S_1^2 S_2^2 S_3^2 \rangle\rangle_r. \end{aligned} \tag{5.3.10}$$

We note that, for the sake of simplicity, the superscript z is omitted from the correlation functions on the right-hand side of Eq. (5.3.10). The coefficients in Eq. (5.3.10) are defined as follows:

$$l_0 = F(0),$$

$$l_1 = \cosh(J\nabla)F(x)|_{x=0}, \qquad k_1 = \sinh(J\nabla)F(x)|_{x=0},$$

$$l_2 = \sinh^2(J\nabla)F(x)|_{x=0}, \qquad k_2 = \cosh(J\nabla)\sinh(J\nabla)F(x)|_{x=0},$$

$$l_3 = \cosh^2(J\nabla)F(x)|_{x=0}, \qquad k_3 = \sinh^3(J\nabla)F(x)|_{x=0},$$

$$l_4 = \cosh(J\nabla)\sinh^2(J\nabla)F(x)|_{x=0}, \qquad k_4 = \cosh^2(J\nabla)\sinh(J\nabla)F(x)|_{x=0},$$

$$l_5 = \cosh^3(J\nabla)F(x)|_{x=0}. \tag{5.3.11}$$

Next, the average value of the perimeter spin in the system can be written as follows, and it is found as

$$m_1 = \langle\langle S_\delta^z \rangle\rangle_r = \langle\langle 1 + S_0^z \sinh(J\nabla) + (S_0^z)^2\{\cosh(J\nabla) - 1\}\rangle\rangle_r F(x+\gamma)|_{x=0}, \tag{5.3.12}$$

$$\langle\langle S_1 \rangle\rangle_r = a_1\left(1 - \langle\langle (S_0)^2 \rangle\rangle_r\right) + a_2\langle\langle S_0 \rangle\rangle_r + a_3\langle\langle (S_0)^2 \rangle\rangle_r, \tag{5.3.13}$$

with the coefficients

$$a_1 = F(\gamma),$$

$$a_2 = \sinh(J\nabla)F(x+\gamma)|_{x=0},$$

$$a_3 = \cosh(J\nabla)F(x+\gamma)|_{x=0}, \tag{5.3.14}$$

where $\gamma = (q-1)A$ is the effective field produced by the $(q-1)$ spins outside the system (see Fig. 4.1) and A is an unknown parameter to be determined self-consistently. With the help of Eq. (5.2.7), quadrupolar moment of the central spin can be obtained as follows

$$\langle\langle (S_0^z)^2 \rangle\rangle_r = \left\langle\left\langle \prod_{j=1}^{q} \left[1 + S_j^z \sinh(J\nabla) + (S_j^z)^2\{\cosh(J\nabla) - 1\}\right]\right\rangle\right\rangle_r G(x)|_{x=0}, \tag{5.3.15}$$

where the function $G(x)$ is defined as

$$G(x) = \int dD_i P(D_i) g(x, D_i). \tag{5.3.16}$$

Definition of the function $g(x, D_i)$ in Eq. (5.3.16) is given as follows and the expression in Eq. (5.3.17) can be evaluated by using the eigenvalues and corresponding eigenvectors of the effective Hamiltonian matrix $-H_i$.

$$
\begin{aligned}
g(x, D_i) &= \frac{1}{\sum_{n=1}^{3} \exp(\beta\lambda_n)} \sum_{n=1}^{3} \langle \varphi_n | \left(S_i^z \right)^2 | \varphi_n \rangle \exp(\beta\lambda_n), &\text{(5.3.17)} \\
&= \frac{2\cosh(\beta x)}{2\cosh(\beta x) + e^{-\beta D_i}}.
\end{aligned}
$$

Hence, we get the quadrupolar moment by expanding the right-hand side of Eq. (5.3.15)

$$
\begin{aligned}
\langle\langle (S_0^z)^2 \rangle\rangle_r &= r_0 + 3n_1 \langle\langle S_1 \rangle\rangle_r + 3(r_1 - r_0)\langle\langle S_1^2 \rangle\rangle_r + 3r_2 \langle\langle S_1 S_2 \rangle\rangle_r \\
&\quad + 6(n_2 - n_1)\langle\langle S_1 S_2^2 \rangle\rangle_r + 3(r_0 - 2r_1 + r_3)\langle\langle S_1^2 S_2^2 \rangle\rangle_r + n_3\langle\langle S_1 S_2 S_3 \rangle\rangle_r \\
&\quad + 3(r_4 - r_2)\langle\langle S_1 S_2 S_3^2 \rangle\rangle_r + 3(n_1 - 2n_2 + n_4)\langle\langle S_1 S_2^2 S_3^2 \rangle\rangle_r \\
&\quad + (-r_0 + 3r_1 - 3r_3 + r_5)\langle\langle S_1^2 S_2^2 S_3^2 \rangle\rangle_r, &\text{(5.3.18)}
\end{aligned}
$$

with

$$
r_0 = G(0),
$$

$$
r_1 = \cosh(J\nabla)G(x)|_{x=0}, \qquad\qquad n_1 = \sinh(J\nabla)G(x)|_{x=0},
$$

$$
r_2 = \sinh^2(J\nabla)G(x)|_{x=0}, \qquad\qquad n_2 = \cosh(J\nabla)\sinh(J\nabla)G(x)|_{x=0},
$$

$$
r_3 = \cosh^2(J\nabla)G(x)|_{x=0}, \qquad\qquad n_3 = \sinh^3(J\nabla)G(x)|_{x=0},
$$

$$
r_4 = \cosh(J\nabla)\sinh^2(J\nabla)G(x)|_{x=0}, \qquad n_4 = \cosh^2(J\nabla)\sinh(J\nabla)G(x)|_{x=0},
$$

$$
r_5 = \cosh^3(J\nabla)G(x)|_{x=0}. \qquad\qquad\qquad\qquad\qquad\text{(5.3.19)}
$$

Corresponding to Eq. (5.3.12), thermal and configurational average of quadrupolar moment of a perimeter spin is

$$
\langle\langle (S_\delta^z)^2 \rangle\rangle_r = \langle\langle 1 + S_0^z \sinh(J\nabla) + (S_0^z)^2\{\cosh(J\nabla) - 1\}\rangle\rangle_r G(x + \gamma), \qquad \text{(5.3.20)}
$$

$$
\langle\langle S_1^2 \rangle\rangle_r = b_1 \left(1 - \langle\langle (S_0^z)^2 \rangle\rangle_r\right) + b_2 \langle\langle S_0^z \rangle\rangle_r + b_3 \langle\langle (S_0^z)^2 \rangle\rangle_r. \qquad \text{(5.3.21)}
$$

where

$$
\begin{aligned}
b_1 &= G(\gamma), \\
b_2 &= \sinh(J\nabla)G(x + \gamma)|_{x=0}, \\
b_3 &= \cosh(J\nabla)\rangle G(x + \gamma)|_{x=0}. &\text{(5.3.22)}
\end{aligned}
$$

Eqs. (5.3.10), (5.3.13), (5.3.18) and (5.3.21) are the fundamental spin identities of the system which can be regarded as basis relations to derive the remaining unknown correlation functions composed of 21 linear equations for honeycomb lattice. The complete set can be found in (Yüksel et al., 2012a). By solving the system of 21 linear equations with the condition

$$\langle\langle S_0^z \rangle\rangle_r = \langle\langle S_1 \rangle\rangle_r \qquad (5.3.23)$$

we can obtain the phase diagrams in various planes, as well as the variation of order parameters as a function of system parameters. Since the effective field γ is very small in the vicinity of $k_B T_c/J$, we can obtain the critical temperature for the fixed set of Hamiltonian parameters by solving Eq. (5.3.23) in the limit of $\gamma \to 0$ then we can construct the whole phase diagrams of the system. Depending on the values of Hamiltonian and crystal field distribution parameters, there may be two solutions [i.e., two critical temperature values which satisfy Eq. (5.3.23)] corresponding to the first (or second) and second-order phase-transition points, respectively. We determine the type of the transition by looking at the temperature dependence of magnetization for selected values of system parameters.

Now, we can discuss the effect of the crystal field distributions defined in Eqs. (5.3.5) and (5.3.6) on the global phase diagrams of the system where the second and first order transitions are shown by solid and dashed curves, respectively with tricritical points (shown by hollow circles) for honeycomb ($q = 3$) and square ($q = 4$) lattices. Also, in order to clarify the type of the transitions in the system, we will give the temperature dependence of the order parameter.

5.3.1 *Phase Diagrams of the System with Dilute Crystal Field*

First, we illustrate the phase diagrams and magnetization curves of the system with a dilute crystal field distribution defined in Eq. (5.3.5) where crystal field D is turned on, or turned off with probabilities p and $(1 - p)$ on the lattice sites, respectively. In Figs. 5.3a and 5.3c, we plot the phase diagrams of the system in ($k_B T_c/J - D/J$) plane for honeycomb and square lattices with coordination numbers $q = 3$ and $q = 4$, respectively.

As seen in Figs. 5.3a and 5.3c, phase diagrams of the system can be divided into three parts with different concentration values p. For the curves in the first group with $p < p^*$, the system always exhibits a second order phase transition with a finite critical temperature $k_B T_c / J$ which extent to $D/J \to -\infty$. If the concentration p reaches its critical value p^* then the critical temperature depresses to zero. Physical reason underlying this behavior can be explained as follows; when we select sufficiently large negative crystal field values (i.e.$D/J \to -\infty$), all of the spins in the system tend to align in $S = 0$ state. As p increases starting from zero, the ratio of spins which aligned in $S = 0$ state increases, and therefore, magnetization weakens, and accordingly, critical temperature of the system decreases. According to our numerical results, the critical concentration value is obtained as $p^* = 0.3795$ for $q = 3$ and $p^* = 0.5875$ for $q = 4$. In the second group of the phase diagrams in Figs. 5.3a and 5.3c, the system exhibits a reentrant behavior of second order, whereas the curves in the third group, exhibit a reentrant behavior of first order with a tricritical point at which a first order transition line turns into a second order transition line. Besides, the curves which exhibit a reentrant behavior of first (or second) order, depress to zero at three successive values of crystal field $D/J = -3.0, -2.0, -1.0$. Moreover, in $D/J \to \infty$ limit, the system behaves like spin-1/2 for $p = 1.0$. In the case of $p \neq 0$, the ratio of spins that behave like $S = \pm 1$ increases as p increases. Therefore, for $0 \leq p \leq 1.0$, all transition lines have finite critical temperatures which increase with increasing p values for $D/J \to \infty$. At this point, we also note that if we select $D/J = 0$ in Eq. (5.3.5), all lattice sites expose to a crystal field $D_i / J = 0$ independent from p. Hence, all transition lines intersect each other on the point $(D/J, k_B T_c / J) = (0, 1.3022)$ for $q = 3$, and $(D/J, k_B T_c / J) = (0, 1.9643)$ for $q = 4$. Meanwhile, previous studies based on EFT are not capable of obtaining first order transition lines of the system. From this point of view, we see that our method improves the results of the other EFT works and we take the conventional EFT method one step forward by investigating the global phase diagrams, especially the first-order transition lines that include reentrant phase transition regions.

On the other hand, Figs. 5.3b and 5.3d show the phase boundary in $(k_B T_c / J - p)$ plane which separates the ferromagnetic and paramagnetic phases with $D/J \to -\infty$.
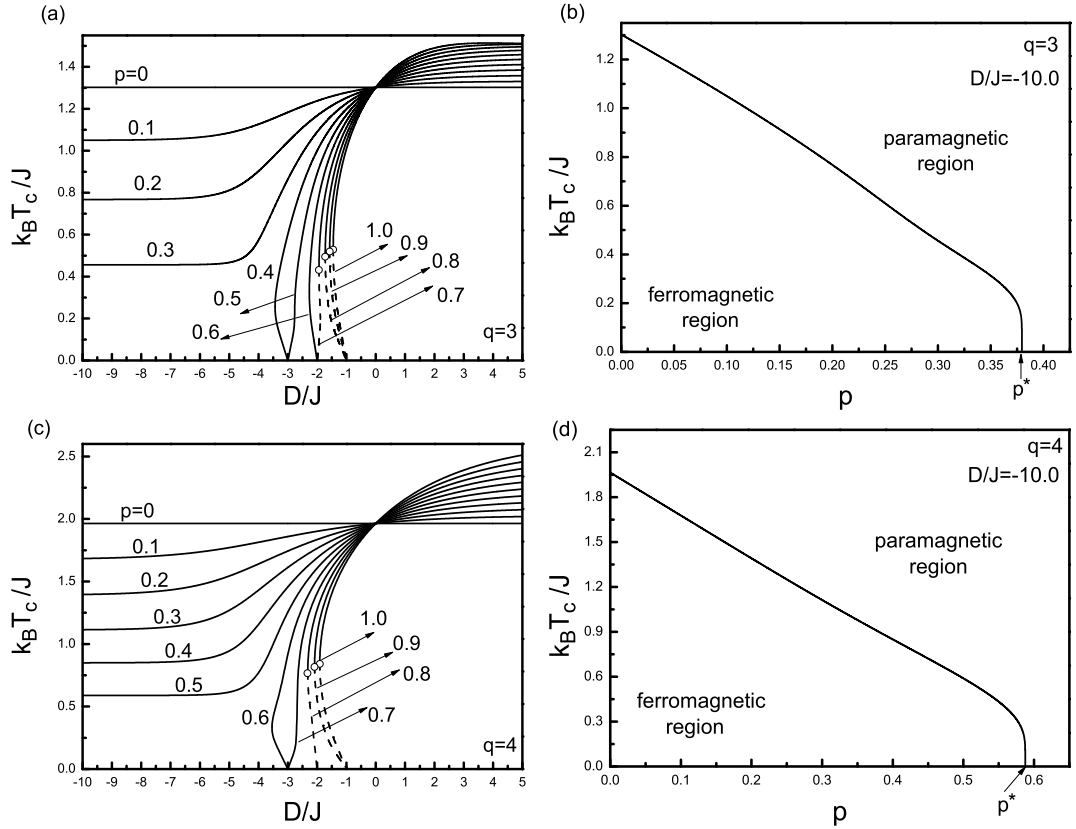
Figure 5.3 (a) Phase diagrams of the system for $q = 3$ in a $(k_BT_c/J - D/J)$ plane corresponding to dilute crystal field distribution defined in Eq. (5.3.5). The solid and dashed lines correspond to second- and first-order phase transitions, respectively. The open circles denote the tricritical points, and the numbers on each curve represent the value of concentration p. (b) Phase diagrams of the system for $q = 3$ in a $(k_BT_c/J - p)$ plane with a selected value of the crystal field $D/J = -10.0$. (c) Phase diagrams of the system for $q = 4$ in a $(k_BT_c/J - D/J)$ plane corresponding to dilute crystal field distribution defined in Eq. (5.3.5). The solid and dashed lines correspond to second- and first-order phase transition, respectively. The open circles refer to the tricritical points, and the numbers on each curve represent the value of concentration p. (d) Phase diagrams of the system for $q = 4$ in a $(k_BT_c/J - p)$ plane with a selected value of the crystal field $D/J = -10.0$.

According to this figure, critical temperature k_BT_c/J of system decreases gradually, and ferromagnetic region gets narrower as p increases, and k_BT_c/J value depresses to zero at $p = p^*$. Such a behavior is an expected fact in dilution problems (Salmon & Tapia, 2010, Kaufman, Klunzinger, & Khurana, 1986, Salmon, Crokidakis, & Nobre, 2009). Numerical value of critical concentration p^* for honeycomb ($q = 3$) and square ($q = 4$) lattices is given in Table 5.3, and compared with the other works in the literature. As seen in Table 5.3, numerical values of p^* for $q = 3$ and $q = 4$

are new results in literature. Furthermore, MFT (Benyoussef, Biaz, Saber, & Touzani, 1987, Carneiro, Henriques, & Salinas, 1989) predicts that the system always has a finite critical temperature and exists in a ferromagnetic state at lower temperatures in $D/J \to -\infty$ limit, except that $p = 1.0$. This artificial result can be regarded as a limitation of the mean field predictions.

Table 5.3 Critical concentration p^* obtained by several methods including EFT based on DA (Kaneyoshi & Mielnicki, 1990, Kaneyoshi, 1992, Yan & Deng, 2002), MFT (Benyoussef, Biaz, Saber, & Touzani, 1987, Carneiro, Henriques, & Salinas, 1989), pair approximation (PA) (Lara & Plascak, 1998) and the present work for honeycomb ($q = 3$) and square ($q = 4$) lattices.

Lattice	DA-I	DA-II	MFT	PA	Present Work
$q = 3$	0.484	0.492	1.0	0.5	0.3795
$q = 4$	0.604	0.610	1.0	0.667	0.5875

In Fig. 5.4, we plot the temperature dependencies of magnetization curves corresponding to the phase diagrams depicted in Fig. 5.3 for $q = 3$. As seen in Fig. 5.4, as p increases then critical temperature $k_B T_c / J$ values decrease for $D/J < 0$, except the reentrant phase transition temperatures which occur at low temperatures. On the other hand, effect of increasing p values on the shape of magnetization curves depends on value of D/J. Namely, in Figs. 5.4a and 5.4b we see that ground state saturation values of magnetization curves decreases as p increases for $D/J = -10.0$ and -3.1. Moreover, for $D/J = -3.1$, magnetization curves of the system exhibit a broad maximum at low temperatures for $p = 0.37$, and a reentrant behavior of second order for $p = 0.4$. If we select $D/J = -2.5$ as in Fig. 5.4c, saturation values of magnetization curves remain unchanged for $p = 0, 0.2, 0.3$ and tend to decrease for $p > 0.3$. If p increases further, a reentrant behavior of second order appears for $p = 0.53$, and we see a broad maximum at low temperatures for $p = 0.517$ and 0.5 which tends to depress as p decreases. This broad maximum behavior of magnetization curves originates from the increase in the number of spins directed parallel to the z-direction with increasing temperature, due to the thermal agitation. For $D/J = -2.0$ in Fig. 5.4d, magnetization curves saturate at $m = 1$ at the ground state and reentrant behavior disappears. If we increase D/J

further, for example for $D/J = -1.5$ (Fig. 5.4e), another type of reentrant behavior occurs in the system in which a first order transition is followed by a second order transition. Finally, for sufficiently large positive values of crystal field, magnetization curves always saturate at $m = 1$ and the system always undergoes a second order phase transition from a ferromagnetic phase to a paramagnetic phase with increasing temperature, which can be seen in Fig. 5.4f with $D/J = 10.0$. As a common property of the curves in Fig. 5.4, we see that effect of p on the saturation values, as well as temperature dependence of magnetization curves strictly depend on the strength of D/J. Hence, according to us, the presence of dilute crystal fields on the system should produce a competition effect on the phase diagrams of the system. We also note that, although it has not been shown in the present work, magnetization curves for $q = 4$ corresponding to the phase diagrams depicted in Fig. 5.3c exhibit qualitatively similar behavior with those of Fig. 5.4 with $q = 3$.

As seen in Fig. 5.3, for a dilute crystal field distribution defined in Eq. (5.3.5), the global phase diagrams which are plotted in $(k_B T_c/J - D/J)$ plane, as well as the phase boundaries in $(k_B T_c/J - p)$ plane for $q = 3$ exhibit qualitatively similar characteristics when compared with those for $q = 4$. Hence, in order to examine the phase diagrams which are plotted in $(k_B T_c/J - D/J)$ plane in Figs. 5.3a and 5.3c in detail, we plot the evolution of the global phase diagrams in Fig. 5.5 only for $q = 4$. From this point of view, Fig. 5.5a shows how the phase diagrams in Fig. 5.3c evolve when the concentration p changes from 0.5 to 0.6. As seen in Fig. 5.5a, we observe a second order phase transition line with a finite critical temperature $k_B T_c/J$ which extent to $D/J \to -\infty$ for $p = 0.575$. If p increases, namely for $p = 0.580$ and 0.583, we see that a low temperature transition line arises between $-4.0 < D/J < -3.0$, as well as a high temperature phase boundary which extents to $D/J \to -\infty$. If p increases further, such as for $p = 0.584$, 0.585 and 0.587, high temperature phase boundary is gradually connected to the transition line which arises between $-4.0 < D/J < -3.0$, and the phase diagrams exhibit a bulge on the right hand side of $(k_B T_c/J - D/J)$ plane, whereas another transition line emerges within the range of $-\infty < D/J < -4.0$, which disappears for $p > 0.587$. Similarly, evolution of the phase diagrams in Fig. 5.3c
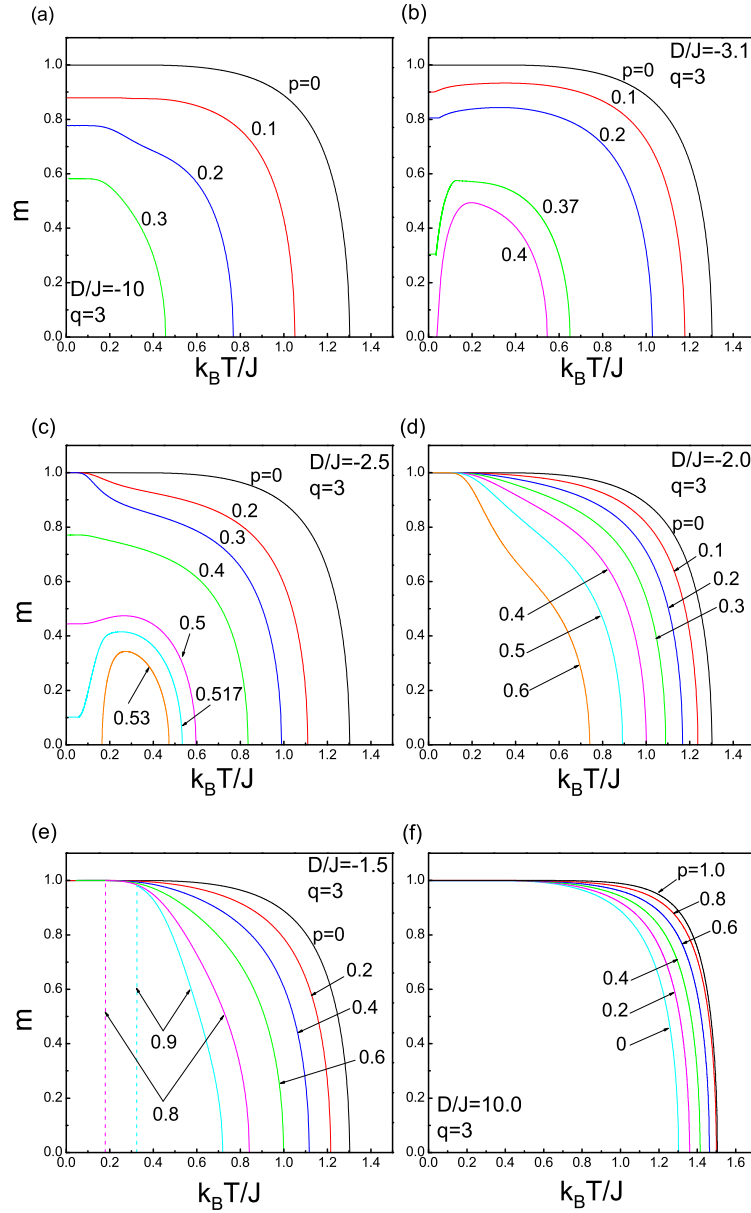
Figure 5.4 Temperature dependence of magnetization corresponding to Fig. 5.3a with some selected values of crystal field. (a) $D/J = -10.0$, (b) $D/J = -3.1$, (c) $D/J = -2.5$, (d) $D/J = -2.0$, (e) $D/J = -1.5$, and (f) $D/J = 10.0$. The numbers on each curve denote the value of concentration p. The solid and dashed lines correspond to second- and first-order phase transitions, respectively.

when the concentration p changes from 0.6 to 0.7 can be seen in Fig. 5.5b. As seen in this figure, the curves for $p = 0.60, 0.62, 0.64, 0.66$ exhibit a reentrant behavior of second order, while for $p = 0.68$ reentrance disappears and for $p = 0.70$ and 0.71 double reentrance with three successive second order phase transitions occurs in a very
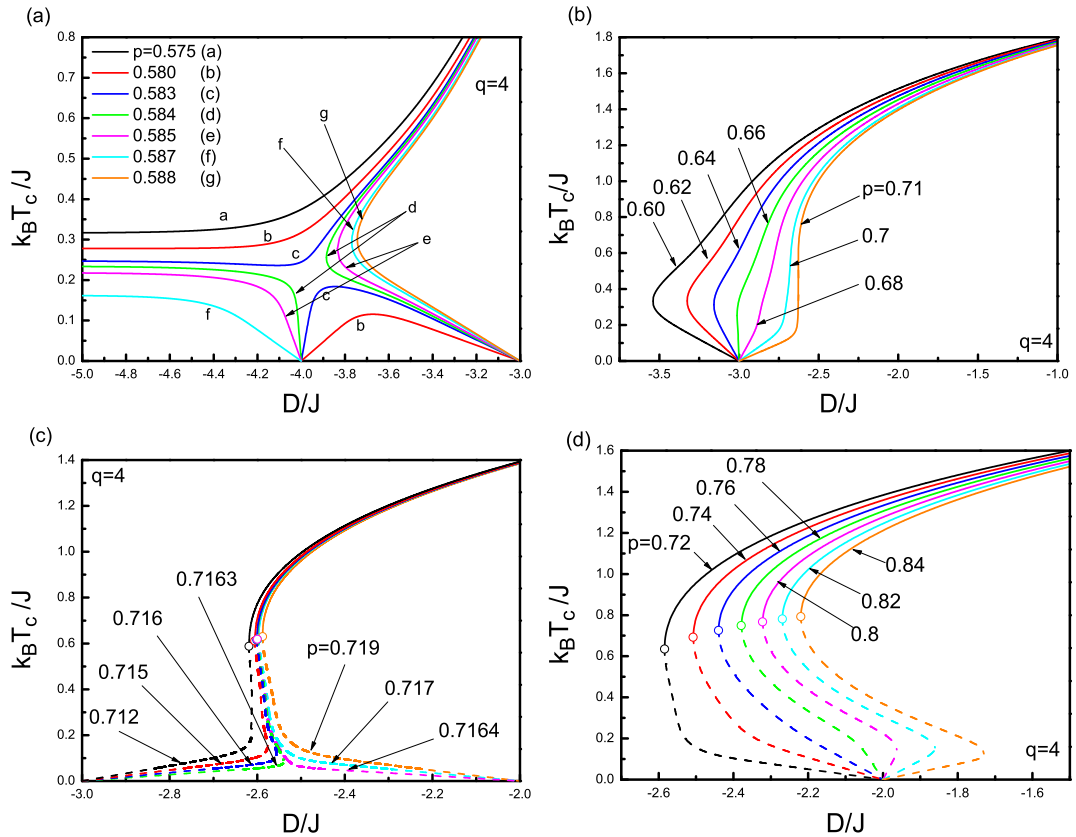
Figure 5.5 Evolution of the phase diagrams corresponding to Fig. 5.3c. The numbers on each curve denote the value of concentration *p*. The solid and dashed lines correspond to second- and first-order phase transitions, respectively. The open circles indicate the tricritical points.

narrow region of D/J. On the other hand, increasing values of p generates first order phase transitions with tricritical points, as well as reentrant behavior of first order. This phenomena is illustrated in Fig. 5.5c. From Fig. 5.5c, we see that, the second order transition temperatures decrease as absolute value of D/J increases, and turn into first order transition lines at tricritical points. Evidently, the phase diagrams change abruptly for $p \geq 0.7164$. Hence, the behavior of the $p = 0.7163$ curve is completely different from that of $p = 0.7164$. Namely, first order transition temperatures of the system for $p \leq 0.7163$ and $p \geq 0.7164$ depress to zero at $D/J = -3.0$ and $D/J = -2.0$, respectively. In order to investigate the phase transition features of the system further, we should continue increasing the value of p. In Fig. 5.5d, we see that the curves for $p = 0.72, 0.74, 0.76$ and 0.78 exhibit a reentrant behavior of first order, whereas the curves with $p = 0.80, 0.82$, and 0.84 exhibit double reentrance with two first order and a second order transition temperature.

5.3.2 Phase Diagrams of the System with Random Crystal Field

Next, in order to investigate the effect of the random crystal fields defined in Eq. (5.3.6) on the thermal and magnetic properties of the system, we represent the phase diagrams and corresponding magnetization curves for honeycomb ($q = 3$) and square lattices ($q = 4$) throughout Figs. 5.6-5.9.
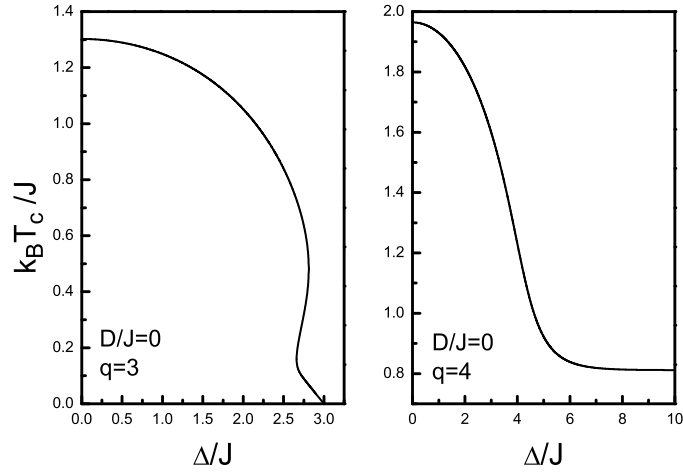

Figure 5.6 Phase diagrams of the system in a ($k_B T_c / J - \Delta / J$) plane for a bimodal crystal field distribution corresponding to Eq. (5.3.6) with $D/J = 0.0$. Left and right-hand side panels are plotted for $q = 3$ and $q = 4$, respectively.

We note that the random crystal field distribution given in Eq. (5.3.6) with $D/J = 0$ corresponds to a bimodal distribution function, while for $\Delta/J = 0$, we obtain a pure BC model with homogenous crystal field D/J. In Fig. 5.6, phase diagrams of the system corresponding to the bimodal distribution function are shown in ($k_B T_c / J - \Delta / J$) plane. For a bimodal distribution, the phase diagrams have a symmetric shape with respect to Δ/J which comes from the fact that $p = 1/2$, and as seen in Fig. 5.6, transition temperatures are second order, and it is clear that the system exhibits different characteristic features depending on the coordination number q. Namely, for $q = 3$, transition temperature decreases with increasing Δ/J and exhibits double reentrance with three second order phase transition temperatures, then falls to zero at $\Delta/J = 3.0$ (left panel in Fig. 5.6). On the other hand, as seen on the right panel in Fig. 5.6, as Δ/J increases the transition temperature of the system for $q = 4$ decreases

and remains at a finite value for $\Delta/J \to \infty$ which means that ferromagnetic exchange interactions for $q = 3$ are insufficient for the system to keep its ferromagnetic order for $\Delta/J > 3.0$, while for $q = 4$ these interactions are dominant in the system, and the presence of a disorder in the crystal fields cannot destruct the ferromagnetic order. In (Lara & Plascak, 1998), the authors reported similar characteristic behavior for $q = 4$ by using pair approximation (PA) with extra isolated multi-phase critical points.
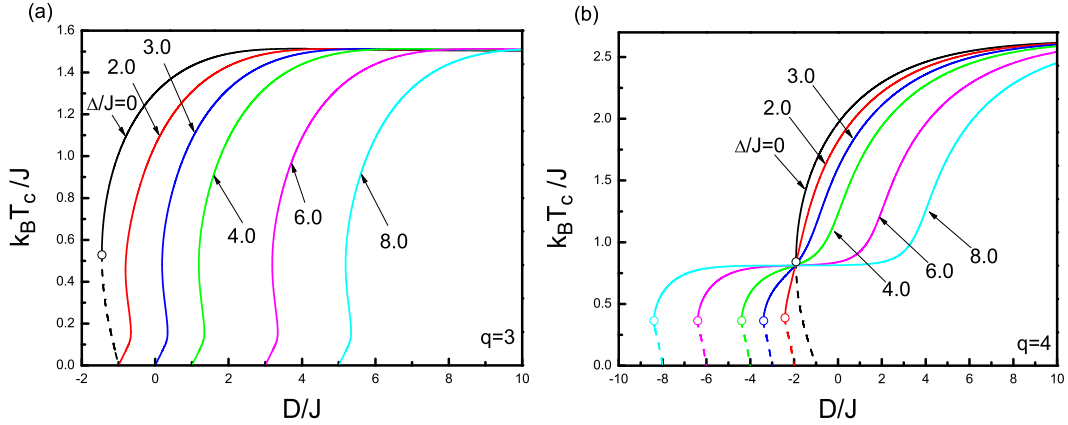

Figure 5.7 Phase diagrams of the system in a $(k_B T_c/J - D/J)$ plane corresponding to random crystal field distribution defined in Eq. (5.3.6) for (a) $q = 3$, (b) $q = 4$. The numbers on each curve denote the value of $\triangle/J$. The open circles represent the tricritical points, and the solid and dashed lines correspond to second- and first-order phase transitions, respectively.

At the same time, in order to see the effect of the random crystal fields with $\triangle/J, D/J \neq 0$ on the phase diagrams and magnetization curves of the system for $q = 3$ and 4, we plot the phase diagrams in $(k_B T_c/J - D/J)$ plane in Fig. 5.7 and variation of the corresponding magnetization curves with temperature in Figs. 5.8 and 5.9, respectively. At first sight, it is obvious that the phase diagrams in Fig. 5.7 represent evident differences in qualitative manner with coordination number q. That is, as seen in Fig. 5.7a, the curve corresponding to $\Delta/J = 0$ represents the phase diagram of pure BC model for a honeycomb lattice which exhibits a reentrant behavior of first order with first and second order transition lines, as well as a tricritical point (Yüksel et al., 2009). From Fig. 5.7a, we see that as Δ/J increases then the tricritical point and first order transitions disappear, and the first order reentrance turns into double reentrance with three transition temperatures of second order, and phase transition lines shift to positive crystal field direction without changing their shapes. On the other hand, the

situation is very different for a square lattice. Namely, as seen in Fig. 5.7a and 5.7b, $\Delta/J = 0$ curves for $q = 3$ and $q = 4$ are qualitatively identical to each other. However, as seen in Fig. 5.7b, for $\Delta/J \neq 0$, first order transition lines and tricritical points do not disappear from the system for $q = 4$, but shift to negative crystal field values. Besides, the system does not exhibit double reentrance for $q = 4$. Furthermore, for $\Delta/J \geq 1.5$ in Fig. 5.7a, all phase diagrams exhibit similar behavior as D/J varies. Strictly speaking, if $\Delta/J \geq 1.5$ then we see that the system does not exhibit a tricritical point. In this case, all the phase transitions are of second order and the qualitative properties of the curves shown in Fig. 5.7a are identical to each other. On the other hand, for $0 \leq \Delta/J < 1.5$ the situation is different. Namely, the curves selected within this interval exhibit first order phase transitions and tricritical points.

It is important to note that these observations are consistent with the results shown in Figs. 5.3a and 5.3c. In other words, the distribution function given in Eq. (5.3.5) with $p = 0.5$ and $D/J = 2D_0/J$ is identical to Eq. (5.3.6) for $\Delta/J = \pm D_0/J$ and $D/J = D_0/J$. For example, according to Eq. (5.3.5), if we select $D_0/J = 4.0$ with $p = 0.5$, it means that half of the spins on the lattice sites expose to a crystal field $D/J = 0$, while a crystal field given by $D/J = 8.0$ acts on the other half of the spins. On the other hand, if we select $\Delta/J = \pm D_0/J$ and $D/J = D_0/J$ by using Eq. (5.3.6), we generate the same distribution again. Hence, we expect to get the same results in Figs. 5.3 and 5.7 for these system parameters. For instance, for $D_0/J = 4.0$ in Fig. 5.3a, we get $D/J = 8.0$, and the system exhibits a ferromagnetic order in the ground state, which can also be seen in Fig. 5.7a with a critical temperature $k_B T_c/J = 1.4395$. These conditions are also valid for $q = 4$, and for the whole temperature region on the phase diagrams. Therefore, the state (para-or ferro), as well as thermal and magnetic properties of a selected $(k_B T/J - D/J)$ point with respect to $p = 0.5$ curves in Figs. 5.3a and 5.3c is identical to the state of a point $(k_B T/J, D/2J)$ in Figs. 5.7a and 5.7b with respect to the curve $\Delta/J = \pm D/J$, respectively. Moreover, the qualitative differences between Figs. 5.7a and 5.7b mentioned above are strongly related to the percolation threshold value of the lattice. Namely, distribution function Eq. (5.3.6) is valid only for $p = 0.5$. However, as seen in Table 5.3, we obtain $p^* < 0.5$ for $q = 3$, and $p^* > 0.5$ for $q = 4$.
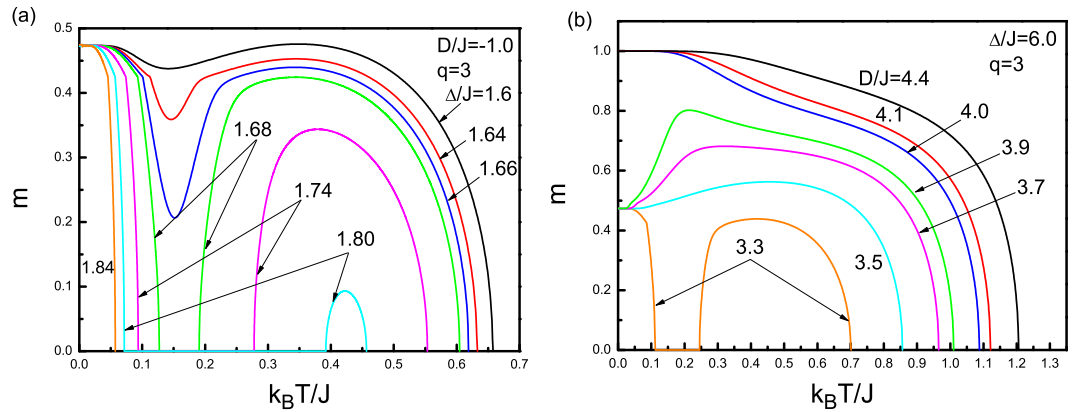
Figure 5.8 Temperature dependence of magnetization curves corresponding to Fig. 5.7a for $q = 3$ (a) with $D/J = -1.0$ and for some selected values of Δ/J, and (b) with $\Delta/J = 6.0$ and for some selected values of D/J.
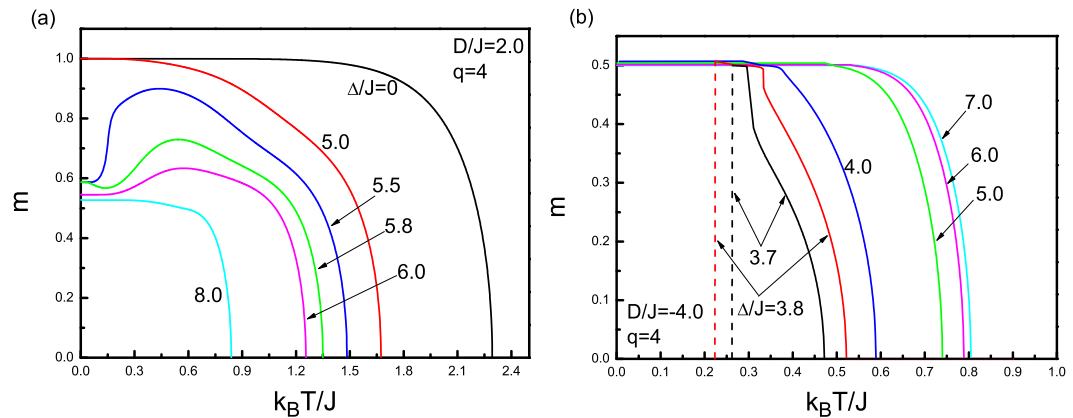

Figure 5.9 Temperature dependence of magnetization curves for $q = 4$ corresponding to Fig. 5.7b for (a) $D/J = 2.0$ and (b) $D/J = -4.0$ with some selected values of Δ/J.

In Fig. 5.8, we examine the temperature dependence of magnetization curves for $q = 3$, corresponding to the phase diagrams shown in 5.7a with $D/J = -1.0$. Fig. 5.8a, shows how the temperature dependence of magnetization curves evolve when Δ/J changes. According to Fig. 5.8a, magnetization curves saturate at a partially ordered state at low temperatures. Besides, for $\Delta/J = 1.68$, 1.74 and 1.80, the system undergoes three successive phase transitions of second order, which confirms the existence of double reentrance. Similarly, Fig. 5.8b shows how the shape of the magnetization curves change as D/J changes for constant $\Delta/J = 6.0$. As seen in Fig. 5.8b, magnetization curves exhibit a second order phase transition from a ferromagnetic (fully ordered) to a paramagnetic phase at certain values of crystal field, namely at

$D/J = 4.0$, 4.1 and 4.4, whereas for $D/J = 3.3$, 3.5, 3.7 and 3.9 the system can only achieve a partially ordered phase. In addition, the curves corresponding to $D/J = 3.5$, 3.7 and 3.9 exhibit a broad maximum at low temperatures, and then decrease as the temperature increases, whereas for $D/J = 3.3$, we observe double reentrance. Fig. 5.9 shows the magnetization curves for $q = 4$, corresponding to the phase diagrams shown in Fig. 5.7b. In Fig. 5.9a, we see that magnetization curves exhibit a second order phase transition from a paramagnetic phase to a fully ordered ferromagnetic phase for $\Delta/J = 0$ and 5.0. On the other hand, the curves corresponding to $D/J = 5.5$, 5.8 and 6.0, saturate at a partially ordered state at low temperatures, and exhibit a broad maximum with increasing temperature which depresses gradually as Δ/J increases, then fall rapidly at a second order phase transition temperature. The broad maximum behavior observed in these curves disappears for $\Delta/J = 8.0$. Additionally, Fig. 5.9b represents the magnetization versus temperature curves for $q = 4$ with $D/J = -4.0$. In Fig. 5.9b, it is clearly evident that, at low temperatures, the system saturates at a partially ordered phase for $\Delta/J = 4.0$, 5.0, 6.0 and 7.0, while for $\Delta/J = 3.7$ and 3.8, a reentrant behavior of first order occurs. Again we see that there is a competition between ferromagnetic exchange interactions and disorder effects in crystal fields which determines the saturation values and temperature dependence of magnetization curves of the system.

5.4   Ising Model in the Presence of Random Magnetic Fields

Ising model in the presence of random magnetic fields, i.e. random field Ising model (RFIM) is probably the most famous model among the other models exhibiting quenched randomness. The model which is actually based on the local fields acting on the lattice sites which are taken to be random according to a given probability distribution was introduced for the first time by (Larkin, 1970) for superconductors and later generalized by (Imry & Ma, 1975). In pure magnets, existence of an ordered state depends on a competition between the energy and entropy. Below a certain critical temperature, the exchange energy between neighboring spins is dominant against the

entropy and the system can exhibit a long range ordered phase which can be easily destroyed in lower dimensions due to the thermal fluctuations. This issue leads to the concept of lower critical dimension d_c above which the system can establish an ordered phase at finite temperature. For pure Ising model, we have $d_c = 1$ (Feng, 1996).

A lower critical dimension d_c of the RFIM has remained an unsolved mystery for many years and various theoretical methods have been introduced. For example, the domain-wall argument of Imry and Ma (Imry & Ma, 1975) suggests that a transition should exist in three and higher dimensions for finite temperature and randomness, which means that $d_c = 2$ (Grinstein & Ma, 1982, Fernandez, Grinstein, Imry, & Kirkpatrick, 1983, Imbrie, 1984, Bricmont & Kupiainen, 1987). On the contrary, dimensional reduction arguments (Parisi & Sourlas, 1979) conclude that the system should not have a phase transition at finite temperature in three dimensions (3D) or fewer, so $d_c = 3$ (Binder, Imry, & Pytte, 1981, Pytte, Imry, & Mukamel, 1981, Mukamel & Pytte, 1982, Niemi, 1982). On the other hand, Frontera and Vives (Frontera & Vives, 1999) showed that a two-dimensional ferromagnetic RFIM with a Gaussian random-field distribution exhibits order at zero temperature. Although the argument of Imry and Ma is regarded as intuitive and nonrigorous, the results obtained on the basis of their theory are considered to be correct at the present (Shukla, 2004).

The Hamiltonian describing the model is defined by

$$\mathcal{H} = -J \sum_{<ij>} S_i S_j - \sum_i h_i S_i, \quad \langle h_i \rangle = 0 , \ \epsilon = \sqrt{\langle h_i^2 \rangle}, \tag{5.4.1}$$

where the random field parameter h_i is drawn from a symmetric probability distribution. In the presence of strong random fields ($h_i >> J$), random field energy is the dominant term in the Hamiltonian, and a particular spin S_i at a site i can easily follow its local field h_i. Hence, it is reasonable to expect that the system can not exhibit a long range ferromagnetic order even at a very low temperature. However, in case of weak random fields ($h_i << J$), the situation needs particular attention. The argument of Imry and Ma clarifies the question whether a d dimensional system can exhibit a long range order in the presence of weak randomness or not in a heuristic manner by considering the possible formation of local domains with size L in which the spins tend to align in the

net direction of random field (Belanger, 1991).

The basic idea of Imry and Ma can be briefly summarized as follows: In the absence of random fields, the ground state configuration (i.e. $T = 0$ configuration) of the system is doubly degenerate. Now, let us consider a finite domain of size L in an infinite system which stays in the fully ordered state with all spins pointing up, i.e. $S_i = 1$ for each lattice site i. The volume of this finite domain is L^d which also defines the number of lattice sites within the domain. The surface of the domain is formed by L^{d-1} spins. If all of the spins in the domain were flipped then the total bulk energy of domain does not change due to the degeneracy condition. However, in this case, the domain of flipped spins acts as a defect in the entire infinite system. Hence, formation of this domain costs a positive exchange energy $E_{ex} \sim JL^{d-1}$ due to the interaction of L^{d-1} pairs of anti-parallel spins along the border of the domain which is called domain wall. On the other hand, in the presence of random fields, the energy of a spin S_i in the domain will be $h_i S_i$ or simply h_i, since $S_i = 1$. Hence, depending on the sign of random field variable h_i this energy would be either positive or negative. Since, $\langle h_i \rangle = 0$ in the entire system, in a statistical manner, random field energy of L^d spins in a particular domain is given by $E_R^2 \sim \epsilon^2 L^d$ where ϵ is the root mean square deviation of fields h_i from their average value (Shukla, 2004). Hence, the total energy cost of the formation of a finite domain of size L in an infinite system is

$$E_d \sim JL^{d-1} - \epsilon L^{d/2}. \tag{5.4.2}$$

According to Eq. (5.4.3), order of the system (ferromagnetic or paramagnetic) is governed by two fundamental factors. Namely, we can mention about a competition between the exchange interactions which tend to align the spins in the ferromagnetic order and the random field energy which has a tendency to destruct the long range order. When $d < 2$, random field energy is dominant at large L even for small random fields whereas for $d > 2$ the exchange energy always dominates against the random field energy. On the other hand, for $d = 2$, both energies become linearly dependent on L, and exchange energy is dominant for weak random fields. However, according to a more sophisticated version of the domain wall argument of Imry and Ma which takes into account the roughening phenomena of domain walls (Villain, Semeria, Lancon, &

Billard, 1983, Imry, 1984, Grinstein, 1984), it is well established that the ferromagnetic ground state is unstable in $d = 2$ (Imry & Ma, 1975).

At the same time, a great many theoretical and experimental works have paid attention to the RFIM and quite noteworthy results have been obtained. Namely, it has been shown that diluted antiferromagnets such as $Fe_xZn_{1-x}F_2$ (Belanger, King, & Jaccarino, 1985, King, Jaccarino, Belanger, & Rezende, 1985), $Rb_2Co_xMg_{1-x}F_4$ (Ferreira, King, Jaccarino, Cardy, & Guggenheim, 1983, Yoshizawa, Cowley, Shirane, Birgeneau, Guggenheim, & Ikeda, 1982) and $Co_xZn_{1-x}F_2$ (Yoshizawa, Cowley, Shirane, Birgeneau, Guggenheim, & Ikeda, 1982) in a uniform magnetic field just correspond to a ferromagnet in a random uniaxial magnetic field (Fishman & Aharony, 1979, Cardy, 1984). The following studies have been devoted to investigate the phase diagrams of these systems in depth, and in the mean-field level it was found that different random-field distributions lead to different phase diagrams for infinite dimensional models. For example, using a Gaussian probability distribution, it has been shown that (Schneider & Pytte, 1977) phase diagrams of the model exhibit only second-order phase-transition properties. Following the same methodology, (Andelman, 1983) discussed the order of the low-temperature transition in terms of the maxima of the distribution function. On the other hand, (Aharony, 1978) and (Mattis, 1985) have introduced bimodal and trimodal distributions, respectively, and they have reported the observation of tricritical behavior. In a recent series of papers, phase-transition properties of infinite dimensional RFIMs with symmetric double- (Crokidakis & Nobre, 2008) and triple-(Salmon, Crokidakis, & Nobre, 2009) Gaussian random fields have also been studied by means of a replica method and a rich variety of phase diagrams have been presented. The situation has also been handled on 3D lattices with nearest-neighbor interactions by a variety of theoretical works such as effective-field theory (EFT) (Borges & Silva, 1987, Liang, Wei, Zhang, Xin, & Song, 2004, Sarmento & Kaneyoshi, 1989, Sebastianes & Figueiredo, 1992, Kaneyoshi, 1985), Monte Carlo (MC) simulations (Landau, Lee, & Kao, 1978, Machta, Newman, & Chayes, 2000, Fytas, Malakis, & Eftaxias, 2008, Fytas & Malakis, 2008), pair approximation (PA) (Albayrak & Canko, 2004), and the series expansion (SE) method

(Gofman, Adler, Aharony, Harris, & Schwartz, 1996). By using EFT, (Borges & Silva, 1987) studied the system for square ($q = 4$) and simple cubic (sc) ($q = 6$) lattices, and they observed a tricritical point only for ($q \geq 6$). Similarly, (Sarmento & Kaneyoshi, 1989) investigated the phase diagrams of RFIMs by means of EFT with correlations for a bimodal field distribution, and they concluded that reentrant behavior of second order is possible for a system with ($q \geq 6$). Recently, (Fytas, Malakis, & Eftaxias, 2008) applied MC simulations on a sc lattice. They found that the transition remains continuous for a bimodal field distribution, while (Hadjiagapiou, 2010) observed reentrant behavior and confirmed the existence of a tricritical point for an asymmetric bimodal probability distribution within the mean-field approximation based on a Landau expansion.

In the aforementioned works based on EFT, decoupling approximation have been utilized which neglects the multi-site correlation functions. On the other hand, as far as we know, EFT studies in the literature dealing with RFIMs are based only on discrete probability distributions (bimodal or trimodal). Hence, in the following, we intend to apply our formalism in RFIM problem and analyze the phase diagrams with single-Gaussian, bimodal, and double-Gaussian random-field distributions on isometric lattices.

As usual, let us consider a spin cluster as depicted in Fig. 4.1 with Hamiltonian (5.4.1) where the first term is a summation over the nearest-neighbor spins with $S_i = \pm 1$ and the second term represents the Zeeman interactions on the lattice. Random magnetic fields are distributed according to a given probability distribution function. The present study deals with three kinds of field distribution, namely, a normal distribution which is defined as

$$P(h_i) = \left(\frac{1}{2\pi\sigma^2} \right)^{1/2} \exp\left[-\frac{h_i^2}{2\sigma^2} \right], \qquad (5.4.3)$$

with a width σ and zero mean, a bimodal discrete distribution

$$P(h_i) = \frac{1}{2} \left[\delta(h_i - h_0) + \delta(h_i + h_0) \right], \qquad (5.4.4)$$

where half of the lattice sites are subject to a magnetic field h_0 and the remaining lattice

sites have a field $-h_0$, and a double peaked Gaussian distribution

$$P(h_i) = \frac{1}{2}\left(\frac{1}{2\pi\sigma^2}\right)^{1/2}\left\{\exp\left[-\frac{(h_i - h_0)^2}{2\sigma^2}\right] + \exp\left[-\frac{(h_i + h_0)^2}{2\sigma^2}\right]\right\}. \qquad (5.4.5)$$

In a double peaked distribution defined in Eq. (5.4.5), random fields $\pm h_0$ are distributed with equal probability and the form of the distribution depends on the h_0 and σ parameters, where σ is the width of the distribution.

According to the Callen identity (Callen, 1963) for the spin-1/2 Ising ferromagnetic system, the thermal average of the spin variables at the site i is given by

$$\langle \{f_i\}S_i\rangle = \left\langle \{f_i\}\tanh\left[\beta\left(J\sum_j S_j + h_i\right)\right]\right\rangle, \qquad (5.4.6)$$

where j expresses the nearest-neighbor sites of the central spin and $\{f_i\}$ can be any function of the Ising variables as long as it is not a function of the site. From Eq. (5.4.6) with $\{f_i\} = 1$, the thermal and random-configurational averages of a central spin can be represented on a sc lattice by introducing the differential operator technique (Honmura & Kaneyoshi, 1979, Kaneyoshi, 1993)

$$m_0 = \left\langle\left\langle S_0^z\right\rangle\right\rangle_r = \left\langle\left\langle \prod_{j=1}^{q=6}\left[\cosh(J\nabla) + S_j\sinh(J\nabla)\right]\right\rangle\right\rangle_r F(x)|_{x=0}, \qquad (5.4.7)$$

where ∇ is a differential operator, q is the coordination number of the lattice, and the inner $\langle...\rangle$ and the outer $\langle...\rangle_r$ brackets represent the thermal and configurational averages, respectively. The function $F(x)$ in Eq. (5.4.7) is defined by

$$F(x) = \int dh_i P(h_i)\tanh[\beta(x + h_i)], \qquad (5.4.8)$$

and it has been calculated by numerical integration and by using the distribution functions defined in Eqs. (5.4.3)-(5.4.5). By expanding the right-hand side of Eq. (5.4.7) we get the longitudinal spin correlation as

$$\begin{aligned}\langle\langle S_0\rangle\rangle_r &= k_0 + 6k_1\langle\langle S_1\rangle\rangle_r + 15k_2\langle\langle S_1 S_2\rangle\rangle_r + 20k_3\langle\langle S_1 S_2 S_3\rangle\rangle_r + 15k_4\langle\langle S_1 S_2 S_3 S_4\rangle\rangle_r \\ &\quad + 6k_5\langle\langle S_1 S_2 S_3 S_4 S_5\rangle\rangle_r + k_6\langle\langle S_1 S_2 S_3 S_4 S_5 S_6\rangle\rangle_r. \qquad (5.4.9)\end{aligned}$$

The coefficients in Eq. (5.4.9) are defined as follows:

$$
\begin{aligned}
k_0 &= \cosh^6(J\nabla)F(x)|_{x=0}, \\
k_1 &= \cosh^5(J\nabla)\sinh(J\nabla)F(x)|_{x=0}, \\
k_2 &= \cosh^4(J\nabla)\sinh^2(J\nabla)F(x)|_{x=0}, \\
k_3 &= \cosh^3(J\nabla)\sinh^3(J\nabla)F(x)|_{x=0}, \\
k_4 &= \cosh^2(J\nabla)\sinh^4(J\nabla)F(x)|_{x=0}, \\
k_5 &= \cosh(J\nabla)\sinh^5(J\nabla)F(x)|_{x=0}, \\
k_6 &= \sinh^6(J\nabla)F(x)|_{x=0}.
\end{aligned}
\tag{5.4.10}
$$

Next, the average value of the perimeter spin in the system can be written as follows, and it is found as

$$
\begin{aligned}
m_1 = \langle\langle S_1 \rangle\rangle_r &= \langle\langle \cosh(J\nabla) + S_0 \sinh(J\nabla) \rangle\rangle_r F(x+\gamma), \\
&= a_1 + a_2 \langle\langle S_0 \rangle\rangle_r.
\end{aligned}
\tag{5.4.11}
$$

The coefficients in Eq. (5.4.11) are defined as

$$
\begin{aligned}
a_1 &= \cosh(J\nabla)F(x+\gamma)|_{x=0}, \\
a_2 &= \sinh(J\nabla)F(x+\gamma)|_{x=0}.
\end{aligned}
\tag{5.4.12}
$$

In Eq. (5.4.12), $\gamma = (q-1)A$ is the effective field produced by the $(q-1)$ spins outside of the system and A is an unknown parameter to be determined self-consistently. In order to evaluate the multi-spin correlation functions in the system, we derive a set of linear equations as usual by using the basis correlation functions in Eqs. (5.4.9) and (5.4.11) with the rules presented in Eq. (4.1.34) and accordingly we obtain a system of linear equations with 12 unknowns for $q = 6$ which can be solved using the condition

$$
\langle\langle S_0 \rangle\rangle_r = \langle\langle S_1 \rangle\rangle_r.
\tag{5.4.13}
$$

The complete sets of linear equations corresponding to $q = 6, 8$ and 12 obtained in this way can be found in (Akinci, Yuksel, & Polat, 2011a).

Now, we can discuss how the type of random-field distribution effects the phase diagrams of the system. Also, in order to clarify the type of transitions in the system, we will give the temperature dependence of the order parameter.

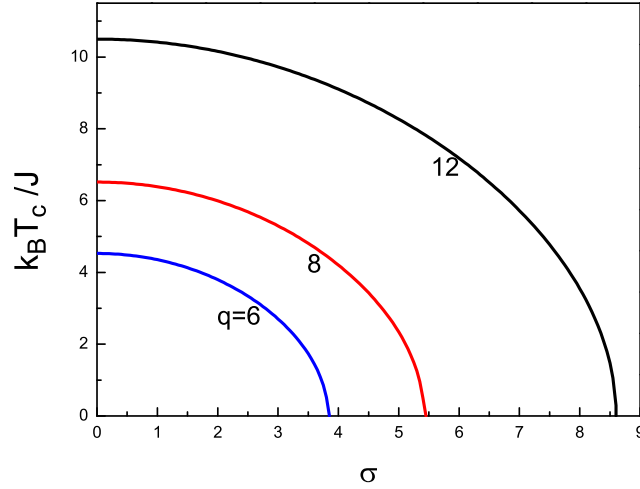*5.4.1   Phase Diagrams of Single-Gaussian Distribution*

Figure 5.10 Phase diagrams of sc ($q = 6$), bcc ($q = 8$), and fcc ($q = 12$) lattices in a ($k_BT_c/J - \sigma$) plane corresponding to a single-Gaussian distribution of random fields. The numbers on each curve denote the coordination numbers.

The form of single-Gaussian distribution which is defined in Eq. (5.4.3) is governed by only one parameter σ which is the width of the distribution. In Fig. 5.10, we show the phase diagram of the system for sc, bcc, and fcc lattices in a ($k_BT_c/J - \sigma$) plane. We can clearly see that as σ increases, then the width of the distribution function gets wider and the randomness effect of the magnetic-field distribution on the system becomes significantly important. Therefore, increasing the σ value causes a decline in the critical temperature k_BT_c/J of the system. We note that the critical temperature of the system reaches zero at $\sigma = 3.8501, 5.450$, and 8.601 for sc ($q = 6$), bcc ($q = 8$), and fcc ($q = 12$) lattices, respectively. Besides, we have not observed any reentrant or tricritical behavior for the single-Gaussian distribution, or, in other words, the system undergoes only a second-order phase transition. The k_BT_c/J value in the absence of any randomness, i.e., when $\sigma = 0$, is obtained as $k_BT_c/J = 4.5274, 6.5157$, and 10.4986 for $q = 6, 8, 12$, respectively. These values can be compared with the other works in the literature. Although, to the best of our knowledge, an exact solution for the Ising model does not exist in 3D, it is well known that the SE method agrees well with highly accurate MC simulations, which gives the best approximate values to the known exact results. Therefore, we see in Table 5.4 that the present work improves
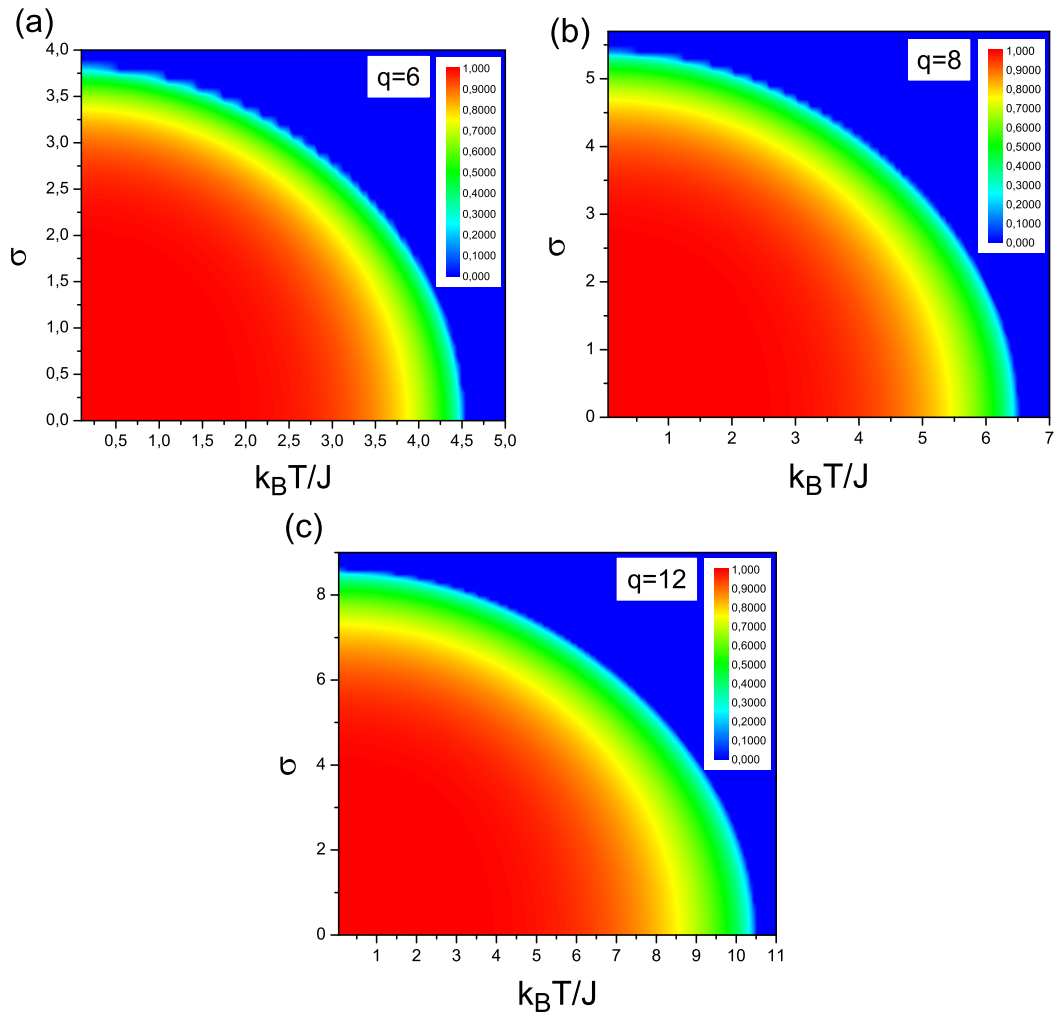
Figure 5.11 Variation of magnetization with $k_B T/J$ and σ corresponding to the phase diagrams in Fig. 5.10 for (a) sc, (b) bcc, and (c) fcc lattices.

the results of the other works based on EFT. The reason is due to the fact that, in contrast to the previously published works mentioned above, there is no uncontrolled decoupling procedure used for the higher-order correlation functions within the present approximation.

Projections of magnetization surfaces on the $(k_B T/J - \sigma)$ plane corresponding to the phase diagrams shown in Fig. 5.10 are depicted in Fig. 5.11 with $q = 6, 8$, and 12. We see that as the temperature increases starting from zero, the magnetization of the system decreases continuously, and it falls rapidly to zero at the critical temperature for all σ values. Moreover, the critical temperature of the system decreases and the saturation value of magnetization curves remains constant for a while then reduces

as σ value increases. This is a reasonable result since, if the σ value increases, then the randomness effects increasingly play an important role on the system, and random fields have a tendency to destruct the long-range ferromagnetic order on the system, and hence magnetization weakens. These observations are common properties of all three lattices.

Table 5.4 Critical temperature $k_B T_c/J$ at $h_0/J = 0$ and $\sigma = 0$ obtained by several methods such as EBPA (Du, Liu, & Yü, 2004), CEFT (Kaneyoshi, Fittipaldi, Honmura, & Manabe, 1981), PA (Balcerzak, 2003), EFT (Kaneyoshi, 1988), BA (Kikuchi, 1951), EFRG (de Sousa & Araújo, 1999, Neto & de Sousa, 2004), MFRG (Reinerhr & Figueiredo, 1998), MC (Landau, 1977, 1976b, Ferrenberg & Landau, 1991) and SE (Fisher, 1967) in comparison with the present work for $q = 6, 8, 12$.

Lattice	EBPA	CEFT	PA	EFT	BA	EFRG	MFRG	MC	SE	Present Work
SC	4.8108	4.9326	4.9328	5.0732	4.6097	4.85	4.93	4.51	4.5103	4.5274
BCC	-	6.9521	-	-	-	6.88	6.95	6.36	6.3508	6.5157
FCC	-	10.9696	-	-	-	-	-	-	9.7944	10.4986

5.4.2 *Phase Diagrams of Bimodal Distribution*

Next, in order to investigate the effect of the bimodal random fields defined in Eq. (5.4.4) on the phase diagrams of the system, we show the phase diagrams in a $(k_B T/J - h_0/J)$ plane and its corresponding magnetization profiles with coordination numbers $q = 6, 8$, and 12 in Figs. 5.12 and 5.13. In these figures the solid and dashed lines correspond to second- and first-order phase-transition points, respectively, and the open circles in Fig. 5.12 denote tricritical points. As seen in Fig. 5.12, increasing values of h_0/J causes the critical temperature to decrease for a while, then the reentrant behavior of first order occurs at a specific range of h_0/J. According to our calculations, the reentrant phenomena and the first-order phase transitions can be observed within the range of $2.0 < h_0/J < 3.0$ for $q = 6$, $3.565 < h_0/J < 3.95$ for $q = 8$, and $4.622 < h_0/J < 5.81$ for $q = 12$. If the h_0/J value is greater than the upper limits of these field ranges, the system exhibits no phase transition. The tricritical temperatures $k_B T_t/J$, which are shown as open circles in Fig. 5.12, are found as $k_B T_t/J = 1.5687, 2.4751$, and 4.3769 for $q = 6, 8$, and 12, respectively.
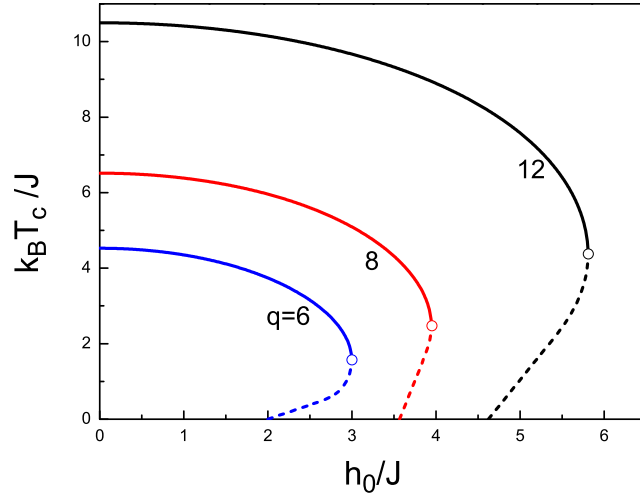
Figure 5.12 Phase diagrams of the system ($q = 6, 8, 12$) in a ($k_B T_c/J - h_0/J$) plane, corresponding to bimodal random field distribution. The solid and dashed lines correspond to second and first-order phase transitions, respectively. The open circles denote the tricritical points.
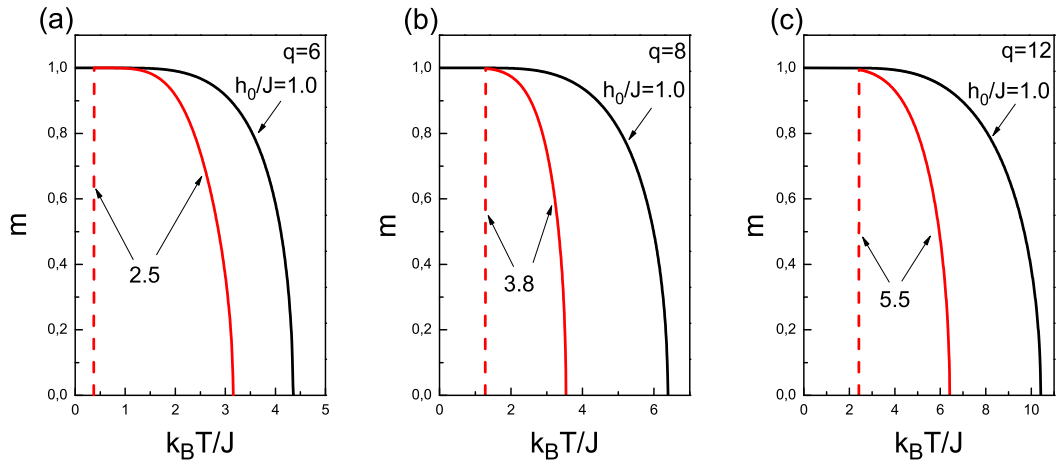

Figure 5.13 Temperature dependence of magnetization corresponding to Fig. 5.11 with $\sigma = 0$ and $h_0/J = 1.0, 2.5$ for a sc lattice (left-hand panel), $h_0/J = 1.0$ and 3.8 for a bcc lattice (middle panel), and $h_0/J = 1.0$ and 5.5 for a fcc lattice (right-hand panel). The solid and dashed lines correspond to second- and first-order phase transitions, respectively.

In Fig. 5.13, we show two typical magnetization profiles of the system. Namely, the system always undergoes a second-order phase transition for $h_0/J = 1.0$. On the other hand, two successive phase transitions (i.e., a first-order transition is followed by a second-order phase transition) occur at the values of $h_0/J = 2.5, 3.8$, and 5.5 for $q = 6, 8$, and 12, respectively, which puts forward the existence of a first-order reentrant

phenomena on the system. We observe that the increasing h_0/J values do not effect the saturation values of magnetization curves.

5.4.3   Phase Diagrams of Double-Gaussian Distribution

To the best of our knowledge, double-Gaussian distribution in Eq. (5.4.5) with nearest-neighbor interactions have not yet been examined in the literature. Therefore, it would be interesting to investigate the phase diagrams of the system with random fields corresponding to Eq. (5.4.5). Now the shape of the random fields is governed by two parameters h_0/J and σ. As shown in the preceding results, increasing the σ value tends to reduce the saturation value of the order parameter and destructs the second-order phase transitions by decreasing the critical temperature of the system without exposing any reentrant phenomena for $h_0/J = 0$. Besides, as the h_0/J value increases, then the second-order phase-transition temperature decreases again and the system may exhibit a reentrant behavior for $\sigma = 0$, while the saturation value of the magnetization curves remains unchanged. Hence, the presence of both h_0/J and σ on the system should produce a competition effect on the phase diagrams of the system. Fig. 5.14 shows the phase diagrams of the system in $(k_B T_c/J - h_0/J)$ and $(k_B T_c/J - \sigma)$ planes for $q = 6, 8$, and 12. As we can see in the left-hand panels in Fig. 5.14, the system exhibits tricritical points and reentrant phenomena for a narrow width of the random-field distribution, and as the width σ of the distribution gets wider, then the reentrant phenomena and tricritical behavior disappear. In other words, both the reentrant behavior and tricritical points disappear as the σ parameter becomes significantly dominant on the system. Our results predict that tricritical points depress to zero at $\sigma = 1.421, 2.238$, and 3.985 for $q = 6, 8$, and 12, respectively. For distribution widths greater than these values, all transitions are of second order, and as we further increase the σ value, then the ferromagnetic region gets narrower. Similarly, in the right-hand panels in Fig. 5.14, we investigate the phase diagrams of the system in a $(k_B T_c/J - \sigma)$ plane with selected values of h_0/J. We note that for the values of $h_0/J \leq 2.0$ ($q = 6$), $h_0/J \leq 3.565$ ($q = 8$), and $h_0/J \leq 4.622$ ($q = 12$), the system always undergoes a second-order phase transition between the paramagnetic and ferromagnetic phases at a critical temperature

which decreases with increasing values of h_0/J as in Fig. 5.10, where $h_0/J = 0$. Moreover, for values of h_0/J greater than these threshold values, the system exhibits a reentrant behavior of first order and the transition lines exhibit a bulge which gets smaller with increasing values of h_0/J, which again means that the ferromagnetic phase region gets narrower. Besides, for $h_0/J > 2.9952$ ($q = 6$), $h_0/J > 3.9941$ ($q = 8$), and $h_0/J > 5.8085$ ($q = 12$), tricritical points appear on the system.
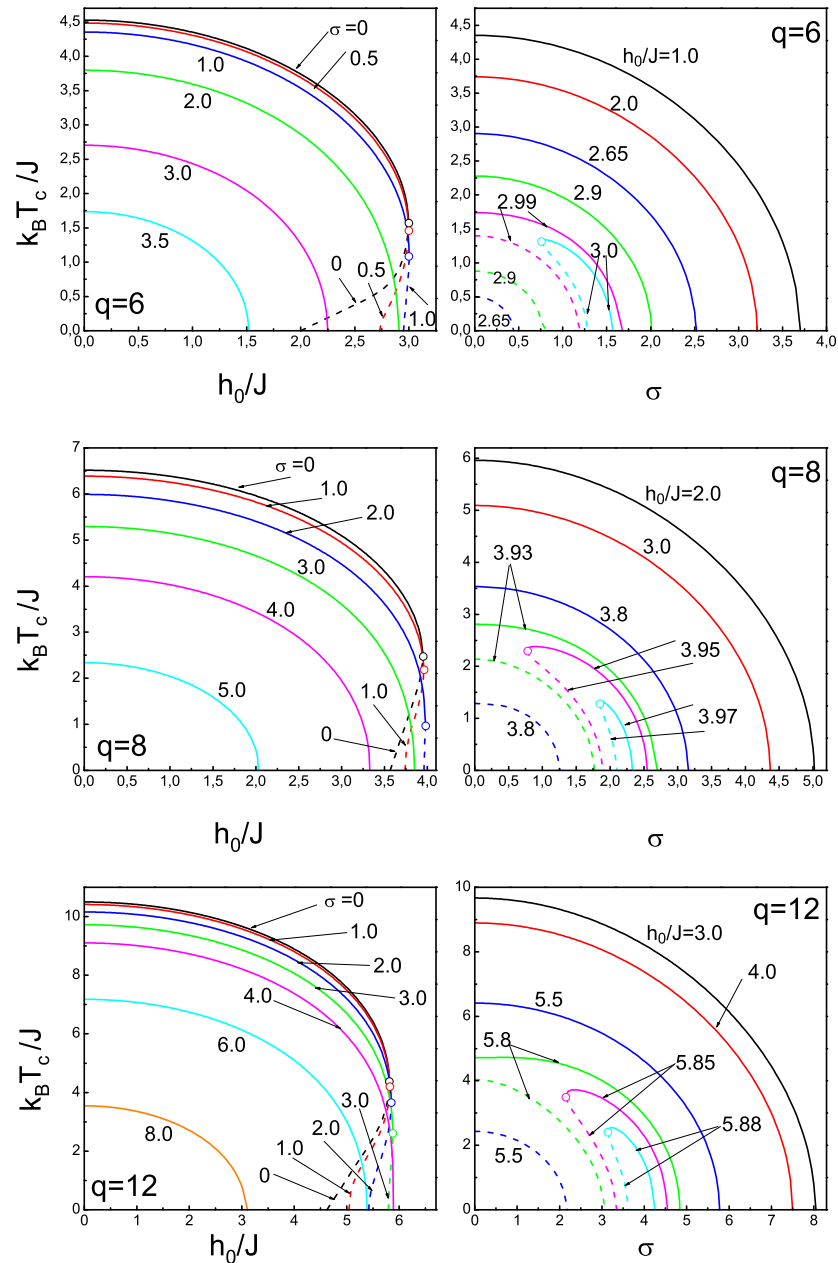

Figure 5.14 Phase diagrams of the system for a double-Gaussian random-field distribution with $q = 6, 8$, and 12 in $(k_B T_c/J - h_0/J)$ and $(k_B T_c/J - \sigma)$ planes.

In Fig. 5.15, we show magnetization curves corresponding to the phase diagrams shown in Fig. 5.14 for a sc lattice. Figure 5.15a shows the temperature dependence of magnetization curves for $q = 6$ with $h_0/J = 0.5$ (left-hand panel) and $h_0/J = 2.5$ (right-hand panel) with selected values of σ. As we can see in Fig. 5.15a, as σ increases, then the critical temperature of the system decreases and first-order phase transitions disappear [see the right-hand panel in Fig. 5.15a]. Moreover, the rate of decrease of the saturation value of the magnetization curves increases as h_0/J increases. On the other hand, in Fig. 5.15b, the magnetization versus temperature curves have been plotted with $\sigma = 0.5$ (left-hand panel) and $\sigma = 2.5$ (right-hand panel) with some selected values of h_0/J. In this figure, it is clear that saturation values of magnetization curves remain unchanged for $\sigma = 0.5$ and tend to decrease rapidly to zero with increasing values of h_0/J when $\sigma = 2.5$. In addition, as h_0/J increases when the value of σ is fixed, then the critical temperature of the system decreases and the ferromagnetic phase region of the system gets narrower. These observations show that there is a competition effect originating from the presence of both h_0/J and σ parameters on the phase diagrams and magnetization curves of the system.
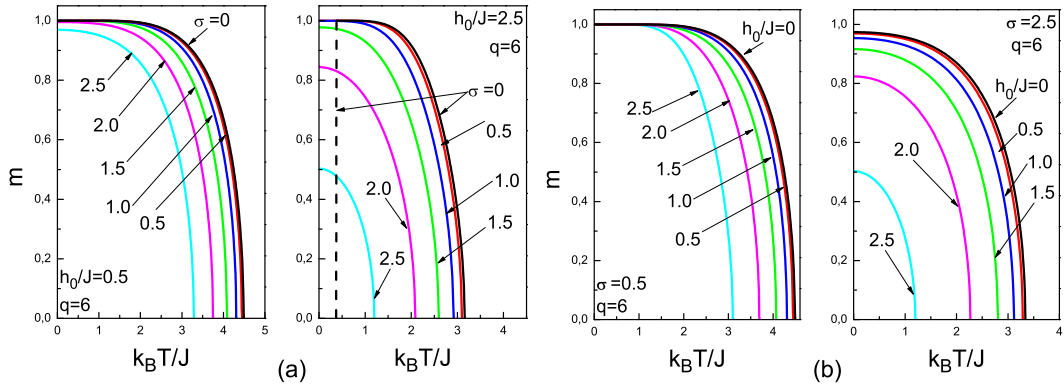
Figure 5.15 Magnetization curves for a sc lattice corresponding to the phase diagrams in Fig. 5.14 for a double-Gaussian distribution with some selected values of h_0/J and σ.

Finally, Fig. 5.16 represents the variation of the tricritical point $(k_BT_t/J, h_t/J)$ with σ for $q = 6, 8$, and 12. As seen from Fig. 5.16, the k_BT_t/J value decreases monotonically as σ increases and reaches zero at a critical value σ_t. According to our calculations, the critical distribution width σ_t value can be given as $\sigma_t = 1.421, 2.238$, and 3.985 for $q = 6, 8$, and 12, respectively. This implies that the σ_t value depends on

the coordination number of the lattice. Besides, h_t/J curves exhibit a relatively small increment with an increasing σ value.

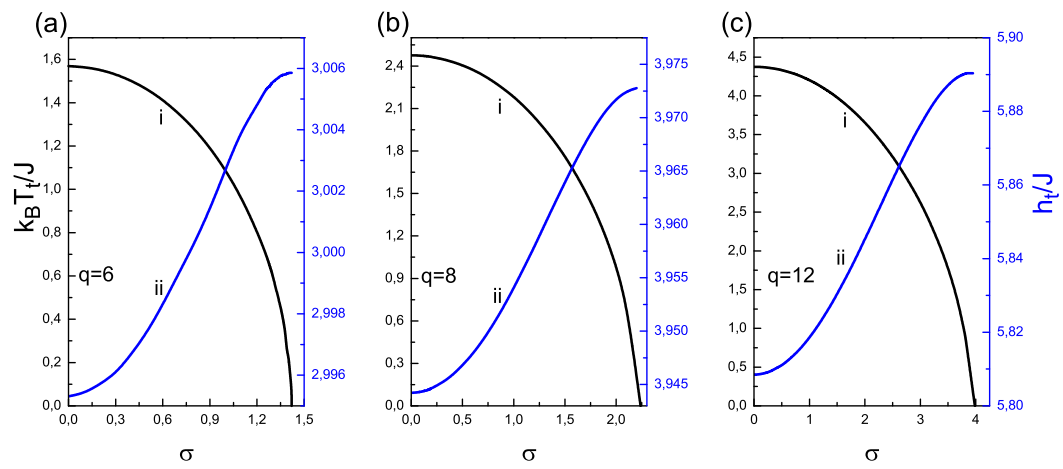Figure 5.16 Variations of tricritical temperature $k_B T_t/J$ (i) and tricritical field h_t/J (ii) as function of distribution width (σ) for (a) sc, (b) bcc, and (c) fcc lattices.

CHAPTER SIX
CONCLUSIONS

In conclusion, concerning the critical phenomena in disordered magnetism, we have introduced an effective-field theory formalism that takes into account the correlations between different spins in the cluster of a considered lattice. The proposed formulation is constructed in a heuristic manner. However, it produces physically quite reasonable outcomes.

First of all, we have applied the method for a pure spin-1 transverse Ising model on a honeycomb lattice ($q = 3$) with crystal field anisotropy in a longitudinal magnetic field (Yüksel & Polat, 2010). We have given the proper phase diagrams, especially the first-order transition lines that include reentrant phase transition regions. A number of interesting phenomena such as reentrant phenomena have been found in the physical quantities originating from the crystal field as well as the transverse and longitudinal components of the magnetic field. We have found that one can observe reentrant behavior in the system for the values of $\Omega/J < \Omega_t/J = 0.861$ and $-1.453 < D/J < -1.02$ and the tricritical points exist for $1.278 < -Dt/J < 1.453$ and $\Omega/J < 0.861$. The results show that the reentrant phenomenon originates from the competition between the crystal field D/J and transverse field Ω/J. Besides, applying a transverse field Ω/J on the system has the tendency to destruct the first-order transitions, while the longitudinal counterpart h/J destructs both the first- and second-order phase transitions. Hence, we believe that the effects of the transverse field Ω/J are very different from those of the longitudinal counterpart h/J since the transverse field can produce quantum effects. These interesting results are not reported in the literature.

In order to have an idea on the feasibility of the formalism in disordered systems, we adopted the formulation for site and bond diluted ferromagnets (Akinci et al., 2011c,b), random crystal field problem (Yüksel et al., 2012a) and for the Ising model in the presence of random magnetic fields (Akinci et al., 2011a), respectively and the outcomes can be briefly summarized as follows:

For a site diluted spin-1/2 ferromagnet (Akinci et al., 2011c), we have found that equations of state obtained within the present approximation can be reduced to those obtained by conventional or improved decoupling approximation techniques which exposes the superiority of the proposed formulation. We have also obtained results that are superior to those estimated by conventional mean field theory (MFT) and effective field theory (EFT) based on a decoupling approximation (DA), especially for the critical site concentration (i.e. site percolation threshold) value c^* for honeycomb ($q = 3$) and square ($q = 4$) lattices. Our estimated values $c^* = 0.6727$ and $c^* = 0.4594$ for $q = 3$ and $q = 4$, respectively are the best approximate values to the results of MC and SE methods among the other works based on MFT or EFT from which it is clearly evident that our method improves the conventional EFT methods based on decoupling approximation.

Moreover, we have studied the phase diagrams of a bond diluted spin-1 transverse Ising model with crystal field interaction on a honeycomb lattice (Akinci et al., 2011b). We have examined the variation of the bond percolation threshold p_c with the crystal and transverse field interactions which has not been reported in the literature before. In the absence of crystal and transverse fields the percolation threshold value is obtained as $p_c = 0.5397$ which improves the results obtained by other EFT based approximations. We have also given the proper phase diagrams, especially the first order transition lines that include reentrant phase transition regions. A number of interesting and unusual phenomena such as the reentrant behavior for positive valued crystal fields and three successive phase transitions that arise for the specific range of Hamiltonian parameters $p, \Omega/J$ and D/J have been found. As a new result, we can conclude that three successive phase transition behaviors can be observed for the systems with bond dilution in the presence of homogeneous crystal and transverse fields, as well as the systems with random crystal fields. Hence, the results show that the type of the transition (first or second order), the existence of reentrant magnetism as well as three successive phase transitions originate from a complicated competition between bond dilution and the strength of crystal and transverse field interactions on the lattice.

Furthermore, we have studied the phase diagrams of a spin-1 Blume-Capel model with diluted and random crystal field interactions on two dimensional lattices (Yüksel et al., 2012a) and examined the phase diagrams as well as magnetization curves of the system for different types of crystal field distributions, namely, dilute crystal fields and a double peaked delta distribution, respectively. For dilute crystal fields, we have given a detailed exploration of the global phase diagrams of the system in $(k_B T_c/J - D/J)$ plane with the second and first order transitions, as well as tricritical points. We have also shown that the system with dilute crystal fields exhibits a percolation threshold value p_c which can not be predicted by standard MFT. In addition, we have observed multi-reentrant phase transitions for specific set of system parameters. On the other hand, we have investigated the effect of the random crystal field distribution characterized by two crystal field parameters D/J and Δ/J on the phase diagrams of the system. As a limited case, we have also focused on a bimodal distribution with $D/J = 0$. Particulary, we have reported the following observations for a bimodal distribution: It has been found that the phase diagrams have symmetric shape with respect to Δ/J which comes from the fact that $p = 1/2$. The transition temperatures are of second order, and the system exhibits different characteristic features depending on the coordination number q. Besides, we have realized that the system may exhibit clear distinctions in a qualitative manner with coordination number q for random crystal fields with $\Delta/J, D/J \neq 0$. Moreover, we have discussed a competition effect which arises from the presence of dilution, as well as random crystal fields, and we have observed that saturation values of the magnetization curves are strongly related to these effects. As a result, we can conclude that all of the points mentioned above show that our method improves the conventional EFT methods based on decoupling approximation and the formalism presented in this work can be easily extended to the systems with continuous-field probability distributions, such as single or double Gaussian field distributions.

Finally, we have studied the phase diagrams as well as magnetization curves of a spin-1/2 Ising model in a random magnetic field on sc, bcc, and fcc lattices for different types of random-field distributions, namely, single-Gaussian, bimodal,

and double-Gaussian distributions (Akinci et al., 2011a). For a single-Gaussian distribution, we have found that the system always undergoes a second-order phase transition between the paramagnetic and ferromagnetic phases. For bimodal and double-Gaussian distributions, we have given the proper phase diagrams, especially the first-order transition lines that include reentrant phase-transition regions. Our numerical analysis clearly indicates that such field distributions lead to a tricritical behavior. Moreover, we have discussed a competition effect which arises from the presence of both h_0/J and σ parameters, and we have observed that saturation values of the magnetization curves are strongly related to these effects. In addition, in the absence of any randomness (i.e., $h_0/J = 0$, $\sigma = 0$) our critical temperature values corresponding to the coordination numbers $q = 6, 8$, and 12 are the best approximate values to the results of MC and SE methods, among the other works given in Table 5.3.

As a result, we can conclude that all of the points mentioned above show that our method improves the conventional EFT methods based on decoupling approximation. However, although we obtain certain improvements in qualitative and quantitative features of the model systems within the present formalism, our method contains some certain deficient points. Namely, we can not distinguish a two dimensional triangular lattice from a three dimensional simple cubic lattice, both of which have a coordination number $q = 6$. Hence, the dimensionality is factitious concept in the present formalism. Moreover, the size of the system of linear equations derived for an arbitrary model increases very fast for $S \geq 1$ and $q \geq 4$ which produces complicated calculation procedures prone to erroneous analysis. On the other hand, calculation of multi-site correlation functions for anti-ferromagnetic and ferrimagnetic systems may be exhaustive and the formulation fails in applications for the systems with next-nearest (and also further) neighbor interactions.

In general, we see that the proposed method has been successfully applied for the investigation of disordered magnetic systems and we hope that the results obtained in this thesis report may be beneficial from both theoretical and experimental points of view.

REFERENCES

Aharony, A. (1978). Tricritical Points in Systems with Random Fields. *Physical Review B*, *18*(7), 3318.

Akinci, U. (2011). An Improved Effective Field Theory Formulation of Spin-1/2 Ising Systems with Arbitrary Coordination Number *z. arXiv:1112.4052v1 [cond-mat.stat-mech], unpublished.*

Akinci, U. (2012). An Improved Effective Field Theory Formulation of Spin-1 Ising Systems with Arbitrary Coordination Number *z. arXiv:1201.3015v1 [cond-mat.stat-mech], unpublished.*

Akinci, U., Yuksel, Y., & Polat, H. (2011a). Effective-Field-Theory Analysis of the Three-Dimensional Random-Field Ising Model on Isometric Lattices. *Physical Review E*, *83*(6), 061103.

Akinci, U., Yuksel, Y., & Polat, H. (2011b). Effects of the Bond Dilution on the Phase Diagrams of a Spin-1 Transverse Ising Model with Crystal Field Interaction on a Honeycomb Lattice. *Physica A*, *390*(4), 541.

Akinci, U., Yuksel, Y., & Polat, H. (2011c). A New Effective Field Theory for Spin-*S* (*S* ≤ 1) Dilute Ising Ferromagnets. *arXiv:1111.2927v1 [cond-mat.stat-mech], unpublished.*

Albayrak, E., & Canko, O. (2004). Trimodal Random-Field Spin-3/2 Ising Systems in a Transverse Field. *Journal of Magnetism and Magnetic Materials*, *270*(3), 333.

Andelman, D. (1983). First- and Second-Order Phase Transitions with Random Fields at Low Temperatures. *Physical Review B*, *27*(5), 3079.

Balcerzak, T. (2001). Cluster Variational Method for Critical Concentration Calculations of Site-Diluted Ising Model. *Journal of Magnetism and Magnetic Materials*, *223*(3), 309.

Balcerzak, T. (2003). Thermodynamics of the Ising Model in Pair Approximation. *Physica A*, *317*(1-2), 213.

Balcerzak, T., Bobák, A., Mielnicki, J., & Truong, V. H. (1985). A New Approach for the Diluted Ising Ferromagnet Description. *Physica Status Solidi B*, *130*(1), 183.

Barreto, F. C. S., Fittipaldi, I. P., & Zeks, B. (1981). New Effective Field Theory for the Transverse Ising Model. *Ferroelectrics*, *39*(1), 1103.

Belanger, D. P. (1991). The Random Field Ising Model. *Journal of Magmnetism and Magnetic Materials*, *100*(1-3), 272.

Belanger, D. P., King, A. R., & Jaccarino, V. (1985). Random-Field Critical Behavior of a $D = 3$ Ising System: Neutron Scattering Studies of $Fe_{0.6}Zn_{0.4}F_2$. *Physical Review B*, *31*(7), 4538.

Benayad, N., Benyoussef, A., & Boccara, N. (1985). The Dilute Spin-1 Ising Model with Crystal-Field Interactions. *Journal of Physics C: Solid State Physics*, *18*(9), 1899.

Benyoussef, A., Biaz, T., Saber, M., & Touzani, M. (1987). The Spin-1 Ising Model with a Random Crystal Field: The Mean-Field Solution. *Journal of Physics C: Solid State Physics*, *20*(32), 5349.

Binder, K. (1981). Critical Properties From Monte Carlo Coarse Graining and Renormalization. *Physical Review Letters*, *47*(9), 693.

Binder, K., Imry, Y., & Pytte, E. (1981). Interface Roughening and Random-Field Instabilities in Ising Systems in Three or Less Dimensions. *Physical Review B*, *24*(11), 6736.

Blume, M. (1966). Theory of the First-Order Magnetic Phase Change in UO_2. *Physical Review*, *141*(2), 517.

Blume, M., Emery, V. J., & Griffiths, R. B. (1971). Ising Model for the λ Transition and Phase Separation in $^3He - ^4He$ Mixtures. *Physical Review A*, *4*(3), 1071.

Blundell, S. (2001). *Magnetism in Condensed Matter*. Oxford University Press Inc., New York.

Bobák, A., & Jaščur, M. (1991). Random-Field Effects in Site-Diluted Ising Ferromagnets. *Journal of Physics: Condensed Matter*, *3*(34), 6613.

Bobák, A., & Jaščur, M. (1994). Correlated Effective-Field Theory of the Site-Diluted Ising Model. *Journal of Magnetism and Magnetic Materials*, *136*(1-2), 105.

Bobák, A., & Karaba, J. (1987). A New Effective Field Theory for Dilute Ising Ferromagnets. *Physica Status Solidi B*, *142*(2), 575.

Bobák, A., Mockovčiak, S., & Sivulka, J. (1993). One- and Two-Spin Cluster Approximations for the Site-Diluted Spin-1 Ising Model. *Physica Status Solidi B*, *176*(2), 477.

Boccara, N. (1983). Dilute Ising Models: A Simple Theory. *Physics Letters A*, *94*(3-4), 185.

Boccara, N., & Saber, M. (1985). Dilute Semi-Infinite Ising Model. *Journal of Physics C: Solid State Physics*, *18*(22), 4275.

Bonfim, O. F. D. A., & Fittipaldi, I. P. (1983). Bond and Site Diluted Ising-Model Systems: A Unified Treatment. *Physics Letters A*, *98*(4), 199.

Borges, H. E., & Silva, P. R. (1987). Thermodynamical Properties of the Random Field Ising Model. *Physica A*, *144*(2-3), 561.

Bouziane, T., & Saber, M. (2009). The Transverse Spin-1 Ising Model with Random Interactions. *Journal of Magnetism and Magnetic Materials*, *321*(1), 17.

Box, G. E. P., & Muller, M. E. (1958). A Note on the Generation of Random Normal Deviates. *The Annals of Mathematical Statistics*, *29*(2), 610.

Bricmont, J., & Kupiainen, A. (1987). Lower Critical Dimension for the Random-Field Ising Model. *Physical Review Letters*, *59*(16), 1829.

Buzano, C., Maritan, A., & Pelizzola, A. (1994). A Cluster Variation Approach to the Random-Anisotropy Blume-Emery-Griffiths Model. *Journal of Physics: Condensed Matter*, *6*(2), 327.

Callen, H. B. (1963). A Note on Green Functions and the Ising Model. *Physics Letters*, *4*(3), 161.

Capel, H. W. (1966). On the Possibility of First-Order Phase Transitions in Ising Systems of Triplet Ions with Zero-Field Splitting. *Physica*, *32*(5), 966.

Cardy, J. L. (1984). Random-Field Effects in Site-Disordered Ising Antiferromagnets. *Physical Review B*, *29*(1), 505.

Carneiro, C. E. I., Henriques, V. B., & Salinas, S. R. (1989). Comment on the Mean-Field Phase Diagram of the Spin-1 Ising Model in a Random Crystal Field. *Journal of Physics: Condensed Matter*, *1*(24), 3687.

Cipra, B. A. (1987). An Introduction to the Ising Model. *The American Mathematical Monthly*, *94*(10), 937.

Crokidakis, N., & Nobre, F. D. (2008). Destruction of First-Order Phase Transition in a Random-Field Ising Model. *Journal of Physics: Condensed Matter*, *20*(14), 145211.

de Sousa, J. R., & Araújo, I. G. (1999). Quantum Influence in the Criticality of the Spin-1/2 Anisotropic Heisenberg Model. *Journal of Magentism and Magnetic Materials*, *202*(1), 231.

Domb, C. (1949). Order-Disorder Statistics II. A Two-Dimensional Model. *Proceedings of the Royal Society A*, *199*(1057), 199–221.

Domb, C., & Sykes, M. F. (1961). Cluster Size in Random Mixtures and Percolation Processes. *Physical Review*, *122*(1), 77.

Du, A., Liu, H. J., & Yü, Y. Q. (2004). Expanded Bethe-Peierls Approximation for the Ising Model with S=1/2 and 1. *Physica Status Solidi B*, *241*(1), 175.

Dutta, A., Divakaran, U., Sen, D., Chakrabarti, B. K., Rosenbaum, T. F., & Aeppli, G. (2012). Quantum Phase Transitions in Transverse Field Spin Models: From Statistical Physics to Quantum Information. *arXiv:1012.0653v2 [cond-mat.stat-mech], unpublished*.

Feng, Q. (1996). *Study of the Three Dimensional Random Field Ising Model: Magnetic X-ray and Neutron Scattering, Magnetization, and Heat Capacity*. Ph.D. thesis, B. A., Lake Forest College, Massachusetts Institute of Tehcnology.

Fernandez, J. F., Grinstein, G., Imry, Y., & Kirkpatrick, S. (1983). Numerical Evidence for $d_c = 2$ in the Random-Field Ising Model. *Physical Review Letters*, *51*(3), 203.

Ferreira, I. B., King, A. R., Jaccarino, V., Cardy, J. L., & Guggenheim, H. J. (1983). Random-Field-Induced Destruction of the Phase Transition of a Diluted Two-Dimensional Ising Antiferromagnet: $Rb_2Co_{0.85}Mg_{0.15}F_4$. *Physical Review B*, *28*(9), 5192.

Ferrenberg, A. M., & Landau, D. P. (1991). Critical Behavior of the Three-Dimensional Ising Model: A High-Resolution Monte Carlo Study. *Physical Review B*, *44*(10), 5081.

Fisher, D. S., Grinsrein, G. M., & Khurana, A. (1988). Theory of Random Magnets. *Physics Today*, *41*(12), 56.

Fisher, M. E. (1967). The Theory of Equilibrium Critical Phenomena. *Reports on Progress in Physics*, *30*(2), 615.

Fishman, S., & Aharony, A. (1979). Random Field Effects in Disordered Anisotropic Antiferromagnets. *Journal of Physics C: Solid State Physics*, *12*(18), L729.

Frontera, C., & Vives, E. (1999). Numerical Signs for a Transition in the Two-Dimensional Random Field Ising Model at T=0. *Physical Review E*, *59*(2), R1295.

Fytas, N. G., & Malakis, A. (2008). Phase Diagram of the 3D Bimodal Random-Field Ising Model. *European Physical Journal B*, *61*(1), 111.

Fytas, N. G., Malakis, A., & Eftaxias, K. (2008). First-Order Transition Features of the 3D Bimodal Random-Field Ising Model. *Journal of Statistical Mechanics: Theory and Experiment*, *2008*(3), P03015.

Gennes, P. G. D. (1963). Collective Motions of Hydrogen Bonds. *Solid State Communications*, *1*(6), 132.

Gofman, M., Adler, J., Aharony, A., Harris, A. B., & Schwartz, M. (1996). Critical Behavior of the Random-Field Ising Model. *Physical Review B*, *53*(10), 6362.

Graf, E. H., Lee, D. M., & Reppy, J. D. (1967). Phase Separation and the Superfluid Transition in Liquid ^{3}He $-^4$ He Mixtures. *Physical Review Letters*, *19*(8), 417.

Grinstein, G. (1984). On the Lower Critical Dimension of the Random Field Ising Model (Invited). *Journal of Applied Physics*, *55*(6), 2371.

Grinstein, G., & Ma, S. K. (1982). Roughening and Lower Critical Dimension in the Random-Field Ising Model. *Physical Review Letters*, *49*(9), 685.

Hadjiagapiou, I. A. (2010). The Random-Field Ising Model with Asymmetric Bimodal Probability Distribution. *Physica A*, *389*(19), 3945.

Heisenberg, W. (1928). On the Theory of Ferromagnetism. *Zeitschrift für Physik*, *49*(4), 619.

Honmura, R., & Kaneyoshi, T. (1979). Contribution to the New Type of Effective-Field Theory of the Ising Model. *Journal of Physics C: Solid State Physics*, *12*(19), 3979.

Htoutou, K., Ainane, A., Saber, M., & de Miguel, J. J. (2005a). The Site Diluted Transverse Spin-1 Ising Model with a Longitudinal Crystal-Field. *Physica A*, *358*(1), 184.

Htoutou, K., Benaboud, A., Ainane, A., & Saber, M. (2004). The Phase Diagrams and the Order Parameters of the Transverse Spin-1 Ising Model with a Longitudinal Crystal-Field. *Physica A*, *338*(3-4), 479.

Htoutou, K., Oubelkacem, A., Ainane, A., & Saber, M. (2005b). Tricritical Behavior in the Diluted Transverse Spin-1 Ising Model with a Longitudinal Crystal Field. *Journal of Magnetism and Magnetic Materials*, *288*(1), 259.

Huang, K. (1987). *Statistical Mechanics (2nd Edition)*. Wiley.

Imbrie, J. Z. (1984). Lower Critical Dimension of the Random-Field Ising Model. *Physical Review Letters*, *53*(18), 1747.

Imry, Y. (1984). Random External Fields. *Journal of Statistical Physics*, *34*(5-6), 849.

Imry, Y., & Ma, S. K. (1975). Random-Field Instability of the Ordered State of Continuous Symmetry. *Physical Review Letters*, *35*(21), 1399.

Ising, E. (1925). Beitrag Zur Theorie Des Ferromagnetismus. *Zeitschrift für Physik*, *31*(1), 253.

Jiang, X. F. (1994). Phase Transition of the Bond-Diluted Spin-1 Transverse Ising Model with Crystal Field Interaction. *Journal of Magnetism and Magnetic Materials*, *134*(1), 167.

Jiang, X. F., Li, J. L., Zhong, J. L., & Yang, C. Z. (1993). Effect of a Crystal Field on Phase Transitions in a Spin-1 Transverse Ising Model. *Physical Review B*, *47*(2), 827.

Kaneyoshi, T. (1980). Comments on Molecular-Field Theory with Correlations. *Physics Letters A*, *76*(1), 67.

Kaneyoshi, T. (1985). Second-Order Phase Transitions and Tricritical Points in the Random-Field Ising Models. *Physica A*, *139*(2-3), 455.

Kaneyoshi, T. (1986). The Tricritical Point in Ising Models with Random Bonds and Crystal-Field Interactions. *Journal of Physics C: Solid State Physics*, *19*(25), L557.

Kaneyoshi, T. (1988). *Review of Solid State Science*, *2*, 39.

Kaneyoshi, T. (1992). Phase Diagrams of a Spin-One Ising Model with a Random Crystal Field in the Correlated Effective-Field Treatment. *Physica Status Solidi B*, *170*(1), 313.

Kaneyoshi, T. (1993). Differential Operator Technique in the Ising Spin Systems. *Acta Physica Polonica A*, *83*(6), 703.

Kaneyoshi, T. (1995a). Some Problems in a Diluted Spin-S ($S > 1/2$) Ising Ferromagnet. *Physica A*, *218*(1-2), 46.

Kaneyoshi, T. (1995b). Theoretical Study of a Diluted Spin-S ($S > 1/2$) Ising Ferromagnet. *Physica A*, *222*(1-4), 450.

Kaneyoshi, T. (1999a). A New Type of Cluster Theory in Ising Models (I). *Physica A*, *269*(12), 344.

Kaneyoshi, T. (1999b). A New Type of Cluster Theory in Ising Models (II). *Physica A*, *269*(12), 357.

Kaneyoshi, T., Fittipaldi, I. P., Honmura, R., & Manabe, T. (1981). New Correlated-Effective Field Theory in the Ising Model. *Physical Review B*, *24*(1), 481.

Kaneyoshi, T., & Jaščur, M. (1992). Critical Concentration of a Diluted Spin-3/2 Ising Ferromagnet. *Physica Status Solidi B*, *173*(2), K37.

Kaneyoshi, T., & Mielnicki, J. (1990). Comparison of Effective-Field and Mean-Field Theories for the Spin-One Ising Model with a Random Crystal Field. *Journal of Physics: Condensed Matter*, *2*(44), 8773.

Kaneyoshi, T., Tamura, I., & Honmura, R. (1984). Dilute Ising Ferromagnet: Its Physical Properties. *Physical Review B*, *29*(5), 2769.

Kaufman, M., Klunzinger, P. E., & Khurana, A. (1986). Multicritical Points in an Ising Random-Field Model. *Physical Review B*, *34*(7), 4766.

Kerouad, M., & Saber, M. (1991). The Re-Entrant Behaviour of the Spin-One Ising Model. *Physica Status Solidi B*, *168*(2), 597.

Kikuchi, R. (1951). A Theory of Cooperative Phenomena. *Physical Review*, *81*(6), 988.

Kim, S. B., Ma, J., & Chan, M. H. W. (1993). Phase Diagram of ^{3}He $-^4$He Mixture in Aerogel. *Physical Review Letters*, *71*(14), 2268.

King, A. R., Jaccarino, V., Belanger, D. P., & Rezende, S. M. (1985). Scaling of the Equilibrium Boundary of Three-Dimensional Random-Field Ising-Model Systems. *Physical Review B*, *32*(1), 503.

Kobe, S. (2000). Ernst Ising 1900-1998. *Brazilian Journal of Physics*, *30*(4), 649.

Landau, D. P. (1976a). Finite-Size Behavior of the Ising Square Lattice. *Physical Review B*, *13*(7), 2997.

Landau, D. P. (1976b). Finite-Size Behavior of the Simple-Cubic Ising Lattice. *Physical Review B*, *14*(1), 255.

Landau, D. P. (1977). Critical Behavior of a BCC Ising Antiferromagnet in a Magnetic Field. *Physical Review B*, *16*(9), 4164.

Landau, D. P., & Binder, K. (2001). *A Guide to Monte Carlo Simulations in Statistical Physics*. Cambridge University Press, Newyork.

Landau, D. P., Lee, H. H., & Kao, W. (1978). Critical Behavior of a 3-D Ising Model in a Random Field. *Journal of Applied Physics*, *49*(3), 1356.

Lara, D., & Plascak, J. (1998). General Spin Ising Model with Diluted and Random Crystal Field in the Pair Approximation. *Physica A*, *260*(3-4), 443.

Larkin, A. I. (1970). Effect of Inhomogeneties on the Structure of the Mixed State of Superconductors. *Journal of Experimental and Theoretical Physics*, *31*(4), 784.

Li, Z. Y., & Yang, C. Z. (1985). Thermodynamical Properties of the Site-Bond Diluted Ising Ferromagnet. *Solid State Communications*, *56*(5), 445.

Liang, Y. Q., Wei, G. Z., Zhang, Q., Xin, Z. H., & Song, G. L. (2004). Phase Diagram and Tricritical Behavior of a Spin-3/2 Transverse Ising Model in a Random Field. *Journal of Magnetism and Magnetic Materials*, *284*(1), 47.

Machta, J., Newman, M. E. J., & Chayes, L. B. (2000). Replica-Exchange Algorithm and Results for the Three-Dimensional Random Field Ising Model. *Physical Review E*, *62*(6), 8782.

Maletta, H., & Felsch, W. (1979). Insulating Spin-Glass System $Eu_xSr_{1-x}S$. *Physical Review B*, *20*(3), 1245.

Maritan, A., Cieplak, M., Swift, M. R., & Toigo, F. (1992). Random-Anisotropy Blume-Emery-Griffiths Model. *Physical Review Letters*, *69*(2), 221.

Marsaglia, G. (1972). Choosing a Point From the Surface of a Sphere. *The Annals of Mathematical Statistics*, *43*(2), 645.

Matsudaira, N. (1973). Ising Ferromagnets with Random Impurities. *Journal of the Physical Society of Japan*, *35*(6), 1593.

Mattis, D. C. (1985). Tricritical Point in Random-Field Ising Model. *Physical Review Letters*, *55*(27), 3009.

Metropolis, N., Rosenbluth, A. W., Rosenbluth, M. N., Teller, A. H., & Teller, E. (1953). Equation of State Calculations by Fast Computing Machines. *Journal of Chemical Physics*, *21*(6), 1087.

Miao, H., Wei, G., Liu, J., & Geng, J. (2009). The Phase Diagrams of a Spin-1 Transverse Ising Model. *Journal of Magnetism and Magnetic Materials*, *321*(2), 102.

Miyatake, Y., Yamamoto, M., Kim, J. J., Toyonaga, M., & Nagai, O. (1986). On the Implementation of the "Heat-Bath" Algorithms for Monte Carlo Simulations of Classical Heisenberg Spin Systems. *Journal of Physics C: Solid State Physics*, *19*(14), 2539.

Mukamel, D., & Pytte, E. (1982). Interface Fluctuations and the Ising Model in a Random Field. *Physical Review B*, *25*(7), 4779.

Mulders, N., Ma, J., Kim, S. B., Yoon, J. S., & Chan, M. H. W. (1995). ^{3}He $-$ ^{4}He Mixtures in Aerogel. *Journal of Low Temperature Physics*, *101*(1), 95.

Néda, Z. (1994). Curie Temperatures for Site-Diluted Ising Ferromagnets. *Journal de Physique I France*, *4*(2), 175.

Neto, M. A., & de Sousa, J. R. (2004). Reentrant Behavior in the Nearest-Neighbor Ising Antiferromagnet in a Magnetic Field. *Physical Review B*, *70*(22), 224436.

Newman, M. E. J., & Barkema, G. T. (2001). *Monte Carlo Methods in Statistical Physics*. Clarendon Press, Oxford.

Niemi, A. (1982). Disorder Solitons. *Physical Review Letters*, *49*(25), 1808.

Onsager, L. (1944). Crystal Statistics I. A Two-Dimensional Model with an Order-Disorder Transition. *Physical Review*, *65*(3-4), 117.

Paetkau, M., & Beamish, J. R. (1998). Tricritical Point and Superfluid Transition in $^3\text{He} - ^4\text{He}$ Mixtures in Silica Aerogel. *Physical Review Letters*, *80*(25), 5591.

Parisi, G., & Sourlas, N. (1979). Random Magnetic Fields, Supersymmetry, and Negative Dimensions. *Physical Review Letters*, *43*(11), 744.

Pytte, E., Imry, Y., & Mukamel, D. (1981). Lower Critical Dimension and the Roughening Transition of the Random-Field Ising Model. *Physical Review Letters*, *46*(18), 1173.

Reinerhr, E. E., & Figueiredo, W. (1998). Phase Diagram of the Dilute Antiferromagnetic Ising Model. *Physics Letters A*, *244*(1-3), 165.

Ritchie, D. S., & Fisher, M. E. (1972). Theory of Critical-Point Scattering and Correlations II. Heisenberg Models. *Physical Review B*, *5*(7), 2668.

Saber, M. (1997). A Simple Approximation Method for Dilute Ising Systems. *Chinese Journal of Physics*, *35*(5), 577.

Saber, M., & Tucker, J. W. (1991). The Site-Diluted Spin-1 Transverse Ising Model. *Journal of Magnetism and Magnetic Materials*, *102*(3), 287.

Salmon, O., Crokidakis, N., & Nobre, F. D. (2009). Multicritical Behavior in a Random-Field Ising Model Under a Continuous-Field Probability Distribution. *Journal of Physics: Condensed Matter*, *21*(5), 056005.

Salmon, O. D., & Tapia, J. R. (2010). Multicriticality in the Blume-Capel Model Under a Continuous-Field Probability Distribution. *Joural of Physics A: Mathematical and Theoretical*, *43*(12), 125003.

Sarmento, E. F., & Kaneyoshi, T. (1989). Phase Transition of Transverse Ising Model in a Random Field. *Physical Review B*, *39*(13), 9555.

Sarmento, E. F., & Kaneyoshi, T. (1993). Phase Diagrams and Tricritical Behavior of a Diluted Spin-1 Transverse Ising Model in a Random Field. *Physical Review B*, *48*(5), 3232.

Sato, H., Arrott, A., & Kikuchi, R. (1959). Remarks on Magnetically Dilute Systems. *Journal of Physics and Chemistry of Solids*, *10*(1), 19.

Schneider, T., & Pytte, E. (1977). Random-Field Instability of the Ferromagnetic State. *Physical Review B*, *15*(3), 1519.

Sebastianes, R. M., & Figueiredo, W. (1992). Phase Diagram of a Trimodal Random Surface Field. *Physical Review B*, *46*(2), 969.

Shukla, P. (2004). Domains and Interfaces in Random Fields. *arXiv:cond-mat/0401253v1 [cond-mat.stat-mech], unpublished*.

Silva, C. J., Caparica, A. A., & Plascak, J. A. (2006). Wang-Landau Monte Carlo Simulation of the Blume-Capel Model. *Physical Review E*, *73*(3), 036702.

Stanley, H. E. (1971). *Introduction to Phase Transitions and Critical Phenomena*. Clarendon Press, Oxford.

Stauffer, D., & Aharony, A. (1991). *Introduction To Percolation Theory*. Taylor & Francis, London.

Sykes, M. F., & Essam, J. W. (1964). Critical Percolation Probabilities by Series Methods. *Physical Review*, *133*(1A), A310.

Sykes, M. F., Gaunt, D. S., & Glen, M. (1976). Percolation Processes in Two Dimensions II: Critical Concentrations and the Mean Size Index. *Journal of Physics A: Mathematical and General*, *9*(1), 97.

Taggart, G. B. (1982). Correlated Effective Field Approximation for the Dilute Ising Ferromagnet. *Physica A*, *116*(1-2), 34.

Tomé, T., & de Oliveira, M. J. (1990). Dynamic Phase Transition in the Kinetic Ising Model Under a Time-Dependent Oscillating Field. *Physical Review A*, *41*(8), 4251.

Tóth, L., & Tóthová, M. (1994). The Spin-1 Ising Model with Random Interactions. *Physica Status Solidi B*, *186*(1), K19.

Tucker, J. W. (1991). Effective Field Theory of Dilute Ising Systems. *Journal of Magnetism and Magnetic Materials*, *102*(1-2), 144.

Tucker, J. W. (1992). Effective Field Theory of a Quenched Dilute Spin-1 Ising Model. *Journal of Magnetism and Magnetic Materials*, *104-107*(1), 191.

Tucker, J. W. (1994). The Random Mixed Bond Spin-1 Ising Model. *Journal of Magnetism and Magnetic Materials*, *132*(1-3), 231.

Tucker, J. W. (2000). A Monte Carlo Study of Thin Spin-1 Ising Films with Surface Exchange Enhancement. *Journal of Magnetism and Magnetic Materials*, *210*(1-3), 383.

Villain, J., Semeria, B., Lancon, F., & Billard, L. (1983). A Controversial Problem: Modified Ising Model in a Random Field. *Journal of Physics C: Solid State Physics*, *16*(32), 6153.

Vyssotsky, V. A., Gordon, S. B., Frisch, H. L., & Hammersley, J. M. (1961). Critical Percolation Probabilities (Bond Problem). *Physical Review*, *123*(5), 1566.

Wiatrowski, G., Balcerzak, T., & Mielnicki, J. (1988). The Anomalous Behaviour of the Specific Heat of the Dilute Ising Ferromagnet at the Critical Concentration Region. *Journal of Magnetism and Magnetic Materials*, *71*(2), 197.

Wood, P. J., & Rushbrooke, G. S. (1966). Classical Heisenberg Ferromagnet. *Physical Review Letters*, *17*(6), 307.

Yan, S. L., & Deng, L. L. (2002). Thermodynamic Properties of Bond Dilution Blume-Capel Model with Random Crystal Field. *Physica A*, *308*(1-4), 301.

Yang, C. Z., & Zhong, J. L. (1989). The Site-Bond Diluted Transverse Ising Model with $S = 1$. *Physica Status Solidi B*, *153*(1), 323.

Yeomans, J. M. (2000). *Statistical Mechanics of Phase Transitions*. Clarendon Press, Oxford.

Yeomans, J. M., & Stinchcombe, R. B. (1978). Critical Properties of the Site-Diluted Ising Ferromagnet. *Journal of Physics C: Solid State Physics*, *11*(13), L525.

Yeomans, J. M., & Stinchcombe, R. B. (1979). Critical Properties of Site- and Bond-Diluted Ising Ferromagnets. *Journal of Physics C: Solid State Physics*, *12*(2), 347.

Yoshizawa, H., Cowley, R. A., Shirane, G., Birgeneau, R. J., Guggenheim, H. J., & Ikeda, H. (1982). Random-Field Effects in Two- and Three-Dimensional Ising Antiferromagnets. *Physical Review Letters*, *48*(6), 438.

Yüksel, Y., Akinci, U., & Polat, H. (2009). An Introduced Effective-Field Approximation and Monte Carlo Study of a Spin-1 Blume-Capel Model on a Square Lattice. *Physica Scripta*, *79*(4), 045009.

Yüksel, Y., Akinci, U., & Polat, H. (2012a). Critical Behavior and Phase Diagrams of a Spin-1 Blume-Capel Model with Random Crystal Field Interactions: An Effective Field Theory Analysis. *Physica A*, *391*(9), 2819.

Yüksel, Y., & Polat, H. (2010). An Introduced Effective-Field Theory Study of Spin-1 Transverse Ising Model with Crystal Field Anisotropy in a Longitudinal Magnetic Field. *Journal of Magnetism and Magnetic Materials*, *322*(24), 3907.

Yüksel, Y., Vatansever, E., & Polat, H. (2012b). Dynamic Phase Transition Properties and Hysteretic Behavior of a Ferrimagnetic Core-Shell Nanoparticle in the Presence of a Time Dependent Magnetic Field. *Journal of Physics: Condensed Matter*, *24*(43), 436004.

Zaim, A., Amraoui, Y. E., Kerouad, M., & Arhchoui, H. (2008). Monte Carlo Study of the Spin-1 Blume-Capel Ising Film. *Journal of Magnetism and Magnetic Materials*, *320*(6), 1030.

Zernike, F. (1940). The Propagation of Order in Cooperative Phenomena: Part I. The AB Case. *Physica*, *7*(7), 565.